ABSTRACT

Theoretical Studies of LHC Physics in the Context of Exact Amplitude-Based Resummation Realized by MC Methods

Aditi Mukhopadhyay, Ph.D.

Advisor: B.F.L. Ward, Ph.D.

With the announcement [1] of the Higgs Boson candidate in the LHC run, it is now required to study the properties of the new particle as well as probe the new physics. Therefore the era of the sub-1% precision on processes such as Z and W production is upon us. In order to study the Standard Model and beyond more rigorously a more precise Monte Carlo simulation is required. With the previous comparisons with the FNAL data it was seen that HERWIRI1.0 gives a precise fit to the data.

In this thesis we present the application of the exact amplitude-based resummation in quantum field theory to precision QCD calculation, by MC event generator methods using HERWIRI1.031 as required by the LHC. Here we discuss the recent results with the interplay of the attendant IR-Improved DGLAP-CS theory and the precision of the exact NLO matrix-element matched parton shower MC's in the HERWIG6.5 environment, the HERWIRI1.031, determined by the recent LHC experimental observations.

The agreement to the new precise data from the LHC is encouraging. For completeness, we also discuss the theoretical perspectives of the exact amplitude-based resummation theory. We present the step towards the sub-1% QCD$\otimes$EW total theoretical precision regime for the LHC physics of the Standard model and beyond.

Theoretical Studies of LHC Physics in the Context of Exact Amplitude-Based Resummation Realized by MC Methods

by

Aditi Mukhopadhyay, B.Sc., M.Sc.

A Dissertation

Approved by the Department of Physics

Gregory A. Benesh, Ph.D., Chairperson

Submitted to the Graduate Faculty of
Baylor University in Partial Fulfillment of the
Requirements for the Degree
of
Doctor of Philosophy

Approved by the Dissertation Committee

B.F.L. Ward, Ph.D., Chairperson

Gerald B. Cleaver, Ph.D.

Kenichi Hatakeyama, Ph.D.

Ronald B. Morgan, Ph.D.

Kenneth T. Park, Ph.D.

Accepted by the Graduate School
August 2014

J. Larry Lyon, Ph.D., Dean

Page bearing signatures is kept on file in the Graduate School.

TABLE OF CONTENTS

LIST OF FIGURES

LIST OF TABLES

ACKNOWLEDGMENTS

I would like to acknowledge my advisor, Dr. B.F.L. Ward who helped me and guided me over the course of the last four years. I owe him my sincerest gratitude.

I would also like to thank Dr. Yost and Dr. Majhi for helpful discussions.

I would also like to thank the members of my committee, Dr. Kenichi Hatakeyama, Dr. Gerald Cleaver, Dr. Ken Park and Dr. Ronald Morgan for their time and patience.

DEDICATION

I would like to dedicate it to my parents Pradip Kumar Mukhopadhyay, Anjana Mukherjee, my PhD advisor Dr. B.F.L. Ward and my fiance Punith Dev Nallathamby, without whom none of this would have been possible.

CHAPTER ONE

Introduction

The successful LHC run during $2010-2012$ has produced a large collection of data samples of the Standard Model processes like the heavy gauge boson production and the decay to lepton pairs $l\bar{l}$ along with the announcement [1] of the Brout-Englert-Higgs (BEH) [2] boson candidate. This has produced the necessity of prediction of QCD processes at precision tag of 1% or better now more than ever.

In order to obtain this desired level of accuracy the infrared (IR) improved DGLAP-CS [3, 4] theory [5, 6] realization with HERWIRI1.031 [7] was done by implementing the set of IR improved DGLAP kernels in HERWIG6.5 [8]. It has been argued that this process allows better than 1% theoretical precision [9, 10].

In Ref. [10] the residuals of hard photon and hard gluons are to be simultaneously calculated in the powers of α and α_s in the perturbation. These residuals require the exact evaluations of higher point and higher loop Feynman diagrams. Using the "Chinese Magic" [11, 12, 13, 14] polarization scheme originally developed for real emission of massless gauge particles, it is possible to get a more accurate evaluation of the above.

In this thesis we give a comparison of the exact amplitude-based resummation theory with the LHC data. In addition we show the theoretical implications, as realized via MC event generator, of our results. To set the stage, we begin with a review of the relevant background information, the standard model and the standard quantum field theoretic methods used to investigate it. We then develop the theory we use, and present our results and implications in Chapters 2–6. Chapter 7 sums it up. The Appendices contain relevant technical details.

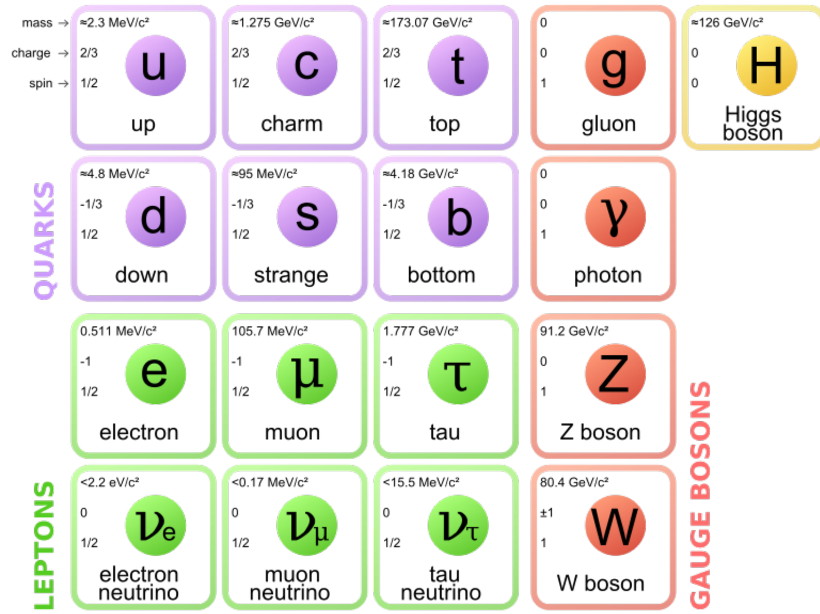

Figure 1.1. Standard Model particles [15].

1.1 Standard Model

The Standard Model is a theory of the strong, weak, and electromagnetic interactions of the fundamental particles. This $SU(3) \times SU(2) \times U(1)$ gauge theory can be considered well established. The structure of this theory is similar to that of the gauge theories coupled to fermions. Fig. (1.1) gives the summary of elementary particles in the Standard Model. It contains the quarks and leptons which are spin $\frac{1}{2}$. The quarks have both charge and color. The electro-weak leptons do not have any color charge. There are three generations each consisting of four particles with different masses but identical quantum numbers. The three generations in order of increasing mass are:

$$\begin{pmatrix} u \\ d \end{pmatrix}_L, u_R, d_R, \begin{pmatrix} \nu_e \\ e \end{pmatrix}_L, e_R, \begin{pmatrix} c \\ s \end{pmatrix}_L, c_R, s_R, \begin{pmatrix} \nu_\mu \\ \mu \end{pmatrix}_L, \mu_R,$$
$$\begin{pmatrix} t \\ b \end{pmatrix}_L, t_R, b_R, \begin{pmatrix} \nu_\tau \\ \tau \end{pmatrix}_L, \tau_R,$$

where L and R are the left and the right handed components defined as:

$$\psi_L = \frac{1-\gamma_5}{2} \tag{1.1}$$

$$\psi_R = \frac{1+\gamma_5}{2} \tag{1.2}$$

where ψ is a lepton or a quark.

In the Standard Model the force carriers are the photon γ, the gauge bosons W^+, W^-, Z, and gluons which are spin 1. The Higgs particle with spin 0 gives masses to fermions and heavy gauge bosons and acts a force carrier. The recent observation [1] of the Higgs like particle at CERN has solidified the proof of the theory.

The photon and the gluons are massless indicating conservation of corresponding symmetry charges. The bosons W^+, W^-, Z are massive indicating the corresponding symmetries to be broken. This breaking is spontaneous to preserve renormalizability.

1.2 Gauge Symmetries

The interactions are dictated by symmetry principles. In order to explain the connection between the symmetries and conservation laws we need to construct the Lagrangian. With each Lagrangian there is associated a corresponding set of Feynman rules.

1.2.1 Noether's Theorem

Consider the Lagrangian

$$\mathscr{L} = i\bar{\psi}\gamma_\mu\partial^\mu\psi - m\bar{\psi} \tag{1.3}$$

where each of the four components of ψ and $\bar{\psi}$ is regarded as an independent field variable. The above Lagrangian (1.3) is invariant under phase transformation

$$\psi(x) \rightarrow e^{i\alpha}\psi(x) \tag{1.4}$$

where α is a real constant. The family of phase transformations, $U(\alpha) \equiv e^{i\alpha}$, forms the unitary Abelian group $U(1)$. Through the Noether's theorem, $U(1)$ invariance implies the presence of a conserved current. Under the infinitesimal transformation,

$$\psi \to (1 + i\alpha)\psi \tag{1.5}$$

the invariance requires the Lagrangian to be stationary.

$$0 = \delta\mathscr{L} \tag{1.6}$$

which reduces to the form of the conserved current equation:

$$\partial_\mu j^\mu = 0, \tag{1.7}$$

where

$$j^\mu = \frac{ie}{2}\left(\frac{\partial\mathscr{L}}{\partial(\partial_\mu\psi)}\psi - \bar{\psi}\frac{\partial\mathscr{L}}{\partial(\partial_\mu\bar{\psi})}\right) = -e\bar{\psi}\gamma^\mu\psi. \tag{1.8}$$

From (1.7) it follows that the charge

$$Q = \int d^3x j^0 \tag{1.9}$$

is also a conserved quantity because of the $U(1)$ invariance.

1.2.2 $U(1)$ Local Gauge Invariance

Generalizing (1.5) into the transformation

$$\psi(x) \to e^{i\alpha(x)}\psi(x) \tag{1.10}$$

where $\alpha(x)$ is both space and time dependent. This is the local gauge invariance. However the Lagrangian (1.3) is not invariant under the transformation (1.10). The second term in the Lagrangian is invariant. However, since the derivative of ψ does not obey (1.10), the invariance of $\mathscr{L}$ is broken.

In order to insist on imposing the invariance of the Lagrangian, the covariant derivative is defined, which transforms like ψ itself under the transformation (1.10)

$$D_\mu\psi \to e^{i\alpha(x)}D_\mu\psi. \tag{1.11}$$

Defining the covariant derivative as

$$D_\mu \equiv \partial_\mu - ieA_\mu, \tag{1.12}$$

the extra term produced due to the transformation of the derivative is canceled due to the transformation properties of the vector field A_μ. A_μ transforms as

$$A_\mu \to A_\mu + \frac{1}{e}\partial_\mu \alpha. \tag{1.13}$$

Therefore, the total Lagrangian is

$$\mathscr{L} = i\bar{\psi}\gamma^\mu D_\mu \psi - m\bar{\psi}\psi = \bar{\psi}(i\gamma^\mu \partial_\mu - m)\psi + e\bar{\psi}\gamma^\mu \psi A_\mu. \tag{1.14}$$

If the new vector field is considered to be the photon field, the Lagrangian should contain a kinetic term for the photon field which can only have field strength tensor,

$$F_{\mu\nu} = \partial_\mu A_\nu - \partial_\nu A_\mu \tag{1.15}$$

which leads to the final Lagrangian of quantum electrodynamics (QED)

$$\mathscr{L} = \bar{\psi}(i\gamma^\mu \partial_\mu - m)\psi + e\bar{\psi}\gamma^\mu \psi A_\mu - \frac{1}{4}F_{\mu\nu}F^{\mu\nu} \tag{1.16}$$

which describes the quantum electrodynamics.

QED is the theory that describes the electromagnetic interactions of the quarks and the leptons. QED is the simplest example of a local gauge theory as it has only one gauge particle namely the photon.

1.2.3 The Non-Abelian Gauge Invariance

The free Lagrangian is denoted by

$$\mathscr{L}_0 = \bar{q}_j(i\gamma^\mu \partial_\mu - m)q_j \tag{1.17}$$

where the q_i's are the three color fields. It is desired that $\mathscr{L}_0$ is invariant under the transformation

$$q(x) \to Uq(x) \equiv e^{i\alpha_a(x)T_a}q(x) \tag{1.18}$$

where T_a with $a = 1, ..., 8$ are the set of independent traceless matrices that generate color transformations. In order for the Lagrangian (1.17) to be stationary under the infinitesimal transformation of (1.18) we replace the derivative in the Lagrangian with the covariant derivative

$$D_\mu = \partial_\mu + igT_a G_\mu^a \tag{1.19}$$

where G_μ^a transforms as

$$G_\mu^a \to G_\mu^a - \frac{1}{g}\partial_\mu \alpha_a - f_{abc}\alpha_b G_c^{\mu\nu}. \tag{1.20}$$

Therefore the complete QCD Lagrangian is given by

$$\mathscr{L} = \bar{q}(i\gamma^\mu \partial_\mu - m)q - g(\bar{q}\gamma^\mu T_a q)G_\mu^a - \frac{1}{4}G_{\mu\nu}^a G_a^{\mu\nu} \tag{1.21}$$

where G_μ represents the vector gluons, q the quarks and the g specified coupling - which describes quantum chromodynamics.

Although it is well known that electromagnetic interactions bind the positronium, it is also evident that it cannot bind the quarks to hadrons. A strong force overrules the effects of the electromagnetic repulsion in order to bind the quarks in a hadron. Thus the color charge is introduced which makes the strong binding possible. Gluons are the quanta of the color field that binds the quarks in nucleons. To repeat, the theory explained is called quantum chromodynamics (QCD). As seen above it is a color gauge theory. Quarks carry color as well as electric charge. There are three colors - Red, Green, and Blue. Color interactions can be assumed to be a copy of the electromagnetic interactions with the replacement of $\sqrt{4\pi\alpha} \to \sqrt{4\pi\alpha_S}$ in each vertex and the introduction of color factors. The exchange of colors occur through eight gluons. Gluons interact with each other unlike photons in QED. At short distances color interactions can be computed using perturbative techniques similar to QED as α_S is sufficiently small there.

1.2.4 Spontaneous Symmetry Breaking

For the Lagrangian, consider

$$\mathscr{L} = \frac{1}{2}\partial_\mu\phi\partial^\mu\phi - V(\phi) \tag{1.22}$$

where the potential is given by

$$V(\phi) = \frac{1}{2}m^2\phi^2 + \frac{\lambda}{4}\phi^4. \tag{1.23}$$

In case of Fig. (1.2 a) where $m^2 > 0$, $\mathscr{L}$ is invariant under the symmetry operation which replaces ϕ by $-\phi$. The conditions of extrema

$$\frac{\partial V}{\partial \phi} = m^2\phi + \lambda\phi^3 = 0 \tag{1.24}$$

and

$$\frac{\partial^2 V}{\partial \phi^2} = m^2 > 0 \tag{1.25}$$

show that $\phi = 0$ is a minima. It simply describes a scalar field with mass m. ϕ is a self interacting field and the ground state (vacuum) corresponds to $\phi = 0$. It obeys the reflection symmetry of the Lagrangian. In the case of Fig (1.2 b) $m^2 < 0$. Now the Lagrangian has the mass term of the wrong sign for the field ϕ, since the relative sign of ϕ^2 and the kinetic energy term is positive. Let $m^2 = -\mu^2$ where $\mu^2 > 0$. Now for the extrema

$$\frac{\partial V}{\partial \phi} = -\mu^2\phi + \lambda\phi^3, \tag{1.26}$$

which gives $\phi = 0$ or $\phi = \pm\sqrt{\frac{\mu^2}{\lambda}}$ and $\frac{\partial^2 V}{\partial \phi^2} = -\mu^2 + 3\lambda\phi^2 < 0$ at $\phi = 0$ and $\frac{\partial^2 V}{\partial \phi^2} = -\mu^2 + 3\lambda\frac{\mu^2}{\lambda} = 2\mu^2 > 0$ at $\phi = \pm\sqrt{\frac{\mu^2}{\lambda}}$. In this case, therefore, there are two minima at $\phi = \pm v$ where $v = \sqrt{\frac{\mu^2}{\lambda}}$. Here also the $\mathscr{L}$ is symmetric under $\phi \to -\phi$ but the ground state does not possess the symmetry of the Lagrangian- this is called Spontaneous Symmetry breaking. Define the vacuum expectation value as $< 0|\phi|0 >$. Now writing $\phi \to \phi + v$ we get

$$< 0|\phi|0 > \to < 0|\phi|0 > + < 0|v|0 >= v. \tag{1.27}$$

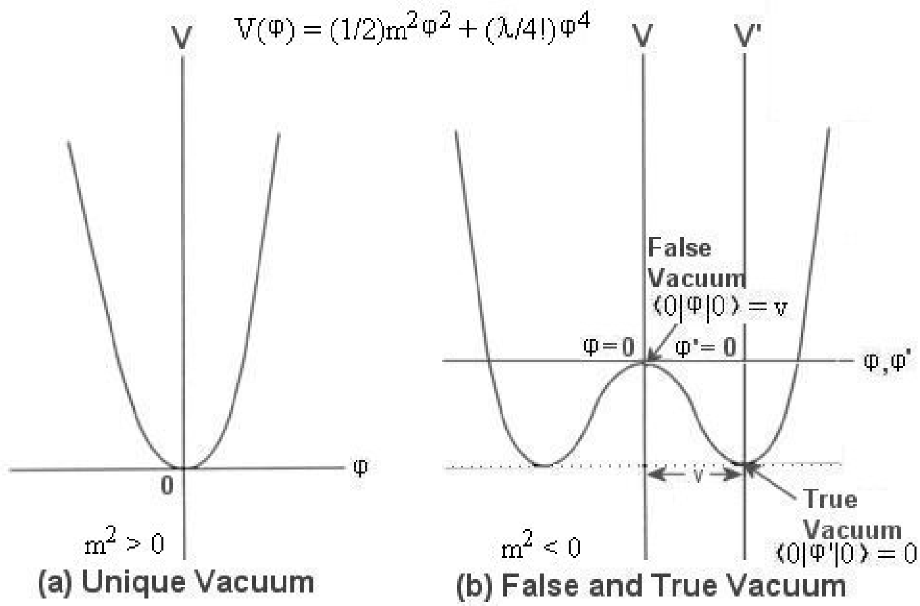

Figure 1.2: The potential $V(\phi) = \frac{1}{2}m^2\phi^2 + \frac{\lambda}{4}\phi^4$ (a) $m^2 > 0$ the Unique Vacuum (b) $m^2 < 0$ False and True Vacuum [15].

The above is in the case of the discrete symmetry $\phi \rightarrow -\phi$. A similar approach is used for continuous symmetry with the spontaneous breaking of the global symmetry. Defining a complex scalar field ϕ such that $\phi^+ = \phi_1 + i\phi_2$ and $\phi^- = \phi_1 - i\phi_2$, the potential is defined as

$$V(\phi_1, \phi_2) = -\frac{1}{2}\mu^2(\phi_1^2 + \phi_2^2) + \frac{\lambda}{4}(\phi_1^2 + \phi_2^2)^2, \tag{1.28}$$

where $\mu^2, \lambda > 0$ and $\phi^+\phi^- = \phi_1^2 + \phi_2^2$. Therefore the total potential is

$$V(\phi) = -\frac{1}{2}\mu^2\phi^+\phi^- + \frac{\lambda}{4}(\phi^+\phi^-)^2. \tag{1.29}$$

Since the potential is invariant under phase transformation, let $\phi^+ \rightarrow e^{i\alpha}\phi^+$ and $\phi^- \rightarrow e^{-i\alpha}\phi^-$. Let $\frac{\partial V}{\partial \phi_i} = 0$ which implies $\phi_i = 0$ or $\phi_1^2 + \phi_2^2 = \frac{\mu^2}{\lambda} = v^2$. Therefore there is now a circle of minima of potential $V(\phi)$ in the ϕ_1, ϕ_2 plane of radius v. Therefore there are an infinite number of stable equilibrium points such that $< \phi_1 >^2 + < \phi_2 >^2 = v^2$ (Fig. (1.3)).

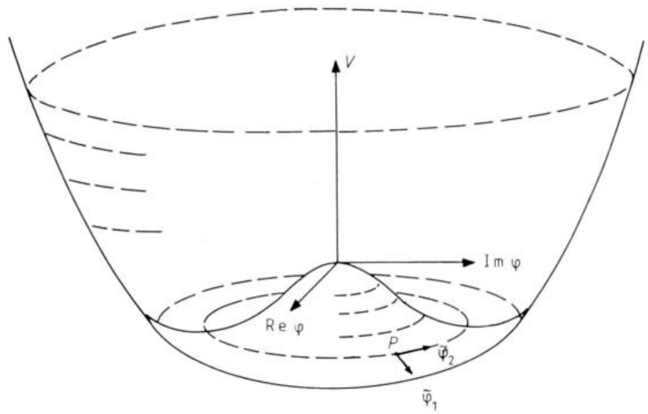

Figure 1.3. The Mexican hat potential [15].

1.2.4.1. *Goldstone Theorem:* Spontaneous breaking of a continuous symmetry is associated with one or more massless excitations also called the Goldstone Bosons.

1.2.5 Higgs Mechanism

Let us consider the simplest case that is the $U(1)$ gauge symmetry. The Lagrangian has to be invariant under the transformation $\phi \rightarrow e^{i\alpha(x)}\phi$, therefore the derivative is replaced by $D_\mu = \partial_\mu + ieA_\mu$. Now constructing the combination $\phi^+ = \phi_1 + i\phi_2$ and $\phi^- = \phi_1 - i\phi_2$ as earlier, the Lagrangian is

$$\mathscr{L} = (D^*_\mu \phi^+)(D^\mu \phi^-) + \frac{\mu^2}{2}\phi^+\phi^- - \frac{\lambda}{4}(\phi^+\phi^-)^2 - \frac{1}{4}F_{\mu\nu}F^{\mu\nu}. \tag{1.30}$$

Minimizing the potential we get $\mu^2 = \lambda v^2$, $<\phi_1>= v$ and $<\phi_2>= 0$ where $v = constant$. On simplifying the kinetic term, the mass term of the gauge field is obtained. After symmetry breaking there is an extra degree of freedom. The Goldstone boson actually does not appear in the theory. This apparent extra degree of freedom is actually spurious because it corresponds only to the freedom to make a gauge transformation. The unwanted massless Goldstone boson has been turned into the badly needed longitudinal polarization of the massive gauge particle, i.e. the Goldstone boson is eaten by the gauge boson which is called the Higgs Mechanism.

1.2.6 Masses of the Gauge Bosons

We want to formulate the Higgs Mechanism so that $W^{\pm}$ and Z^0 become massive and the photon remains massless. To do this four real scalar fields ϕ_i are introduced. So, $SU(2)$ is taken which gives the weak interaction, and abelian $U(1)$ is put in by hand to allow for the electromagnetic interaction. Thus a $SU(2) \times U(1)$ gauge invariant term for the scalar fields is added to the Lagrangian. To keep the term gauge invariant, ϕ_i must belong to an $SU(2) \times U(1)$ multiplet. Introducing a new quantum number, the weak hypercharge, Y, the covariant derivative is defined as

$$D_\mu = \partial_\mu + i\frac{g}{2}\vec{T} \cdot \vec{W}_\mu + i\frac{g'}{2} Y B_\mu. \tag{1.31}$$

The most economical choice of ϕ_i is to arrange the four fields in an isospin doublet of weak hypercharge $Y = 1$.

$$\phi = \begin{pmatrix} \phi^+ \\ \phi^0 \end{pmatrix}, \tag{1.32}$$

with $\phi^+ \equiv (\phi_1 + i\phi_2)/\sqrt{2}$ and $\phi^0 \equiv (\phi_3 + i\phi_4)/\sqrt{2}$ which is the original choice made by Weinberg [4]. The most appropriate choice for $< \phi^0 >$ is

$$< \phi >= \frac{1}{\sqrt{2}} \begin{pmatrix} 0 \\ v \end{pmatrix}. \tag{1.33}$$

In order to determine the masses of the gauge Bosons we calculate $(D^\mu \phi)^\dagger (D_\mu \phi)$. This gives the masses of the $W^{\pm}$ bosons as $\frac{gv}{2}$, the Z boson as $\frac{v}{2}\sqrt{g^2 + g\prime^2}$ and the photon as 0 where

$$\frac{m_W}{m_Z} = \cos(\theta)$$

$$\cos(\theta) = \frac{g}{\sqrt{g^2 + g\prime^2}}. \tag{1.34}$$

The angle θ called the Weinberg angle is the weak mixing angle given by [4]

$$\sin^2(\theta) = 0.23 \tag{1.35}$$

For $SU(2) \times U(1)$ couplings, the two relevant quantum numbers are T_3 and Y. Now, ϕ^0 is neutral, therefore, $Q = 0$. Here, $T_3 = -\frac{1}{2}$ and $Y = 1$. Therefore

$$Q = T_3 + \frac{Y}{2}. \tag{1.36}$$

1.2.7 Masses of the Fermions

Under weak interaction the left handed neutrino and electron form a doublet, i.e., $\begin{pmatrix} \nu_e \\ e \end{pmatrix}_L$ with $Y_{e_L} = -1$, and the right chiral electron under $SU(2)$ forms a singlet where $Y_{e_R} = -2$.

The Lagrangian in this case is given by

$$\mathscr{L} = -G_e \left[(\bar{\nu_e}, \bar{e})_L \begin{pmatrix} \phi^+ \\ \phi^0 \end{pmatrix} e_R + \bar{e}_R(\phi^-, \bar{\phi^0}) \begin{pmatrix} \nu_e \\ e \end{pmatrix}_L \right] \tag{1.37}$$

The symmetry is spontaneously broken by using $\frac{1}{\sqrt{2}} \begin{pmatrix} 0 \\ v + h(x) \end{pmatrix}$ where the neutral $h(x)$ is the only remaining part of the Higgs doublet. Substituting and choosing G_e such that $m_e = \frac{G_e v}{\sqrt{2}}$ generate the required electron mass. Similarly a Lagrangian can be written for the quarks to generate their mass.[1] A deficiency to the theory is that the mass of the neutral Higgs m_h is not predicted by the theory. From the definition of the potential it is found that, $m_h^2 = v^2\lambda/2$.

1.3 Calculations in Quantum Field Theory

In the accelerated beam experiments to probe the behaviors of the elementary particles, two particles are collided, whose momenta are known and the end product is observed. The final state is expressed in terms of the cross section. The cross section is an inherent property of the colliding particles. In order to define the cross

[1] The explanation of the Standard Model is based on "Quarks an Leptons" by Halzen and Martin

section, we consider a target at rest of particle type $\mathcal{A}$, with density $\rho_{\mathcal{A}}$. The target is bombarded with particles type $\mathcal{B}$ with density $\rho_{\mathcal{B}}$ and velocity v. If the lengths of the bunches of the particles be defined as $l_{\mathcal{A}}$ and $l_{\mathcal{B}}$, then the cross section is defined as

$$\sigma \equiv \frac{\text{Number of scattering events}}{\rho_{\mathcal{A}} l_{\mathcal{A}} \rho_{\mathcal{B}} l_{\mathcal{B}} A}, \tag{1.38}$$

where A is the effective area of the beams. The symmetry in $\mathcal{A}$ and $\mathcal{B}$ means that either the target could be rest or it could also be done in any other reference frame.[2] The above quantity has the units of area. Now assuming that the range of interactions between the particles and the width of the individual particles are small in comparison to the beam diameter $\rho_{\mathcal{A}}$ and $\rho_{\mathcal{B}}$ can be considered constant, therefore we get

$$\text{Number of events} \;=\; \sigma l_{\mathcal{A}} l_{\mathcal{B}} \int d^2x \rho_{\mathcal{A}}(x) \rho_{\mathcal{B}}(x). \tag{1.39}$$

Now if the densities are constant, for an effective area A of the beams, we can write

$$\text{Number of events} = \frac{\sigma N_{\mathcal{A}} N_{\mathcal{B}}}{A}, \tag{1.40}$$

where $N_{\mathcal{A}}$ and $N_{\mathcal{B}}$ are the total number of the particles $\mathcal{A}$ and $\mathcal{B}$ respectively. Now, we define the differential cross section $\frac{d\sigma}{d^3p_1 \ldots d^3p_n}$ as the quantity which, when integrated over small $d^3p_1 \ldots d^3p_n$, gives the cross section for scattering. The formula for the differential cross section is given by

$$d\sigma = \frac{|\mathcal{M}|^2}{F} dQ, \tag{1.41}$$

where

$$dQ = \prod_{f=1}^{n} \frac{d^3p_f}{(2\pi)^3} \frac{1}{2E_f} (2\pi)^4 \delta^4(p - \sum p_f)$$

[2] This section follows the treatment of "An Introduction to Quantum Field Theory" by Michael E. Peskin and Daniel V. Schroeder.

is the n-body phase space factor and F is the incident flux. Standard Feynman diagrammatic methods are used to obtain the invariant Feynman amplitude $\mathcal{M}$ in (1.41).

Similarly we define the decay rate of an unstable particle $\mathcal{A}$ assumed to be at rest, decaying to two or more particles as

$$\Gamma = \frac{\text{Number of decays per unit time}}{\text{Number of } \mathcal{A} \text{ particles present}}. \tag{1.42}$$

In the non-relativistic quantum mechanics, near resonance energy E_0, using the Breit-Wigner formula the scattering amplitude is given by

$$f(E) \propto \frac{1}{E - E_0 + i\frac{\Gamma}{2}}. \tag{1.43}$$

The cross section therefore satisfies

$$\sigma \propto \frac{1}{(E - E_0)^2 + \frac{\Gamma^2}{4}}. \tag{1.44}$$

We see that the width of the resonance peak gives the value of the decay rate of the unstable state mentioned earlier.

1.4 Experimental Tests at the Large Hadron Collider (LHC)

The LHC run from 2010–2012 produced a large amount of data for standard model processes leading to the discovery of the Brout-Englert-Higgs (BEH) boson candidate. The searches of the Standard Model Higgs boson were performed at $\sqrt{s} = 7$ and 8 TeV. The searches were performed in the five decay modes $\gamma\gamma$, ZZ, W^+W^-, $\tau^+\tau^-$, and $b\bar{b}$. The results are presented in the following Figs. (1.4) - (1.10) [1]. An excess of events was observed above the expected background, with a local significance of $> 5\sigma$, the mass of which was near 125 GeV, indicating the presence of a new particle.The mass m_X of the observed boson is determined by observing the $\gamma\gamma$ and ZZ decay modes, with the former dominating the precision of the measurement.Now the decay of the new particle to two photons indicates that the new particle is a boson with spin $\neq 1$. These results are consistent, within uncertainties, with the SM Higgs boson.

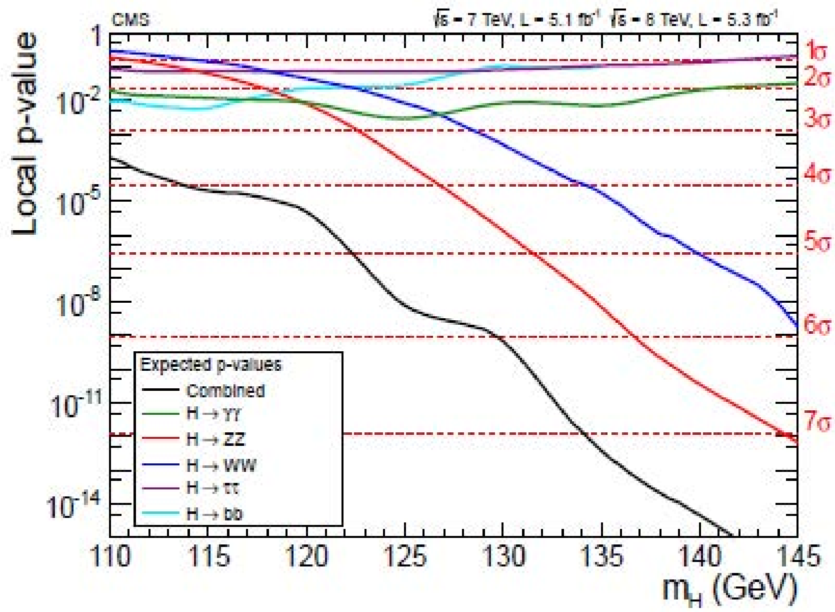

Figure 1.4: Expected local p-values for a SM Higgs boson as a function of m_H for the decay modes $\gamma\gamma$, ZZ, WW, $\tau\tau$, bb, and their combination [1]

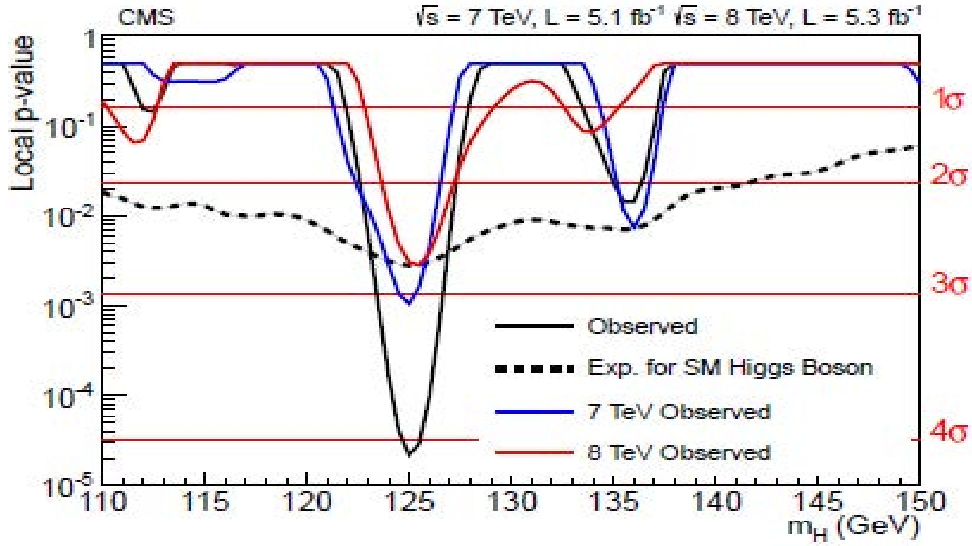

Figure 1.5: The local p-value as a function of 8 TeV data sets. The additional lines show the values for two data sets taken individually. The dashed line shows the expected local p-value for the combined data sets, should a SM Higgs boson exist with mass m_H [1]

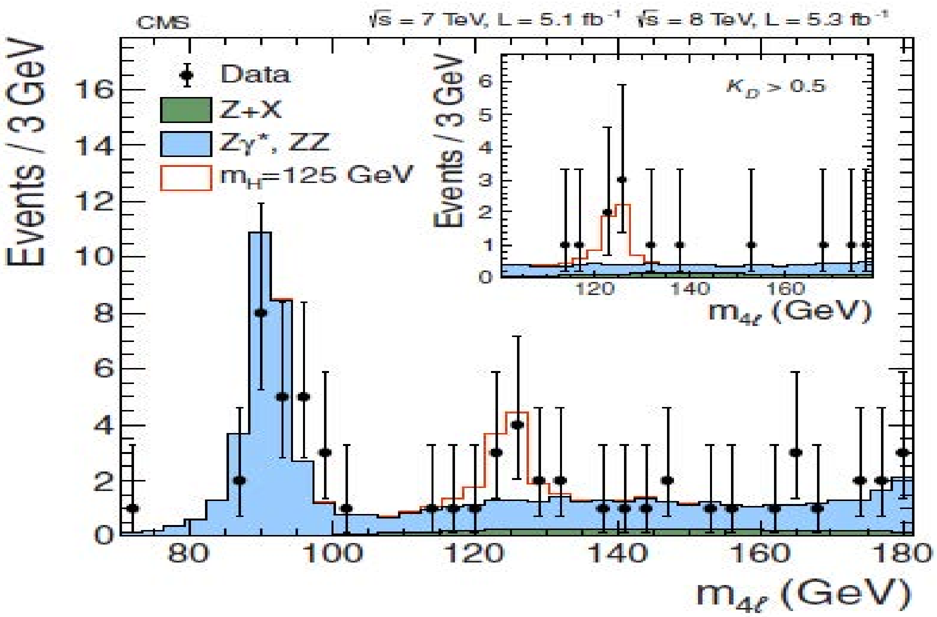

Figure 1.6: Distribution of the four-lepton invariant mass for the $ZZ \rightarrow 4l$ analysis. The points represent the data, the filled histograms represent the background, and the open histogram shows the signal expectation for the Higgs boson of mass $m_H = 125$ GeV, added to the background expectation. The inset shows the m_{4l} distribution after selection of events with $K_D > 0.5$. [1]

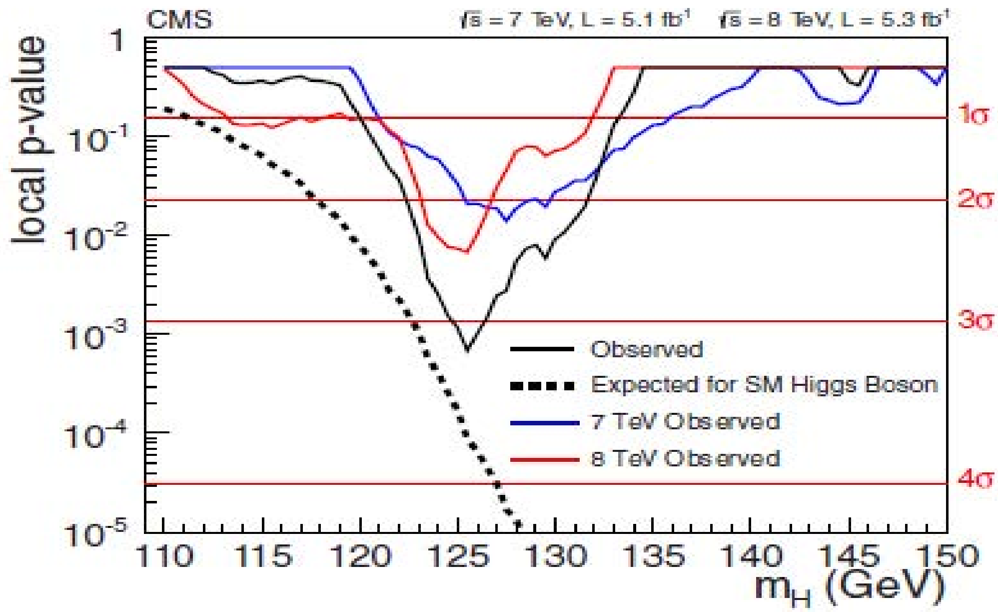

Figure 1.7: The observed local $p-$value for the ZZ decay mode as a function of the SM Higgs boson mass. The dashed line shows the expected local $p-$values for a SM Higgs boson with a mass m_H. [1]

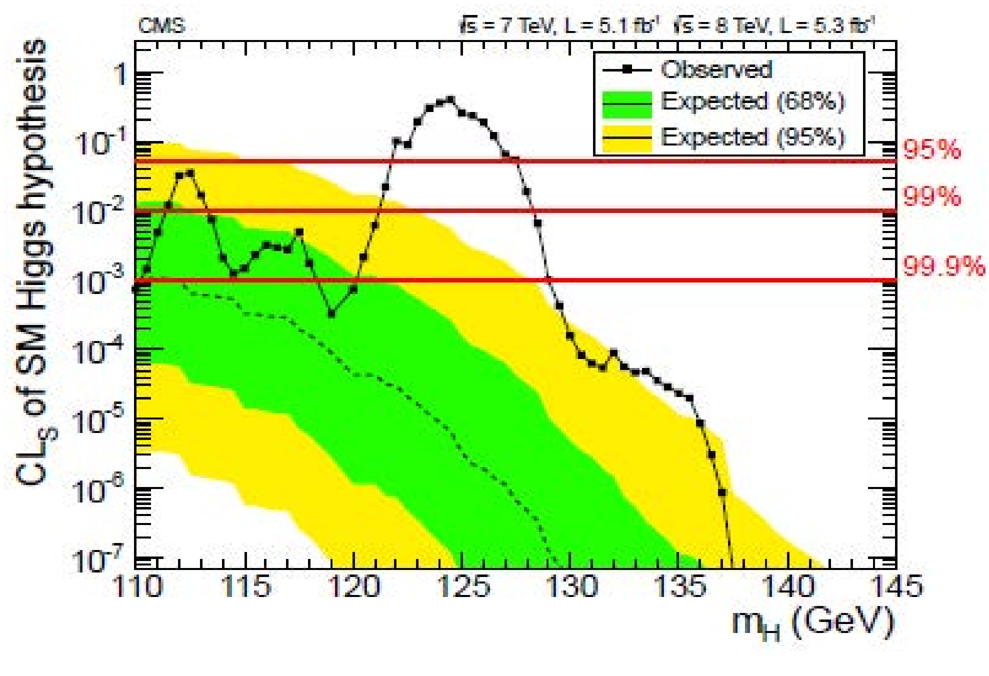

Figure 1.8: The CL_s values for the SM Higgs boson hypothesis as a function of Higgs boson mass in the range $110 - 145$ GeV. The background-only expectations are represented by their median (dashed line) and by the 68% and 95% CL bands. [1]

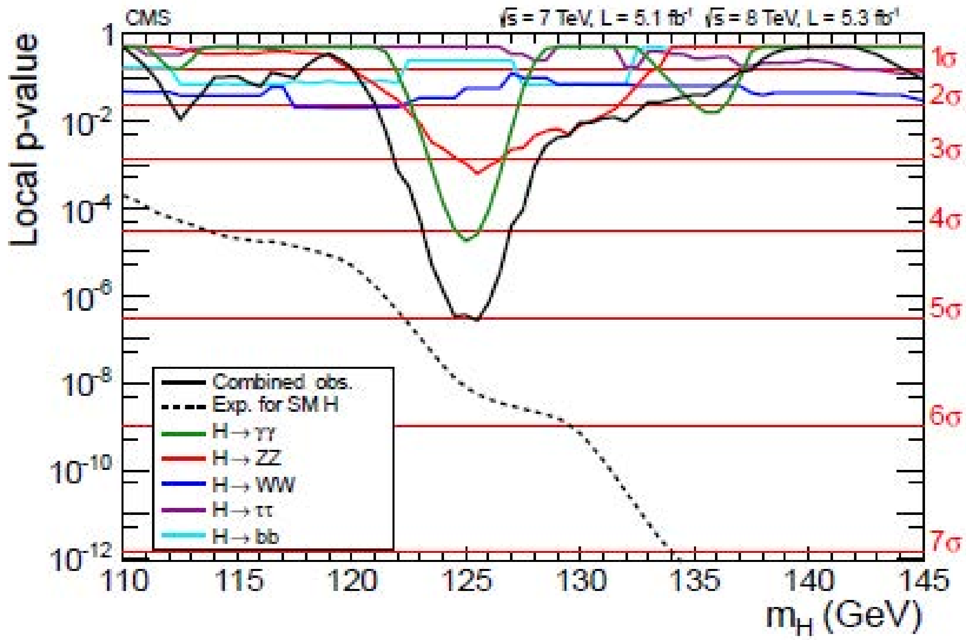

Figure 1.9: The observed local p-value for the five decay modes and the overall combination as a SM Higgs boson mass. The dashed line show the expected local p-values for a SM Higgs boson with mass m_H. [1]

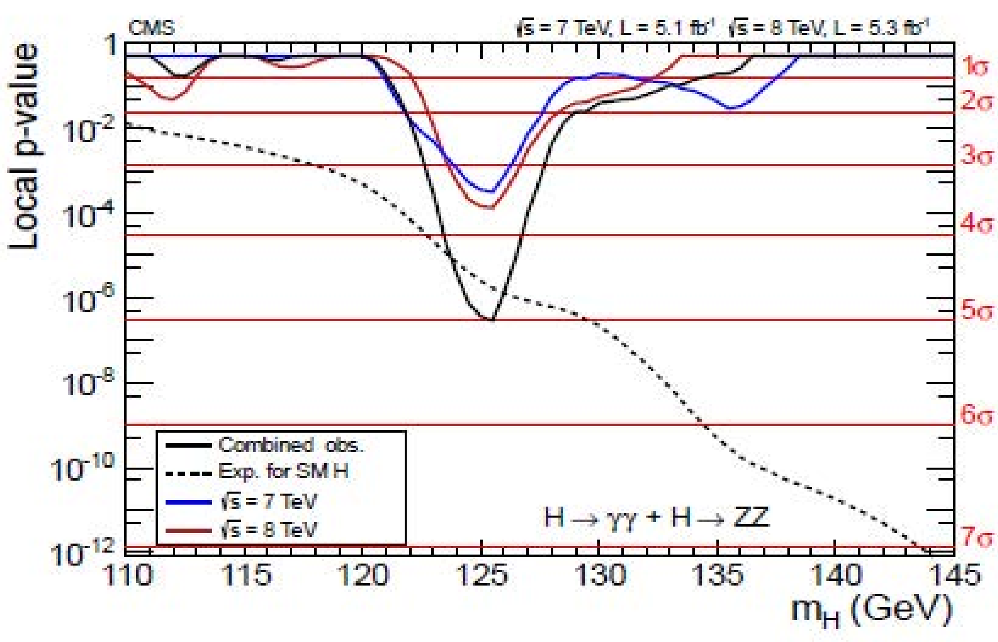

Figure 1.10: The observed local p-value for decay modes with high mass-resolution channels,$\gamma\gamma$ and ZZ, as a function of SM Higgs boson mass. The dashed line shows the expected local p-values for a SM Higgs boson with mass m_H. [1]

CHAPTER TWO

Exact Amplitude-Based Resummation Theory

2.1 Resummation

Resummation "is the art of constructing, from a subset of terms in a finite order perturbation series, an all-orders expression whose expansion gives at least those terms back" Eric Laenen, Theory Meeting, Nikhef, Sept 14, 2007. For a perturbation series, one describes the observables as $O = \sum_n (c_n \alpha_S^n + R_n)$ where c_n are computed using Feynman diagrams and R_n is the remainder at order n. In order for this approach to work the following conditions have to be satisfied: O is infrared safe, R_n has to be very small, α_S small enough and c_n should be well behaved at large n.

Resummation is based on the organization of large logarithms in perturbative expansions and can be explained as

$$\begin{aligned}\hat{O} &= 1 + \alpha_S(L^2 + L + 1) + \alpha_S^2(L^4 + L^3 + L^2 + L + 1) + \ldots \\ &= \exp\left(Lg_1(\alpha_S L) + g_2(\alpha_S L) + \alpha_S g_3(\alpha_S L) + \ldots\right) C(\alpha_S)\end{aligned} \tag{2.1}$$

where α_S is the coupling in the theory and L is a logarithm. This process not only restores the predictive power, it also gives a better description of the physics and increases the theoretical accuracy. The issue is that the residuals in any practical application are the limits on precision.

2.2 QED $\otimes$ QCD *Exponentiation*

2.2.1 QED Exponentiation

We therefore focus on the YFS theory [17] as a general rearrangement of the renormalized perturbation theory based on its IR behavior. We review the YFS exponentiation to the prototypical process example of the Abelian gauge theory,

$e^+e^- \rightarrow \bar{f}f + n(\gamma)$, in this section. The process $e^+(p_1)e^-(q_1) \rightarrow \bar{f}(p_2)f(q_2) + n(\gamma)(k_1, \ldots, k_n)$ is represented by

$$d\sigma_{exp} = e^{2\alpha ReB+2\alpha\tilde{B}} \sum_{n=0}^{\infty} \frac{1}{n!} \int \prod_{j=1}^{n} \frac{d^3k_j}{k_j^0} \int \frac{d^4y}{(2\pi)^4} e^{iy(p_1+q_1-p_2-q_2-\sum_j k_j)+D}$$
$$\bar{\beta}_n(k_1, \ldots, k_n) \frac{d^3p_2 d^3q_2}{p_2^0 q_2^0} \tag{2.2}$$

where $\tilde{B}$ is the real infrared function, B is the virtual infrared function, $\bar{\beta}_n$ are the hard photon residuals and where

$$2\alpha\tilde{B} = \int^{k \leq K_{max}} \frac{d^3k}{k_0} \tilde{S}(k)$$
$$D = \int d^3k \frac{\tilde{S}(k)}{k_0} (e^{-iy.k} - \theta(K_{max} - k)). \tag{2.3}$$

The standard YFS infrared emission factor is

$$\tilde{S} = \frac{\alpha}{4\pi} \left[Q_f Q_{(\bar{f})'} (\frac{p_1}{p_1 k} - \frac{q_1}{q_1 .k})^2 + (\ldots) \right] \tag{2.4}$$

if Q_f is the electric charge of f in units of the charge of the positron. This result (2.2) has been used in Ref. [10] to achieve precision predictions for the LEP physics such as .054% precision on the luminosity process of low angle Bhabha scattering.

2.2.2 QCD Exponentiation

Here we present the QCD exponentiation theory [6, 18, 19]. We use the process in Fig. (2.1) as a prototypical process. This process contains all the theoretical issues to form an extension of the original Yennie, Frautschi and Suura (YFS) [17] theory, QCD soft exponentiation using the MC methods [6]. Using the GPS convention of Ref. [20] for spinors $\{u, v, \mathfrak{u}\}$, the photon and gluon polarization vectors are given by

$$(\epsilon^\mu_\sigma(\beta))^* = \frac{\bar{u}_\sigma(k)\gamma^\mu u_\sigma(\beta)}{\sqrt{2}\bar{u}_{-\sigma}(k)u_\sigma}, \ \ (\epsilon^\mu_\sigma(\zeta))^* = \frac{\bar{u}_\sigma(k)\gamma^\mu \mathfrak{u}_\sigma(\zeta)}{\sqrt{2}\bar{u}_{-\sigma}(k)\sigma(\zeta)} \tag{2.5}$$

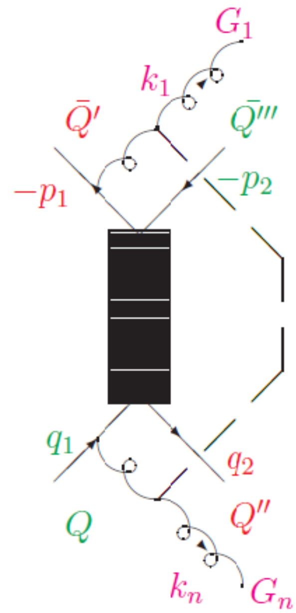

Figure 2.1: The process $\bar{Q}'Q \to \bar{Q}''' + Q'' + n(G)$. The four momenta are indicated in the standard manner: q_1 is the four momentum of the incoming Q, q_2 is the four momentum of the outgoing Q'', etc., and $Q = u, d, s, c, b, G$.

with $\beta^2 = 0$, $\zeta_\uparrow = (1,0,0,1)$ and $\zeta_\downarrow = (1,0,0,-1)$. Now the amplitude of the process $\bar{Q}'^{\bar{\alpha}} + Q^\alpha \to \bar{Q}'''^{\bar{\gamma}} Q''^{\gamma} + n(G)$ is given by

$$\mathcal{M}_{\gamma\bar{\gamma}^{(n)}\alpha\bar{\alpha}} = \sum_l M_{\gamma\bar{\gamma}l}^{(n)\alpha\bar{\alpha}}, \tag{2.6}$$

where, $\alpha, \bar{\alpha}, \gamma, \bar{\gamma}$ are the color indices and $M_l^{(n)}$ is the contribution to $\mathcal{M}^{(n)}$ from the Feynman diagrams with l virtual loops. On symmetrization, we get

$$M_l^{(n)} = \frac{1}{l!} \int \prod_{j=1}^{l} \frac{d^4 k_j}{(2\pi)^4 (k_j^2 - \lambda^2 + i\epsilon)} \rho_l^{(n)}(k_1, \ldots, k_l), \tag{2.7}$$

from which we get that $\rho_l^{(n)}$ is symmetric in its arguments $k_1, \ldots, k_l$. λ is the infrared gluon regulator mass for IR singularities.

We define the virtual IR emission factor S_{QCD} for a gluon of 4−momentum k for the $k \to 0$ regime of the loop integral, (2.7), as

$$\lim_{k\to 0} k^2 (\rho_{\gamma\bar{\gamma}1}^{(n)\alpha\bar{\alpha}}(k)|_{\text{leading Casimir contribution}} - S_{\mathrm{QCD}}(k) \rho_{\gamma\bar{\gamma}0}^{(n)\alpha\bar{\alpha}}) = 0. \tag{2.8}$$

Here the restriction to the leading color Casimir terms at one loop is introduced.

The virtual gluons are all on equal footing in $\rho_l^{(n)}$, therefore we can define the residual amplitude $\beta_l^1(k_1,\ldots,k_{l-1};k_l)$ through the equation,

$$\rho_l^{(n)} = S_{\mathrm{QCD}}(k_l) * \rho_{l-1}^{(n)}(k_1,\ldots,k_{l-1}) + \beta_l^1(k_1,\ldots,k_{l-1};k_l). \tag{2.9}$$

Two properties of the residual amplitude worth mentioning are:

- It is symmetric in its first $l-1$ arguments.
- The IR singularities in S_{QCD} for the gloun l are no longer contained in the residual amplitude.

Continuing iteratively, reapplying (2.9), we finally get the contribution to $\rho_l^{(n)}$ as

$$\rho_l^{(n)} = S_{\mathrm{QCD}}(k_1)\ldots S_{\mathrm{QCD}}(k_l) + \sum_{i=1}^{l}\prod_{j\neq i} S_{\mathrm{QCD}}(k_j)\beta_1^1(k_i) + \ldots + \beta_l^l(k_1,\ldots,k_l), \tag{2.10}$$

where the virtual gluon residuals $\beta_i^i(k_1',\ldots,k_i')$ have the following properties:

- they are symmetric functions of their arguments
- they do not contain any of the IR singularities which the product $S_{\mathrm{QCD}}(k_1')\ldots S_{\mathrm{QCD}}(k_i')$ contains.

We denote β_i^i as β_i henceforward. (2.10) is an exact rearrangement of the contributions of the Feynman diagrams which in turn contribute to $\rho_l^{(n)}$. Yennie, Frautschi and Suura (YFS) [17] have already shown that Feynman diagrammatic perturbation is still non-rigorous from the constructive quantum field theoretic perspective if the above approach is used.

Using (2.10) in (2.6) we get the "YFS representation"

$$\mathcal{M}^n = e^{\alpha_S B_{\mathrm{QCD}}} \sum_{j=0}^{\infty} m_j^{(n)}, \tag{2.11}$$

where it is defined that

$$\alpha_S(Q) B_{\mathrm{QCD}} = \int \frac{d^4 k_i}{(2\pi)^4 (k^2 - \lambda^2 + i\epsilon)} S_{\mathrm{QCD}} \tag{2.12}$$

and

$$m_j^{(n)} = \frac{1}{j!}\int \prod_{i=1}^{j} \frac{d^4k_i}{(2\pi)^4(k_i^2-\lambda^2+i\epsilon)}\beta_j(k_1,\ldots,k_j). \tag{2.13}$$

Here we have not proved $\beta_i(k_1,\ldots,k_i)$ is completely free of IR singularities yet. In a non-Abelian gauge theory, IR divergences other than the one arising out of the divergences from the product $S_{\rm QCD}(k_1)\ldots S_{\rm QCD}(k_i)$ are also possible. However, (2.11) does have an improved IR divergence structure. We write the differential cross section associated with the $\mathcal{M}^{(n)}$

$$\begin{aligned} d\hat{\sigma}^n = {}& \frac{e^{2\alpha_S ReB_{\rm QCD}}}{n!}\int \prod_{m=1}^{n} \frac{d^3k_m}{(k_m^2+\lambda^2)^{\frac{1}{2}}}\delta(p_1+q_1-p_2-q_2-\sum_{i=1}^{n}k_i) \\ & *\,\bar{\rho}^{(n)}(p_1,q_1,p_2,q_2,k_1,\ldots,k_n)\frac{d^3p_2d^3q_2}{p_2^0q_2^0}, \end{aligned} \tag{2.14}$$

where

$$\bar{\rho}^{(n)}(p_1,q_1,p_2,q_2,k_1,\ldots,k_n) = \sum_{\text{color,spin}} \|\sum_{j=0}^{\infty} m_j^{(n)}\|^2 \tag{2.15}$$

in the $Q\bar{Q}$ cms system.

For the functions, $\rho^{(n)}(p_1,q_1,p_2,q_2,k_1,\ldots,k_n) \equiv \bar{\rho}^{(n)}(k_1,\ldots,k_n)$, which are symmetric functions of their arguments $k_1,\ldots,k_n$, at first for $n=1$ we define

$$\lim_{|\vec{k}\to 0|} \vec{k}^2(\bar{\rho}^1(k)\mid_{\text{leading Casimir contribution}} - \tilde{S}_{\rm QCD}(k)\bar{\rho}^0) = 0. \tag{2.16}$$

We repeat all the steps we did for $S_{\rm QCD}$

$$\begin{aligned} d\hat{\sigma}_{exp} &= \sum_n d\hat{\sigma}^n_{exp} \\ &= e^{SUM_{IR}(\rm QCD)}\sum_{n=0}^{\infty}\int\prod_{j=1}^{n}\frac{d^3k_j}{k_j^0}\int\frac{d^4y}{(2\pi)^4}e^{iy.(p_1+q_1-p_2-q_2-\sum_j k_j)+D_{\rm QCD}} \\ & *\,\bar{\beta}_n(k_1,\ldots,k_n)\frac{d^3p_2}{p_2^0}\frac{d^3q_2}{q_2^0} \qquad , \end{aligned} \tag{2.17}$$

where

$$SUM_{IR}(\text{QCD}) = 2\alpha_S ReB_{\rm QCD} + 2\alpha_S\tilde{B}_{\rm QCD}(K_{max}),$$
$$2\alpha_S\tilde{B}_{\rm QCD}(K_{max}) = \int\frac{d^3k^0}{k^0}\tilde{S}_{\rm QCD}(k)\theta(K_{max}-k),$$

$$D_{\rm QCD} = \int \frac{d^3k}{k} \tilde{S}_{\rm QCD}(k) \left[e^{-iy.k} - \theta(K_{max} - k) \right], \tag{2.18}$$

$$\frac{1}{2}\bar{\beta}_0 = d\sigma^{(1-loop)} - 2\alpha_S Re B_{\rm QCD} d\sigma_B,$$
$$\frac{1}{2}\bar{\beta}_1 = d\sigma_{B_1} - \tilde{S}_{\rm QCD}(k) d\sigma_B, \ldots . \tag{2.19}$$

Here $\bar{\beta}_n$ are the QCD hard gluon residuals . They are the non-Abelian analogs of the residuals defined by Yennie Frautschi Suura.

The two things to be noted about the right hand side of the (2.17) are:

- There is no dependence on the dummy parameter K_{max} which was introduced for the cancellation of the infrared divergences in SUM_{IR}(QCD) to all orders in $\alpha_S(Q)$ [21]. Q is the hard scale in the parton scattering process described here.
- Its analog can also be derived in the new CEEX format [18].

Since the left hand side of (2.17) and SUM_{IR}(QCD) are infrared finite, it follows that

$$d\bar{\hat{\sigma}}_{exp} \equiv e^{-SUM_{IR}({\rm QCD})} d\hat{\sigma}_{exp} \tag{2.20}$$

should also be infrared finite to all orders in α_S.

Now we define the left over non-Abelian infrared divergence part of each contribution ($\bar{\beta}_n^{(l)}$) as

$$\bar{\beta}_n^l = \tilde{\bar{\beta}}_n^l + D\bar{\beta}_n^l. \tag{2.21}$$

The new function $\tilde{\bar{\beta}}_n^{(l)}$ is completely free of infrared divergences . Therefore, the part $D\bar{\beta}_n^l$ contains all the infrared divergences of non-Abelian origin. $D\bar{\beta}_n^l$ is normalized so as to vanish in the Abelian limit $f_{abc} \to 0$.

At $\mathcal{O}(\alpha_S^n(Q))$, the IR finiteness of the contribution to $\bar{\hat{\sigma}}_{exp}$ requires

$$d\bar{\hat{\sigma}}_{exp}^{(n)} \equiv \int \sum_{l=0}^{n} \frac{1}{l!} \prod_{j=1}^{l} \int_{k_j \geq K_{max}} \frac{d^3k_j}{k_j^0} \tilde{S}_{\rm QCD}(k_j) \sum_{i=0}^{n-l} \frac{1}{i!} \prod_{j=l+1}^{l+i} \int \frac{d^3k_j}{k_j^0}$$
$$* \, \bar{\beta}_i^{(n-l-i)}(k_{l+1}, \ldots, k_{l+i}) \frac{d^3p_2}{p_2^0} \frac{d^3q_2}{q_2^0} \tag{2.22}$$

is finite. This, therefore, shows

$$D d\bar{\bar{\sigma}}^{(n)}_{exp} \equiv \int \sum_{l=0}^{n} \frac{1}{l!} \prod_{j=1}^{l} \int_{k_j \geq K_{max}} \frac{d^3k_j}{k_j^0} \tilde{S}_{\rm QCD}(k_j) \sum_{i=0}^{n-l} \frac{1}{i!} \prod_{j=l+1}^{l+i} \int \frac{d^3k_j}{k_j^0} \times D\bar{\beta}_i^{(n-l-i)}(k_{l+1}, \ldots, k_{l+i}) \frac{d^3p_2}{p_2^0} \frac{d^3q_2}{q_2^0} \tag{2.23}$$

is also finite. Therefore, we can drop $D\bar{\beta}^{(l)}_n$ because they do not have a contribution in the final parton cross-section $\hat{\sigma}_{exp}$. Now, in order to show how we arrive at the above result we define $D\bar{\beta}^{(l)}_n$ as

$$\int dPh D\bar{\beta}^{(l)}_n \equiv \sum_{i=1}^{n=l} d_i^{n,l} \ln^i(\lambda^2), \tag{2.24}$$

where the coefficient functions $d_i^{n,l}$ are independent of λ for $\lambda \to 0$ and dPh is the respective n-gluon Lorentz invariant phase space. In the above we have defined $D\bar{\beta}^{(l)}_n$ by a minimal subtraction of the respective IR divergences in it so that if we would use dimensional regularization it would only contains powers of the actual pole and transcendental constants, $\frac{1}{\epsilon} - C_E + \ln(4\pi)$ for $\epsilon = 2 - \frac{d}{2}$, where d is the dimension of space-time. Here, C_E is the Euler constant. Since the integration region for the final particles is arbitrary, the independent powers of the IR regulator $\ln(\lambda^2)$ in (2.23) gives a zero contribution.

Therefore, finally we get

$$\begin{aligned} d\hat{\sigma}_{exp} &= \sum_n d\hat{\sigma}^n_{exp} \\ &= e^{SUM_{IR}(\rm QCD)} \sum_{n=0}^{\infty} \int \prod_{j=1}^{n} \frac{d^3k_j}{k_j^0} \int \frac{d^4y}{(2\pi)^4} e^{iy.(p_1+q_1-p_2-q_2-\sum_j k_j)+D_{\rm QCD}} \\ &\times \tilde{\bar{\beta}}_n(k_1, \ldots, k_n) \frac{d^3p_2}{p_2^0} \frac{d^3q_2}{q_2^0} \quad , \end{aligned} \tag{2.25}$$

where, the hard gluon residuals are defined as

$$\tilde{\bar{\beta}}_n(k_1, \ldots, k_n) = \sum_{l=0}^{\infty} \tilde{\bar{\beta}}^{(l)}_n(k_1, \ldots, k_n). \tag{2.26}$$

The hard gluon residuals are now free of all infrared divergences to all orders in $\alpha_S(Q)$.

2.2.3 QED $\otimes$ QCD *Exponentiation*

We start with the prototypical process $pp \to \bar{l}l + n(\gamma) + m(g) + X$ where, $l = e, \mu$. In this case we make the following replacements

$$
\begin{aligned}
B^{nls}_{\text{QCD}} &\to B^{nls}_{\text{QCD}} + B^{nls}_{\text{QED}} \equiv B^{nls}_{QCED} \\
\tilde{B}^{nls}_{\text{QCD}} &\to \tilde{B}^{nls}_{\text{QCD}} + \tilde{B}^{nls}_{\text{QED}} \equiv \tilde{B}^{nls}_{QCED} \\
\tilde{S}^{nls}_{\text{QCD}} &\to \tilde{S}^{nls}_{\text{QCD}} + \tilde{S}^{nls}_{\text{QED}} \equiv \tilde{S}^{nls}_{QCED}
\end{aligned} \tag{2.27}
$$

in the YFS [17] exponentiation algebra. Here the superscript *nls* denotes the infrared functions are DGLAP-CS synthesized [3, 4]. Now we start from the basic algebra

$$
d\hat{\sigma}_{exp} = e^{SUM_{IR}(QCED)} \sum_{n=0}^{\infty} \int \prod_{j_1=1}^{n} \frac{d^3k_{j_1}}{k_{j_1}} \prod_{j_2=1}^{m} \frac{d^3k_{j_2}}{k_{j_2}} \int \frac{d^4y}{(2\pi)^4} e^{iy.(p_1+q_1-p_2-q_2-\sum_j k_j)+D_{QCED}} \\
* \tilde{\bar{\beta}}_{n,m}(k_1, \ldots, k_n; k'_1, \ldots, k'_m) \frac{d^3p_2}{p_2^0} \frac{d^3q_2}{q_2^0}, \tag{2.28}
$$

where the new YFS residuals, $\tilde{\bar{\beta}}_{n,m}(k_1, \ldots, k_n; k'_1, \ldots, k'_m)$, with n hard photons and m hard gluons represent the successive application of the YFS expansion. The infrared functions are now given by

$$
\begin{aligned}
SUM_{IR}(QCED) &= 2\alpha_S \mathcal{R} B^{nls}_{QCED} + 2\alpha_S \tilde{B}^{nls}_{QCED} \\
D_{QCED} &= \int \frac{dk}{k^0} (e^{-iky} - \theta(K_{max} - k^0)) \tilde{S}^{nls}_{QCED}
\end{aligned} \tag{2.29}
$$

which is independent of K_{max}. However the dummies in QED and QCD were set to the same value for the purpose of the calculation. This is denoted as Quantum ChromoElectroDynamics (QCED). In the (2.28) $SUM_{IR}(QCED)$ sums up to the infinite order the maximal leading IR singular terms in the cross section for soft emission below a dummy parameter K_{max}, D_{QCED} does the same for the regime above K_{max}, which therefore implies that (2.28) is independent of K_{max}. Here the entire soft gluon phase space is included in the representation. After the DGLAP-CS synthesization, the residuals are truly perturbative and the leading order $\tilde{\bar{\beta}}^{(0,0)}_{0,0}$ gives a good estimate of the size of the effects being studied.

CHAPTER THREE

IR-improved DGLAP-CS Theory

3.1 DGLAP-CS

The motivation of the improvement can be seen in the kernels that determine the evolution of the structure functions by the attendant DGLAP-CS evolution of the corresponding parton densities. Now, we consider the evolution of the non-singlet (NS) parton density function $q^{NS}(x)$, where x is the Bjorken variable [22]. We start the analysis with the infrared divergence in the kernel that determines the evolution

$$\frac{dq^{NS}(x,t)}{dt} = \frac{\alpha_S(t)}{2\pi}\int_x^1 \frac{dy}{y} q^{NS}(y,t) P_{qq}(\frac{x}{y}) \tag{3.1}$$

where the kernel $P_{qq}(z)$ is for $z < 1$

$$P_{qq}(z) = C_F \frac{1+z^2}{1-z} \tag{3.2}$$

when t is set to $t = \ln\frac{\mu^2}{\mu_0^2}$ for a particular reference scale μ_0 with respect to which the evolution of the scale of interest μ is studied. Here $C_F = \frac{N_C^2-1}{2N_C}$, the quark color representation's quadratic Casimir invariant where N_C is the number of colors, which is 3. There is an unintegrable IR singularity at $z = 1$ which is the point of zero energy gluon emission. Regularizing is possible by the replacement

$$\frac{1}{(1-z)} \rightarrow \frac{1}{(1-z)_+} \tag{3.3}$$

with the distribution $\frac{1}{(1-z)_+}$ defined such that

$$\int_0^1 dz \frac{f(z)}{(1-z)_+} = \int_0^1 dz \frac{f(z)-f(1)}{(1-z)}. \tag{3.4}$$

Now, we may also write

$$\frac{1}{(1-z)_+} = \frac{1}{(1-z)}\theta(1-\epsilon-z) + \ln\epsilon\,\delta(1-z) \tag{3.5}$$

where $\epsilon \downarrow 0$. Here, $\theta(x)$ is the step function from 0 for $x < 1$ to 1 for $x \geq 0$ and $\delta(x)$ is the Dirac delta function. Now, we impose the final result

$$\int_0^1 dz P_{qq}(z) = 0, \tag{3.6}$$

which is satisfied by adding the effects of virtual corrections at $z = 1$ so that we finally get

$$P_{qq}(z) = C_F \left(\frac{1+z^2}{(1-z)_+} + \frac{3}{2}\delta(1-z) \right). \tag{3.7}$$

The smooth behavior in the original real emission result from the Feynman rules with a divergent $\frac{1}{1-z}$ behavior as $z \to 1$ has been replaced with a mathematical artifact such that the regime $1 - \epsilon < z < 1$ now has no probability at all and at $z = 1$ there is a large negative integrable contribution so that we end-up finally with a zero value for the total integral of $P_{qq}(z)$.

Now the momentum conservation at the QCD vertex, at $z < 1$, gives

$$\begin{aligned} P_{qq}(z) &= P_{Gq}(1-z) \\ P_{qG}(z) &= P_{qG}(1-z) \\ P_{GG}(z) &= P_{GG}(1-z). \end{aligned} \tag{3.8}$$

Therefore using (3.7) and (3.8) we get

$$P_{Gq} = C_F \frac{1+(1-z)^2}{z}. \tag{3.9}$$

Upon including the pair production contribution to the evolution of the quark density the evolution equation becomes

$$\frac{dq(x,t)}{dt} = \frac{\alpha_S(t)}{2\pi} \int_x^1 \frac{dy}{y} (q(y,t) P_{qq}(\frac{x}{y}) + g(y,t) P_{qG}(\frac{x}{y})). \tag{3.10}$$

In (3.10) we have

$$P_{qG} = \frac{1}{2}(z^2 + (1-z)^2), \tag{3.11}$$

which includes the probability that a gluon annihilates into a $q\bar{q}$ pair such that the quark has a fraction z of its momenta.

Now we write the gluon evolution equation as

$$\frac{dg(x,t)}{dt} = \frac{\alpha_S}{2\pi}\int_x^1 \frac{dy}{y}\left(q(y,t)P_{Gq}(\frac{x}{y}) + g(y,t)P_{GG}(\frac{x}{y})\right) \tag{3.12}$$

where g(y,t) is the gluon density in the proton. In (3.12) we have

$$P_{GG}(z) = 2C_G\left(\frac{1-z}{z} + \frac{z}{1-z} + z(1-z)\right). \tag{3.13}$$

Again from the momentum conservation of the partons it may be written

$$\int_0^1 dzz[P_{qq}(z) + P_{Gq}(z)] = 0,$$
$$\int dzz[2n_f P_{qG}(z) + P_{GG}(z)] = 0, \tag{3.14}$$

where n_f = number of quark flavors. Therefore

$$P_{GG}(z) = 2C_G\left[\frac{1-z}{z} + \frac{z}{1-z} + z(1-z) + \left(\frac{11}{12} - \frac{1}{3}\frac{T}{C_G}\delta(1-z)\right)\right], \tag{3.15}$$

where C_G and T are the Casimir operators for the color group and for the representation of the fermions. Summing up we write

$$\begin{aligned}
P_{qq}(z) &= C_F\left(\frac{1+z^2}{(1-z)_+} + \frac{3}{2}\delta(1-z)\right),\\
P_{Gq} &= C_F\frac{1+(1-z)^2}{z},\\
P_{qG} &= \frac{1}{2}(z^2+(1-z)^2),\\
P_{GG}(z) &= 2C_G\left[\frac{1-z}{z} + \frac{z}{1-z} + z(1-z)\left(\frac{11}{12} - \frac{1}{3}\frac{T}{C_G}\delta(1-z)\right)\right]
\end{aligned} \tag{3.16}$$

3.2 IR-Improved DGLAP-CS

The question that concerns us is how much of the complete soft limit of the DGLAP-CS theory is contained in the anomalous dimensions of the leading twist operators in Wilson's expansion which resides on the tip of the light cone. Here the

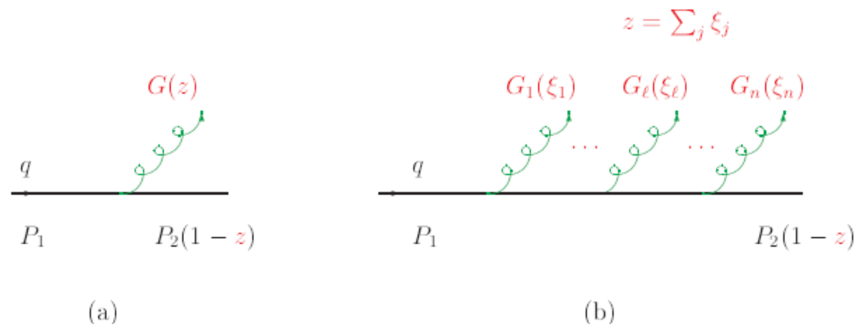

Figure 3.1: (a) The process $q \to q(1-z) + G(z)$, (b) The multiple gluon improvement $q \to q(1-z) + G_1(\xi_1) + \ldots + G_n(\xi_n)$.

long wavelength gluon effects to DGLAP-CS theory is calculated. [5, 6] The idea is to sum up the leading IR terms in the corrections of P_{qq} with the goal that the IR singularity is integrable. We apply the QCD exponentiation to the gluon emission transition in Fig. (3.1) that corresponds to $P_{qq}(z)$.

We start with splitting $A \to B + C$:

$$P_{BA} = P^0_{BA} \equiv \frac{1}{2} z(1-z) \bar{\sum_{spins}} \frac{|V_{A\to B+C}|^2}{p_\perp^2}$$
$$\Rightarrow \tag{3.17}$$
$$P_{BA} = \frac{1}{2} z(1-z) \bar{\sum_{spins}} \frac{|V_{A\to B+C}|^2}{p_\perp^2} z^{\gamma_q} F_{YFS}(\gamma_q) e^{\frac{1}{2}\delta_q}$$

where $A = q$, $B = G$, $C = q$ and $V_{A\to B+C}$ is the lowest order amplitude for $q \to G(z) + q(1-z)$. Therefore the un-normalized exponentiated result is

$$P_{qq}(z) = C_F F_{YFS}(\gamma_q) e^{\frac{1}{2}\delta_q} \frac{1+z^2}{1-z}(1-z)^{\gamma_q} \tag{3.18}$$

where

$$\gamma_q = C_F \frac{\alpha_S}{\pi} t = \frac{4C_F}{\beta_0} \tag{3.19}$$

$$\delta_q = \frac{\gamma_q}{2} + \frac{\alpha_S C_F}{\pi}\left(\frac{\pi^2}{3} - \frac{1}{2}\right) \tag{3.20}$$

and

$$F_{YFS}(\gamma_q) = \frac{e^{-C_E\gamma_q}}{\Gamma(1+\gamma_q)}. \tag{3.21}$$

Here

$$\beta_0 = 11 - \frac{2}{3}n_f, \tag{3.22}$$

where n_f = the number of active quark flavors and C_E is the Euler constant and $\Gamma(w)$ is the Euler gamma function. The function F_{YFS} was introduced by Yennie, Frautschi and Suura [17] in their analysis of the IR behavior of QED. It can be seen that the exponentiation has removed the unintegrable IR divergence at $z = 1$. To see how equation(2.25) leads to (3.18) we write

$$\begin{aligned} SUM_{IR}(\text{QCD}) &= 2\alpha_S Re B_{\text{QCD}} + 2\alpha_S \tilde{B}_{\text{QCD}}(K_{max}) \\ &= \frac{1}{2}(2C_F\frac{\alpha_S}{\pi}t\ln\frac{K_{max}}{E} + C_F\frac{\alpha_S}{2\pi}t + \frac{\alpha_S C_F}{\pi}(\frac{\pi^2}{3}-\frac{1}{2})) \end{aligned} \tag{3.23}$$

where on the RHS of the last result the DGLAP-CS synthesization procedure has already been applied. When the soft gluon effects for energy fraction $< z \equiv K_{max}/E$

are taken into account we get

$$\int \frac{\alpha_S}{2\pi} P_{BA} dt dz = e^{SUM_{IR}(\mathrm{QCD})(z)} \int \left\{ \tilde{\bar{\beta}}_0 \int \frac{d^4y}{(2\pi)^4} e^{\left\{ iy.(p_1-p_2)+\int^{k<K_{max}} \frac{d^3k}{k} \tilde{S}_{\mathrm{QCD}}(k)\left[e^{-iy.k}-1\right] \right\}} \right\}$$
$$+ \left\{ \tilde{\bar{\beta}}_0 \int \frac{d^3k_1}{k_1} \tilde{\bar{\beta}}_1(k_1) \int \frac{d^4y}{(2\pi)^4} e^{\left\{ iy.(p_1-p_2-k_1)+\int^{k<K_{max}} \frac{d^3k}{k} \tilde{S}_{\mathrm{QCD}}(k)\left[e^{-iy.k}-1\right] \right\}+\ldots} \right\}$$
$$\frac{d^3p_2}{p_2^0}\frac{d^3q_2}{q_2^0}$$
$$= e^{SUM_{IR}(\mathrm{QCD})(z)} \int \left\{ \tilde{\bar{\beta}}_0 \int \frac{d^4y}{(2\pi)^4} e^{\left\{ iy.(E_1-E_2)+\int^{k<K_{max}} \frac{d^3k}{k} \tilde{S}_{\mathrm{QCD}}(k)\left[e^{-iy.k}-1\right] \right\}} \right\}$$
$$+ \left\{ \tilde{\bar{\beta}}_0 \int \frac{d^3k_1}{k_1} \tilde{\bar{\beta}}_1(k_1) \int \frac{d^4y}{(2\pi)^4} e^{\left\{ iy.(E_1-E_2-k_1^0)+\int^{k<K_{max}} \frac{d^3k}{k} \tilde{S}_{\mathrm{QCD}}(k)\left[e^{-iy.k}-1\right] \right\}+\ldots} \right\}$$
$$\frac{d^3p_2}{p_2^0}\frac{d^3q_2}{q_2^0} \tag{3.24}$$

where it has been set $E_i = p_i^0$, $i = 1, 2$ and the real infrared function $\tilde{S}_{\mathrm{QCD}}$ is given by

$$\tilde{S}_{\mathrm{QCD}}(k) = -\frac{\alpha_S C_F}{8\pi^2}\left(\frac{p_1}{kp_1} - \frac{p_2}{kp_2}\right)^2 {}_{|DGLAP-CS\ synthesized} \tag{3.25}$$

The two important integrals required here are

$$\begin{aligned} I_{YFS}(zE, 0) &= \int_{-\infty}^{\infty} \frac{dy}{2\pi} e^{\left[iy(zE)+\int^{k<zE} \frac{d^3k}{k} \tilde{S}_{\mathrm{QCD}}(k)(e^{-iyk}-1) \right]} \\ &= F_{YFS}(\gamma_q)\frac{\gamma_q}{zE} \\ I_{YFS}(zE, k_1) &= \int_{-\infty}^{\infty} \frac{dy}{2\pi} e^{\left[iy(zE-k_1)+\int^{k<zE} \frac{d^3k}{k} \tilde{S}_{\mathrm{QCD}}(k)(e^{-iyk}-1) \right]} \\ &= \left(\frac{zE}{zE-k_1}\right)^{1-\gamma_q} I_{YFS}(zE, 0) \end{aligned} \tag{3.26}$$

Therefore, we can identify the factor

$$\int(\bar{\tilde{\bar{\beta}}}_0\frac{\gamma_q}{zE}+\int dk_1k_1d\Omega_1\bar{\tilde{\bar{\beta}}}_{k_1}(\frac{zE}{zE-k_1})^{1-\gamma_q}\frac{\gamma_q}{zE})\frac{d^3p_2}{E_2q_2^0}=\int dt\frac{\alpha_S(t)}{2\pi}P^0_{BA}dz+\mathcal{O}(\alpha_S^2). \tag{3.27}$$

This leads finally to the exponentiated result by elementary differentiation:

$$P_{BA}=P^0_{BA}z^{\gamma_q}F_{YFS}(\gamma_q)e^{\frac{1}{2}\delta_q} \tag{3.28}$$

It is noted that the terms exponentiated here are not included in the standard treatment of the Wilson expansion. The normalization condition, $\int_0^1 dzP_{qq}(z)=0$, along with the IR improvement gives the final expression

$$P_{qq}(z)=C_FF_{YFS}(\gamma_q)e^{\frac{1}{2}\partial_q}\left[\frac{1+z^2}{1-z}(1-z)^{\gamma_q}-f_q(\gamma_q)\delta(1-z)\right] \tag{3.29}$$

where

$$f_q(\gamma_q)=\frac{2}{\gamma_q}-\frac{2}{\gamma_q+1}+\frac{1}{\gamma_q+2} \tag{3.30}$$

The latter result is the IR-Improved kernel for NS DGLAP-CS evolution in QCD. The DGLAP-CS theory shows that the kernel $P_{Gq}(z)$ is related to $P_{qq}(1-z)$ directly. For $z<1$ we have

$$P_{Gq}(z)=P_{qq}(1-z)=C_FF_{YFS}(\gamma_q)e^{\frac{1}{2}\delta_q}\frac{1+(1-z)^2}{z}z^{\gamma_q}. \tag{3.31}$$

This gives a non-trivial check of the new IR-improved theory, the conservation of momentum leads to

$$\int_0^1 dzz(P_{Gq}(z)+P_{qq}(z))=0. \tag{3.32}$$

Now, using the check, the following integral vanishes

$$I=\int_0^1 dzz(\frac{1+(1-z)^2}{z}z^{\gamma_q}+\frac{1+z^2}{1-z}(1-z)^{\gamma_q}-f_q(\gamma_q)\delta(1-z)). \tag{3.33}$$

We note

$$\frac{z}{1-z}=\frac{z-1+1}{1-z}=-1+\frac{1}{1-z}. \tag{3.34}$$

Introducing (3.34) in (3.33) we get

$$I = \int_0^1 dz \left\{ (1+(1-z)^2)z^{\gamma_q} - (1+z^2)(1-z)^{\gamma_q} + \frac{1+z^2}{1-z}(1-z)^{\gamma_q} - f_q(\gamma_q)\delta(1-z) \right\}. \tag{3.35}$$

The first two terms in the integral on the RHS cancel by using the change in variable $z \to 1-z$. The last two terms cancel from the normalization condition. Therefore, it can be concluded that

$$I = 0. \tag{3.36}$$

Therefore the quark momentum sum rule is satisfied.

Now,we note the standard formula for $P_{qG}(z)$

$$P_{qG}(z) = \frac{1}{2}(z^2 + (1-z)^2), \tag{3.37}$$

which is already well behaved in the IR regime. We therefore next consider the $P_{GG}(z)$, which in the lowest order form is

$$P_{GG}(z) = 2C_G(\frac{1-z}{z} + \frac{z}{1-z} + z(1-z)) \tag{3.38}$$

which has unintegrable singularities at $z = 1$ and $z = 0$. Now applying the exponentiated analysis to the squared amplitude for the process $G \to G(z) + G(1-z)$ we get the exponentiated un-normalized result

$$P_{GG}(z) = 2C_G F_{YFS}(\gamma_G) e^{\frac{1}{2}\delta_G}(\frac{1-z}{z}z^{\gamma_G} + \frac{z}{1-z}(1-z)^{\gamma_G} + \frac{1}{2}(z^{1+\gamma_G}(1-z) + z(1-z)^{1+\gamma_G})), \tag{3.39}$$

where we have gotten the γ_G and δ_G from the expressions of the γ_q and δ_q by using the substitution $C_F \to C_G$, which gives

$$\gamma_G = C_G \frac{\alpha_S}{\pi} t = \frac{4C_G}{\beta_0} \tag{3.40}$$

$$\delta_G = \frac{\gamma_G}{2} + \frac{\alpha_S C_G}{\pi}(\frac{\pi^2}{3} - \frac{1}{2}). \tag{3.41}$$

From this it can be seen that the singularities at $z = 1$ and $z = 0$ have been rendered integrable. We use the gluon momentum sum rule to normalize P_{GG} such that

$$\int_0^1 dzz(2n_f P_{qG}(z) + P_{GG}(z)) = 0. \tag{3.42}$$

We then arrive at the final IR-improved result

$$\begin{aligned} P_{GG}(z) &= 2C_G F_{YFS}(\gamma_G) e^{\frac{1}{2}\delta_G} \left\{ \frac{1-z}{z} z^{\gamma_G} + \frac{z}{1-z}(1-z)^{\gamma_G} \right\} \\ &+ 2C_G F_{YFS}(\gamma_G) e^{\frac{1}{2}\delta_G} \left\{ \frac{1}{2}(z^{1+\gamma_G}(1-z) + z(1-z)^{1+\gamma_G}) - f_G(\gamma_G)\delta(1-z) \right\} \end{aligned} \tag{3.43}$$

where $f_G(\gamma_G)$ is given by

$$\begin{aligned} f_G(\gamma_G) = \frac{n_f}{6C_G F_{YFS}(\gamma_G)} e^{-\frac{1}{2}\delta_G} &+ \frac{2}{\gamma_G(1+\gamma_G)(2+\gamma_G)} + \frac{1}{(1+\gamma_G)(2+\gamma_G)} \\ &+ \frac{1}{2(3+\gamma_G)(4+\gamma_G)} + \frac{1}{(2+\gamma_G)(3+\gamma_G)(4+\gamma_G)} \end{aligned} \tag{3.44}$$

Therefore the improved results of $P_{qq}(z)$, $P_{Gq}(z)$ and $P_{GG}(z)$ together with the standard result $P_{qG}(z)$ give the IR-improved DGLAP-CS theory. In summary, listing the above results, we have

$$P_{qq}^{exp}(z) = C_F F_{YFS}(\gamma_q) e^{\frac{1}{2}\delta_q} \left[\frac{1+z^2}{1-z}(1-z)^{\gamma_q} - f_q(\gamma_q)\delta(1-z) \right], \tag{3.45}$$

$$P_{Gq}^{exp}(z) = C_F F_{YFS}(\gamma_q) e^{\frac{1}{2}\delta_q} \frac{1+(1-z)^2}{z} z^{\gamma_q}, \tag{3.46}$$

$$\begin{aligned} P_{GG}^{exp}(z) = 2C_G F_{YFS}(\gamma_G) e^{\frac{1}{2}\delta_G} \{ &\frac{1-z}{z} z^{\gamma_G} + \frac{z}{1-z}(1-z)^{\gamma_G} \\ &+ \frac{1}{2}(z^{1+\gamma_G}(1-z) + z(1-z)^{1+\gamma_G}) - f_G(\gamma_G)\delta(1-z) \}, \end{aligned} \tag{3.47}$$

$$P_{qG}(z) = \frac{1}{2}(z^2 + (1-z)^2). \tag{3.48}$$

The superscript *exp* is used to denote the exponentiated result. In the actual applications, we also IR-improve $P_{qG}(z)$, so that we have

$$P_{qG}^{exp}(z) = F_{YFS}(\gamma_G) e^{\frac{1}{2}\delta_G} \frac{1}{2} \{ z^2(1-z)^{\gamma_G} + (1-z)^2 z^{\gamma_G} \} \tag{3.49}$$

with a corresponding change in f_G to $\bar{f}_G$, where[1]

$$\bar{f}_G(\gamma_G) = \frac{n_f}{C_G}\frac{1}{(1+\gamma_G)(2+\gamma_G)(3+\gamma_G)} + \frac{2}{\gamma_G(1+\gamma_G)(2+\gamma_G)} + \frac{1}{(1+\gamma_G)(2+\gamma_G)}$$
$$\frac{1}{2(3+\gamma_G)(4+\gamma_G)} + \frac{1}{(2+\gamma_G)(3+\gamma_G)(4+\gamma_G)} \tag{3.50}$$

The new scheme has improved MC stability. In the attendant parton shower MC based on the new kernels there is no need for an IR cut-off 'k_0' parameter. The new kernels agree with the usual kernels at $\mathcal{O}(\alpha_S)$ as the differences between them start in $\mathcal{O}(\alpha_S^2)$. This means that the NLO matching formulas in the MC@NLO [25] and POWHEG [26] apply directly to the new kernels for the realization of the exact NLO ME/shower matching. We point-out finally here that the new IR-improvement exponents $\gamma_A, A = q, G$, are genuine quantum loop effects; they vanish when $\hbar \to 0$.

3.2.1 Phenomenological Effects of IR-Improvement

In the non-singlet case we can write [6]

$$\frac{dM_n^{NS}}{dt} = \frac{\alpha_S(t)}{2\pi} A_n^{NS} M_n^{NS}(t) \tag{3.51}$$

where

$$M_n^{NS}(t) = \int_0^1 dz z^{n-1} q^{NS}(z,t) \tag{3.52}$$

and

$$\begin{aligned} A_n^{NS} &= \int_0^1 dz z^{n-1} P_{qq}^{exp}(z), \\ &= C_F F_{YFS}(\gamma_q) e^{\frac{1}{2}\delta_q} \left[B(n,\gamma_q) + B(n+2,\gamma_q) - f_q(\gamma_q)\right] \end{aligned} \tag{3.53}$$

where the beta function is given by

$$B(x,y) = \frac{\Gamma(x)\Gamma(y)}{\Gamma(x+y)}. \tag{3.54}$$

[1] The improvement in (3.45-3.49) should be distinguished from the resummation in parton density evolution for "$z \to 0$" Regge regime – see for example Refs. [23, 24]. This latter improvement must also be taken into account for precision LHC predictions.

The IR- improved exponent approaches a constant which is a multiple of $-f_q$ as $n \to \infty$ for $0 \le z < 1$. At finite n, example n=2, $A_2^{NS} = C_F(-0.966)$ where $\alpha_S \cong .118$.

Now the un-IR-improved result is

$$A_n^{NS} \equiv C_F \left[-\frac{1}{2} + \frac{1}{n(n+1)} - 2\sum_{j=2}^{n} \frac{1}{j} \right]. \tag{3.55}$$

The asymptotic behavior for large n shows that the above diverges as $-2C_F \ln n$ as $n \to \infty$. Also, for the sake of comparison, for a finite value $n = 2$, $A_2^{NS} = C_F(-1.33)$.

The solution to (3.51) is given by

$$\begin{aligned} M_n^{NS}(t) &= M_n^{NS}(t_0) e^{\int_{t_0}^{t} dt\prime \frac{\alpha_S(t\prime)}{2\pi} A_n^{NS}(t\prime)} \\ &= M_n^{NS}(t_0) e^{\bar{a}_n [E_i(\frac{1}{2}\delta_1 \alpha_S(t_0)) - E_i(\frac{1}{2}\delta_1 \alpha_S(t))]} \\ &\Longrightarrow_{t,t_0\, large\, with\, t \gg t_0} \; M_n^{NS}(t_0) \left(\frac{\alpha_S(t_0)}{\alpha_S(t)} \right)^{\bar{a}\prime_n} \end{aligned} \tag{3.56}$$

where $E_i(x) = \int_{-\infty}^{x} dr \frac{e^r}{r}$ is the exponential integral function,

$$\begin{aligned} \bar{a}_n &= \frac{2C_F}{\beta_0} F_{YFS}(\gamma_q) e^{\frac{\gamma_q}{4}} [B(n,\gamma_q) + B(n+2,\gamma_q) - f_q(\gamma_q)] \\ \bar{a}\prime_n &= \bar{a}_n \left(1 + \frac{\delta_1}{2} \frac{(\alpha_s(t_0) - \alpha_s(t))}{\ln(\alpha_s(t_0)/\alpha_s(t))} \right) \end{aligned} \tag{3.57}$$

Here δ_1 is given by $\delta_1 = \frac{C_F}{\pi}\left(\frac{\pi^2}{3} - \frac{1}{2}\right)$.

Therefore, the size of γ_q is what is expected from analogy with QED,and with $\alpha_S \cong .118$ we get that γ_q is 10 times γ_e. The values of γ_j can be improved as needed using perturbative results for the functions SUM_{IR}(QCD), $\tilde{S}_{\rm QCD}$, $\tilde{\bar{\beta}}_n$, which is consistent with what is needed for the precise data.

3.2.2 Impact of IR-Improvement on the Standard Methodology

Now we address the relationship between the re-arrangement made of the exact leading-logs in the QCD perturbabtion theory and the non-exponentiated DGLAP-

CS theory [6]. Expanding the the exponentiated kernels

$$(1-z)^{a-1} = \frac{1}{a}\delta(1-z) + \frac{1}{(1-z)_+} + \sum_{j=1}^{\infty}\frac{a^j}{j!}\left[\frac{ln^j(1-z)}{1-z}\right]_+, \qquad (3.58)$$

where it can be seen that P_{qq} and P_{qq}^{exp} agree to the leading order. Therefore, the leading log series which they generate for the respective NS parton distributions agree through leading order in $\frac{\alpha_S}{\pi}L$, where L is the respective big-log in momentum space. If we denote the parton densities that we generate with IR-improvement by $\{F_i'\}$ and the reduced cross section by $\hat{\sigma}'$, such that the same perturbative QCD cross section is obtained order by order in perturbation theory, then we should have

$$\begin{aligned}\sigma &= \sum_{i,j}\int dx_1 dx_2 F_i(x_1)F_j(x_2)\hat{\sigma}(x_1x_2s)\\ &= \sum_{i,j}\int dx_1 dx_2 F_i'(x_1)F_j'(x_2)\hat{\sigma}'(x_1x_2s). \qquad (3.59)\end{aligned}$$

The mass singularities are factorized using the exponentiated kernels from the un-factorized reduced cross-section and this generates the $\hat{\sigma}'$. The analogous result holds for deep inelastic scattering. Also, if exponentiated kernels are used to generate the respective parton distributions, these kernels are used to factorize the respective hard scattering cross-section and this gives the same perturbative QCD prediction for deep inelastic structure functions. Thus the IR-improved theory has the same leading log series as the un exponentiated DGLAP-CS kernels. The advantage is however that the lack of +-functions in the generation of the configuration space functions $\{F_i', \hat{\sigma}'\}$ means that these functions lend themselves to Monte Carlo realization to arbitrarily soft radiative effects. Unlike the the standard un-exponentiated kernels, the exponentiated ones contain powers of the product $\alpha_S L$ that describe the large IR effects being resummed.

CHAPTER FOUR

Monte Carlo Realization of the IR-Improved DGLAP-CS Theory in HERWIRI1.031

In this section we show the implementation of the IR-improved kernels in the HERWIG6.5 environment achieve a new MC which we will denote as HERWIRI1.0. The kernels in module HWBRAN in the HERWIG6.5 are modified using the substitution

$$DGLAP-CS\ P_{AB} \Rightarrow IR-I\ DGLAP-CS\ P^{exp}_{AB} \tag{4.1}$$

where the hard processes have been left alone for the moment. Following [27], the probability that no branching occurs above virtuality cutoff Q_0^2 is $\Delta_a(Q^2, Q_0^2)$ such that

$$d\Delta_a(t, Q_0^2) = \frac{-dt}{t}\Delta(t, Q_0^2)\sum_b \int dz \frac{\alpha_S}{2\pi}P_{ba}(z). \tag{4.2}$$

This implies

$$\Delta_a(Q^2, Q_0^2) = exp\left[-\int_{Q_0^2}^{Q^2}\frac{dt}{t}\sum_b\int dz\frac{\alpha_S}{2\pi}P_{ba}(z)\right]. \tag{4.3}$$

The non-branching probability appearing in the evolution equation is given by

$$\Delta(Q^2, t) = \frac{\Delta_a(Q^2, Q_0^2)}{\Delta_a(t, Q_0^2)},\ \ t = k_a^2 \text{ the virtuality of gluon a.} \tag{4.4}$$

The virtuality of parton a is generated with

$$\Delta_a(Q^2, t) = R, \tag{4.5}$$

where R is a random number uniformly distributed in [0,1]. Using $\alpha_S(Q) = \dfrac{2\pi}{b_0\ln(\frac{Q}{\Lambda})}$ we get

$$\begin{aligned}\int_0^1 dz\frac{\alpha_S(Q^2)}{2\pi}P_{qG}(z) &= \frac{4\pi}{2\pi b_0\ln(\frac{Q}{\Lambda})}\int_0^1 dz\frac{1}{2}[z^2 + (1-z)^2]\\ &= \frac{2}{3}\frac{1}{b_0\ln(\frac{Q^2}{\Lambda^2})}.\end{aligned} \tag{4.6}$$

The integration over dt gives

$$
\begin{aligned}
I &= \int_{Q_0^2}^{Q^2} \frac{1}{3}\frac{dt}{t}\frac{2}{b_0\ln(\frac{t}{\Lambda^2})} \\
&= \frac{2}{3b_0}\ln\ \ln\frac{t}{\Lambda^2}|_{Q_0^2}^{Q^2} \\
&= \frac{2}{3b_0}\left[\ln(\frac{\ln(\frac{Q^2}{\Lambda^2})}{\ln(\frac{Q^2}{\Lambda^2})})\right]. \qquad (4.7)
\end{aligned}
$$

On introduction of I in (4.2) we get

$$
\begin{aligned}
\Delta_a(Q^2, Q_0^2) &= \exp\left[-\frac{2}{3b_0}\ln(\frac{\ln(\frac{Q^2}{\Lambda^2})}{\ln(\frac{Q_0^2}{\Lambda^2})})\right] \\
&= \left[\frac{\ln(\frac{Q^2}{\Lambda^2})}{\ln(\frac{Q_0^2}{\Lambda^2})}\right]. \qquad (4.8)
\end{aligned}
$$

If we let $\Delta_a(Q^2, t) = R$ then we get

$$
\left[\frac{\ln(\frac{t}{\Lambda^2})}{\ln(\frac{Q^2}{\Lambda^2})}\right]^{-\frac{2}{3b_0}} = R \qquad (4.9)
$$

which in turn gives

$$
t = \Lambda^2(\frac{Q^2}{\Lambda^2})^{R^{\frac{3b_0}{2}}}. \qquad (4.10)
$$

Now, in HERWIG6.5

$$
\begin{aligned}
b_0 &= (\frac{11}{3}n_c - \frac{2}{3}n_f) \\
&= \frac{1}{3}(11n_c - 10),\ \ n_f = 5 \\
&\equiv \frac{2}{3}BETAF \qquad (4.11)
\end{aligned}
$$

using the notation of HERWIG6.5. The momentum available after a $q\bar{q}$ split in HERWIG6.5 [8] is given by

$$
QQBAR = QCDL3(\frac{QLST}{QCDL3})^{R^{BETAF}}, \qquad (4.12)
$$

in agreement with (4.10) with the identifications $t = QQBAR^2$, $\Lambda \equiv QCDL3$, $Q = QLST$.

Now repeating aforementioned calculations with the IR-improved kernels (3.48, 3.49), we have

$$P_{qG}^{exp}(z) = F_{YFS}(\gamma_G) e^{\delta_G/2} \frac{1}{2}[z^2(1-z)^{\gamma_G} + (1-z)^2 z^{\gamma_G}], \tag{4.13}$$

such that

$$\int_0^1 dz \frac{\alpha_S}{2\pi} P_{qG}(z)^{exp} = \frac{4F_{YFS}(\gamma_G)e^{\delta_G/2}}{b_0 \ln(\frac{Q^2}{\Lambda^2})(\gamma_G+1)(\gamma_G+2)(\gamma_G+3)}. \tag{4.14}$$

Therefore, the integral over dt is

$$\begin{aligned} I &= \int_{Q_0^2}^{Q^2} \frac{dt}{t} \frac{4F_{YFS}(\gamma_G)e^{\delta_G/2}}{b_0 \ln(\frac{t}{\Lambda^2})(\gamma_G+1)(\gamma_G+2)(\gamma_G+3)} \\ &= \frac{4F_{YFS}(\gamma_G)e^{\delta_G/2}}{(\gamma_G+1)(\gamma_G+2)(\gamma_G+3)} Ei\left(1, \frac{8.369604402}{b_0 \ln(\frac{t}{\Lambda^2})}\right) \Big|_{Q_0^2}^{Q^2} . \end{aligned} \tag{4.15}$$

In the above we have used

$$\delta_G = \frac{\gamma_G}{2} + \frac{\alpha_S C_G}{\pi}\left(\frac{\pi^2}{3} - \frac{1}{2}\right), \tag{4.16}$$

where $C_G = 3$. The final IR-improved formula is

$$\Delta_a(Q^2, t) = exp[-(F(Q^2) - F(t))], \tag{4.17}$$

where,

$$F(Q^2) = \frac{4F_{YFS}(\gamma_G)e^{0.25\gamma_G}}{b_0(\gamma_G+1)(\gamma_G+2)(\gamma_G+3)} E_i\left(1, \frac{8.269604402}{b_0 \ln\left(\frac{Q^2}{\Lambda^2}\right)}\right), \tag{4.18}$$

where E_i is the exponential integral function. In Fig. (4.1) the difference between the two results for $\Delta_a(Q^2, t)$ is shown. They agree within a few % except for the softer values of t, as expected.

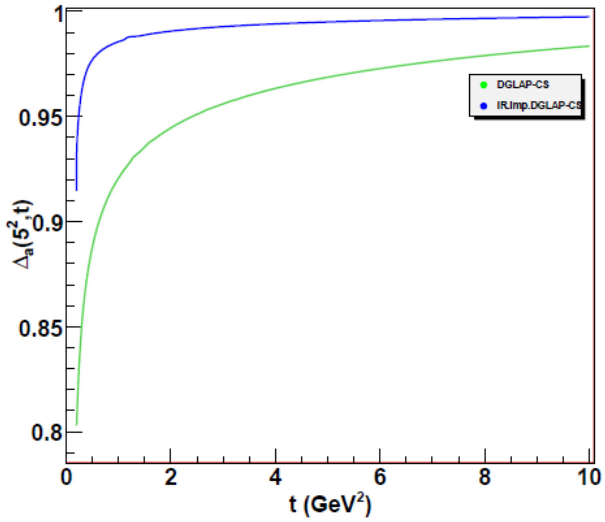

Figure 4.1: Graph of $\Delta_a(Q^2, t)$ for the DGLAP-CS and IR.Imp.DGLAP-CS kernels [3]. Q^2 is a typical virtuality closer to squared scale of the hard sub-process - here we use $Q^2 = 25\ GeV^2$ for illustration.

For further illustration, noting the $q \to qG$ branching process in HERWIG6.5 [8], the implementation of the usual DGLAP-CS [3, 4] kernels is given by the following

```
      WMIN = MIN(ZMIN*(1. -ZMIN), ZMAX*(1.-ZMAX))
      ETEST = (1. + ZMAX**2) * HWUALF(5-SUDORD*2, QNOW*WMIN)
      ZRAT = ZMAX/ZMIN
30    Z1 = ZMIN * ZRAT**HWRGEN(0)
      Z2 = 1. - Z1
      PGQW = (1. + Z2*Z2)                                        (4.19)
      ZTEST = PGQW * HWUALF(5-SUDORD*2, QNOW*Z1*Z2)
      IF (ZTEST .LT. ETEST*HWRGEN(1)) GOTO 30
      ...
```

where the branching of q to G at $z =$ Z1 occurs in the interval from ZMIN to ZMAX set by the inputs to the program and the current value of the virtuality QNOW. HWUALF is the respective function for α_S in the program and the HWRGEN are uniformly distributed random numbers in the interval of 0 to 1. To realize the same with IR-improved kernel, the following is used in place of the code (4.19)

```
      NUMFLAV = 5
      B0 = 11. - 2./3.*NUMFLAV
      L = 16./(3.*B0)
      DELTAQ = L/2 + HWUALF(5-SUDORD*2, QNOW*WMIN)*1.184056810
      ETEST = (1. + ZMAX**2) * HWUALF(5-SUDORD*2, QNOW*WMIN)
            * EXP(0.5*DELTAQ) * FYFSQ(NUMFLAV-1) * ZMAX**L
      ZRAT = ZMAX/ZMIN
30    Z1 = ZMIN * ZRAT**HWRGEN(0)
      Z2 = 1. - Z1                                                   (4.20)
      DELTAQ = L/2 + HWUALF(5-SUDORD*2, QNOW*Z1*Z2)*1.184056810
      PGQW = (1. + Z2*Z2) * EXP(0.5*DELTAQ) * FYFSQ(NUMFLAV-1)
           * Z1**L
      ZTEST = PGQW * HWUALF(5-SUDORD*2, QNOW*Z1*Z2)
      IF (ZTEST .LT. ETEST*HWRGEN(1)) GOTO 30
      ...
```

which with the identifications $\gamma_q \equiv L$, $\delta_q \equiv DELTAQ$, $F_{YFS}(\gamma_q) \equiv$ FYFSSQ (NUMFLAV $-$ 1) realizes the IR-improved DGLAP-CS kernel P_{Gq}^{exp}. Continuing in the similar manner all the kernels in the IR-improved DGLAP-CS were implemented in HERWIG6.5 environment, with its angle-ordered showers. This resulted in the new MC, HERWIRI1.031 (see Appendices A and B for more details).

CHAPTER FIVE

Review of Previous Comparisons of MC Realization of IR-Improved DGLAP-CS Theory and Fermilab Collider Data

Following the Ref. [7] we review the comparison of the MC realization of the IR-Improved DGLAP-CS theory in HERWIRI1.031 and HERWIG6.5 in relation to data at Fermilab (FNAL) Tevatron collider energies.

In order to see what type of effects we can expect, we begin with some theoretical comparisons between the IR-improved and the unimproved MC's. With an eye already toward LHC, we use prototypical processes at 14 TeV.

For the generic hard processes at planned LHC energies (14 TeV) the comparison is shown in Figs. (5.1), (5.2) for the respective ISR z-distribution and p_T^2 distribution at the parton level. Here, z is defined as E_{parton}/E_{beam} where E_{beam} is the cms beam energy and E_{parton} is the respective parton energy in the cms system. There are no cuts on the MC data. We see the expected softening of the spectra.

In the next part we concentrate on the luminosity process of single Z production again at the planned 14 TeV LHC energy in Figs. (5.3),(5.4), (5.5) it is shown respectively the ISR parton energy fraction distribution, the Z p_T distribution, and the Z rapidity distribution with cuts on the acceptance as $M_Z > 40$ GeV, $p_T^l > 5$ GeV for the $Z \to \mu^+\mu^-$ - all lepton rapidities are included. For the energy fraction distribution and the p_T distribution a softer spectra is seen in the former and similar spectra in the latter in the IR-improved case. In the case of the rapidity plot, the migration of some events to the higher values of Y is seen. It is consistent with a softer spectrum for the IR-improved case. This sets the stage for the confrontation with actual collider data. We now turn to FNAL data in this regard.

To this end, we review the results for the comparison discussion, by making a comparison with the FNAL data on the Z p_T and rapidity spectra as reported in Ref. [6]. The results are for 1.96 TeV cms energy in Figs. (5.6) and (5.7). Both HERWIRI1.031 and HERWIG6.5 give a reasonable overall representation of the CDF rapidity data [28] but HERWIRI1.031 is somewhat closer to the data for small values of Y. The χ^2/d.o.f are 1.77 and 1.54 for HERWIG6.5 and HERWIRI1.031 respectively. The data errors in Fig. (5.6) do not include luminosity and PDF errors, so that they can only be used conditionally. Also, including the NLO contributions to the hard process via MC@NLO/HERWIG6.510 and MC@NLO/HERWIRI1.031 improves the agreement for both HERWIG6.5 and for HERWIRI1.031. In this case the χ^2/d.o.f are 1.40 and 1.42 respectively. They are both consistent with one another and within 10% of the data in the low Y region.

Also, the HERWIRI1.031 gives a better fit to the $D0$ p_T data [29] in Fig. (5.6) compared to HERWIG6.5 for low p_T, showing that IR-improvement makes a better representation of the QCD in the soft regime for a given fixed order in perturbation theory. After adding the MC@NLO for the two programs we see that $\mathcal{O}(\alpha_S)$ correction improves the χ^2/d.o.f for HERWIRI1.031 in both the soft and hard regimes. The $\mathcal{O}(\alpha_S)$ correction improves the HERWIG6.510 χ^2/d.o.f for p_T near 3.75 GeV where the distribution peaks. The χ^2/d.o.f for MC@NLO/HERWIRI1.031 is 1.5 and for MC@NLO/HERWIG6.510 is worse for $p_T < 7.5$ GeV.

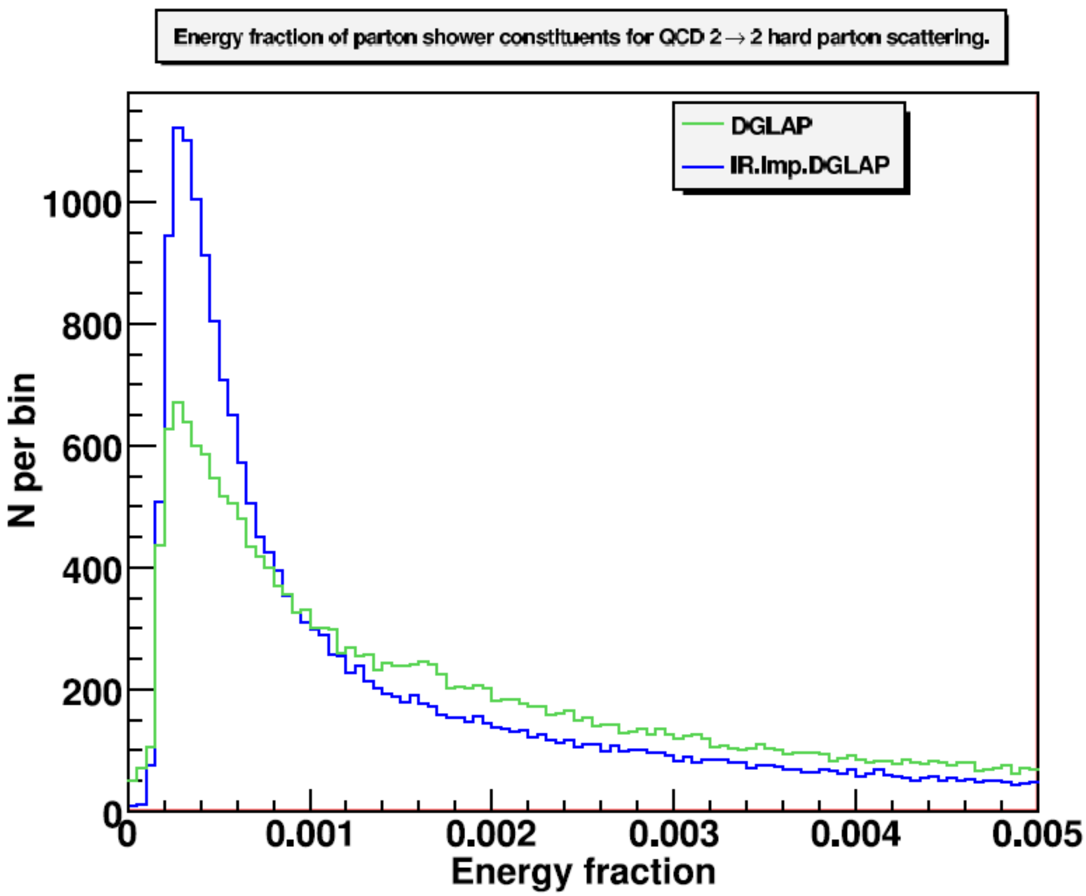

Figure 5.1: The z-distribution (ISR parton energy fraction) shower comparison in HERWIG6.5 [7]

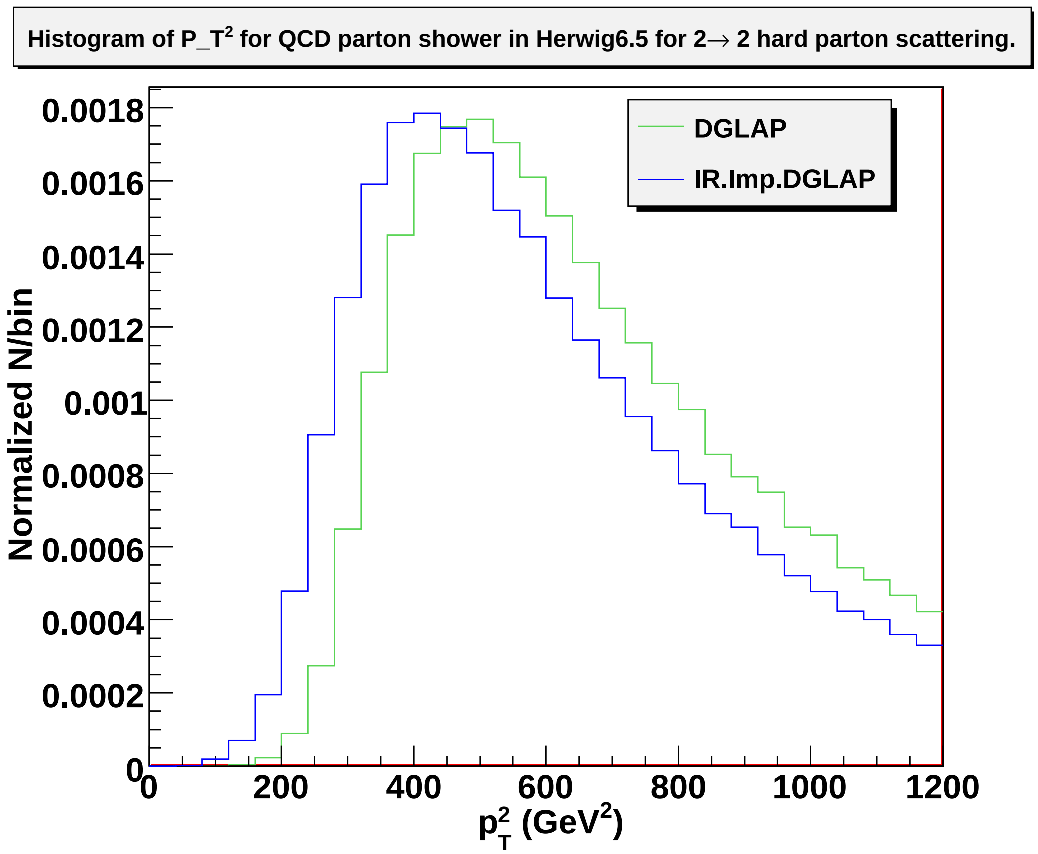

Figure 5.2. The ${p^2}_T$-distribution (ISR parton) shower comparison in HERWIG6.5 [7]

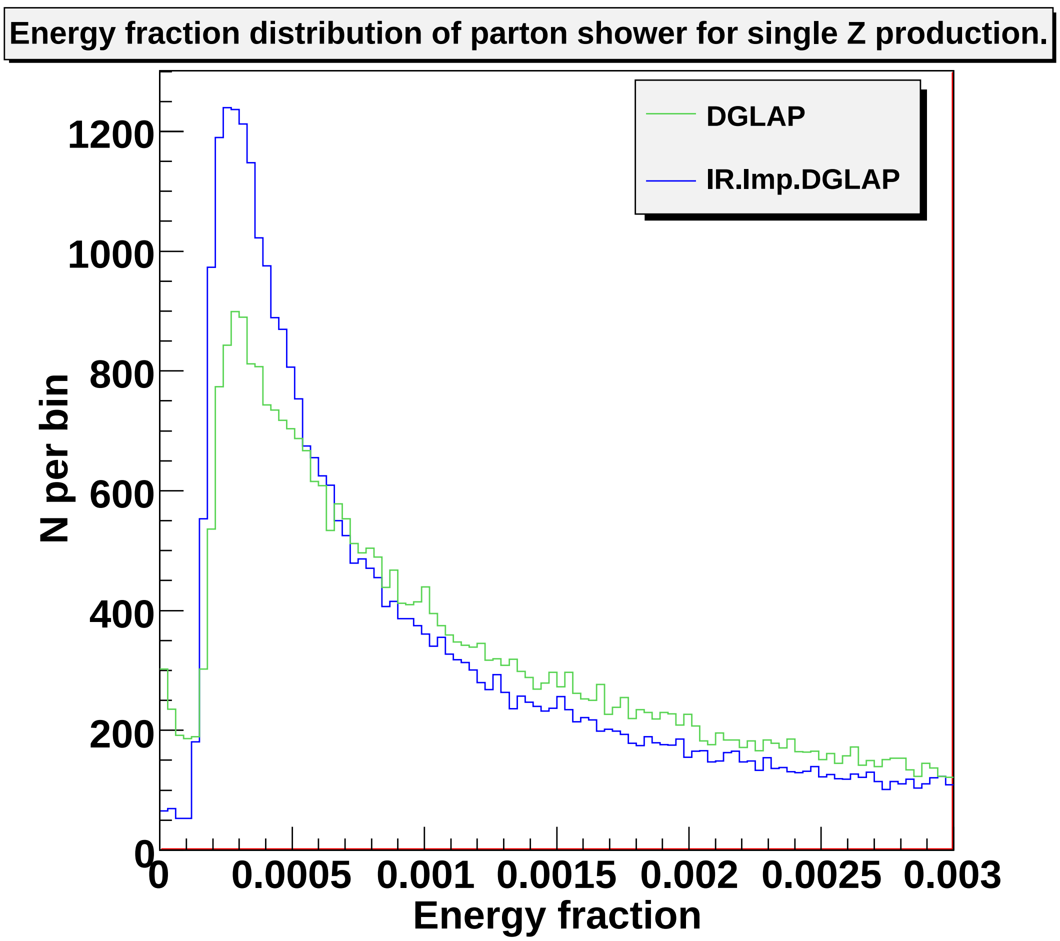

Figure 5.3: The z-distribution (ISR parton energy fraction) shower comparison in HERWIG6.5 [7]

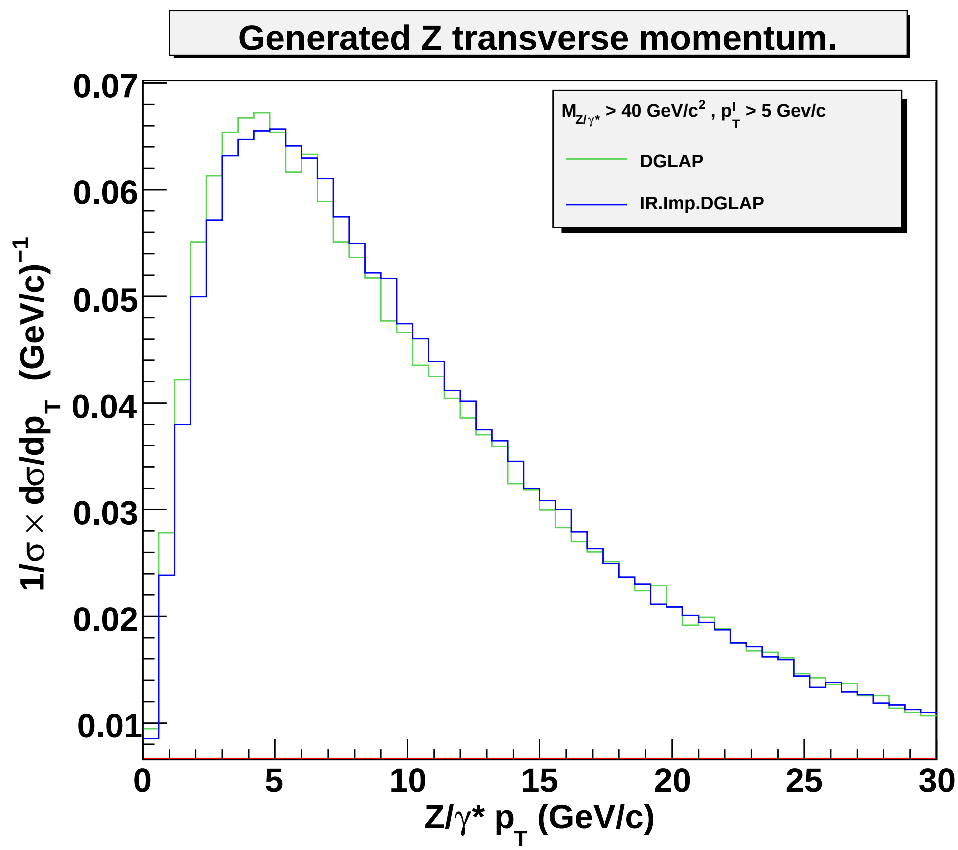

Figure 5.4. The $Z\,p_T$-distribution (ISR parton shower effect) comparison in HERWIG6.5 [7]

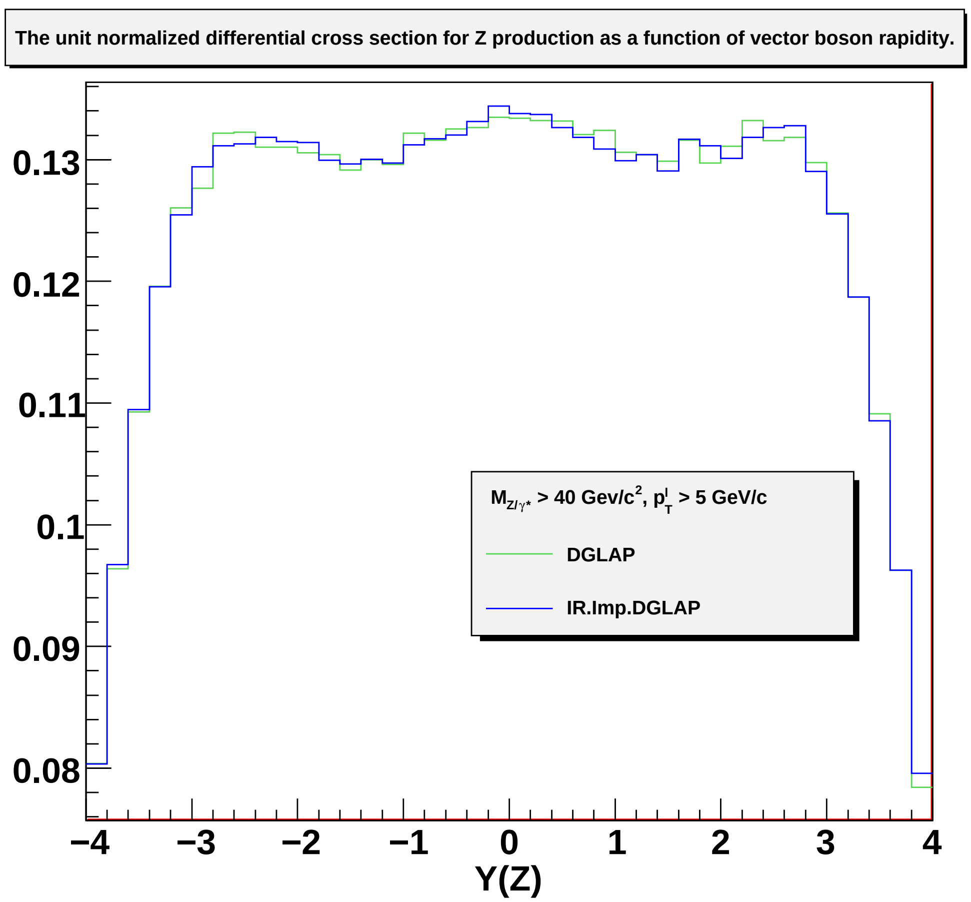

Figure 5.5. The Z rapidity-distribution (ISR parton shower) comparison in HERWIG6.5 [7]

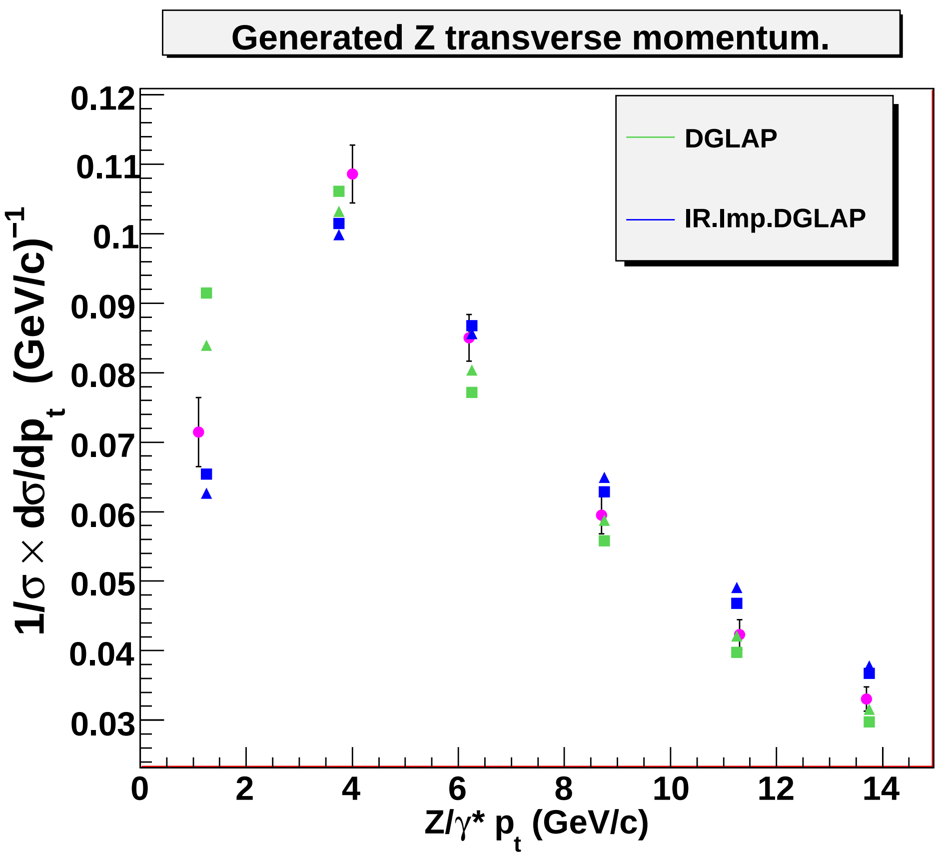

Figure 5.6: Comparison with the FNAL data: D0 p_T spectrum data on (z/γ^*) production to e^+e^- pairs, the circular dots are the data, the blue triangles are HERWIRI1.031, the green triangles are HERWIG6.510, the blue squares are MC@NLO/HERWIRI1.031 and green squares are MC@NLO/HERWIG6.510 [7]

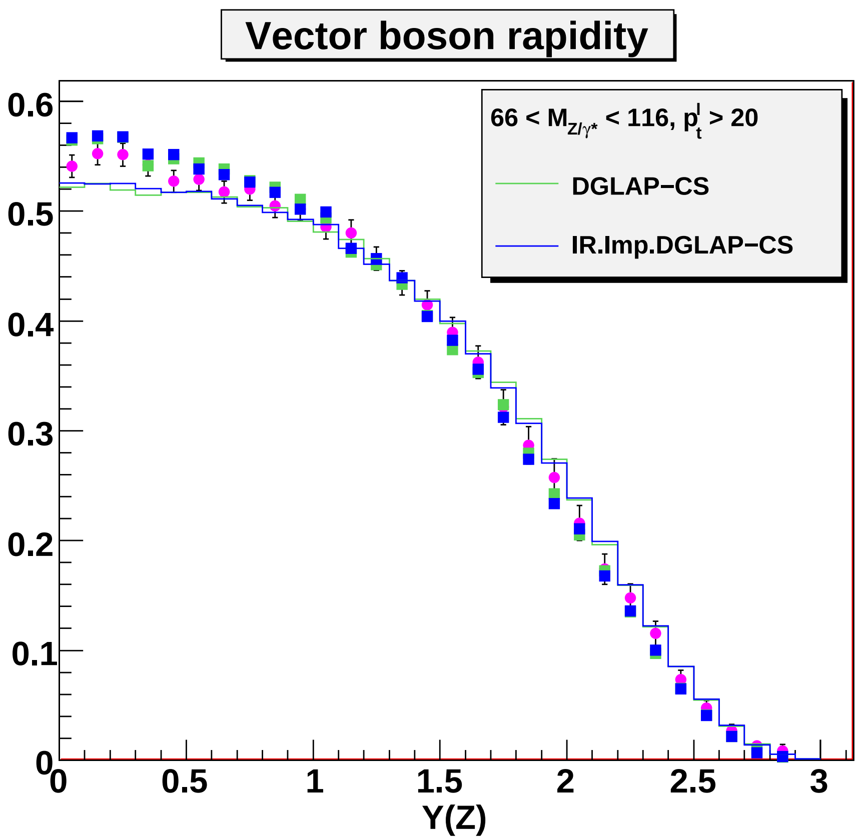

Figure 5.7: Comparison with the FNAL data: CDF rapidity data on (Z/γ^*) production to e^+e^- pairs, the circular dots are the data, the blue squares are MC@NLO/HERWIRI1.031 and the green squares are MC@NLO/HERWIG6.510 [7]

CHAPTER SIX

Results of Comparison of the MC Realization Exact Amplitude-Based Resummation Theory with LHC data and Theoretical Perspectives of Exact Amplitude-Based Resummation Theory

6.1 Results

The comparisons with the FNAL data were encouraging- the IR-improved MC did have better agreement with the data compared to the unimproved MC. The key point is the ability to improve the accuracy of the IR-improved results without physical precision barriers like ad hoc "k_0"-parameters. The new data from the LHC open up a new era for precision in QCD. In the single Z^0/γ^* production with decay to lepton pairs, each of ATLAS and CMS have over 10^7 events, so that in measuring the p_T spectra, each bin will have per mille level statistical precision. Although it is currently not available, we can expect that the respective systematic errors will also be of a similar size. This means that the theoretical errors at the sub-1% regime will be necessary to fully exploit such data.

This exploitation impacts both the comparison between theory and experiment for SM and beyond the SM processes. Indeed, if the theoretical prediction for standard candle processes such as single Z^0/γ^* production and decay to lepton pairs is not under theoretical control,how can we believe any statement that the data for any process, either SM or BSM, is consistent with expectations? Thus, we turn to the new LHC data on single Z^0/γ^* production as a vehicle by which to assess the interplay of our IR-improved amplitude-based results with issues of NLO matrix-element matched MC precision in LHC physics.

In the new MC HERWIRI1.031 [7] is the first realization of the new IR-improved kernels in HERWIG6.5 [8] environment. Using recent LHC data as the baseline HERWIRI1.031 is compared [30] to HERWIG6.510 with and without the exact $\mathcal{O}(\alpha_S)$ correction via MC@NLO. In Fig. (6.1) for the single Z/γ^* production of the LHC the comparison of the CMS rapidity data with the MC theory predictions is given. In Fig. (6.2) the analogous comparison with ATLAS p_T is shown. (See Appendices C and D for the ATLAS and CMS data used here.) The rapidity data are the combined e^+e^-,$\mu^+\mu^-$ results. The p_T data is for the bare e^+e^- case. The results are better appreciated if they are compared to the results obtained in the comparison with the FNAL data on the single Z/γ^* production in $\bar{p}$ collision at 1.96 TeV. It is seen that with the intrinsic rms p_T parameter set to zero in HERWIG6.5, the MC@NLO/HERWIG6.5 gives a good fit to the CDF rapidity distribution data,but does not give a satisfactory fit to the $D0$ p_T spectra.The corresponding comparison the simulation data for MC@NLO/HERWIRI1.031 gives a good fit to both sets of data with PTRMS=0. Here PTRMS corresponds to the rms value of an assumed intrinsic Gaussian distribution in p_T. To get a good fit to both sets of data the authors of HERWIG have put in an intrinsic PTRMS$\cong$ 2 GeV [31, 32]. Therefore in analyzing the new LHC data we have set PTRMS=2.2 GeV in HERWIG6.510 simulation and PTRMS=0 in HERWIRI simulations. In addition, as a cross-check, we have also set PTRMS=0 in HERWIG6.510 simulations. In Fig. (6.1) we show both the results with and without the exact $\mathcal{O}(\alpha_S)$ corrections which are realized using MC@NLO and which we continue to reference as MC@NLO/A, where A = HERWIG6.510, HERWIRI1.031. The difference between the leading order results in the solid lines and their NLO exact ME matched parton shower analog in the squares shows the size of the exact $\mathcal{O}(\alpha_S)$ correction in the CMS rapidity distribution for single Z/γ^* production at the LHC. The latter correction is clearly needed to describe the data. In Fig. (6.2), we show the analogous plots against the ATLAS p_T data. In the case of p_T note that it is important to compare the squares with the corresponding solid lines to see the size of the exact $\mathcal{O}(\alpha_S)$ correction, as these simulations have the same value of PTRMS – the triangles shown in Fig. (6.2) have PTRMS = 0.

Again, we see that the exact $\mathcal{O}(\alpha_S)$ correction is clearly needed to describe the data. Quantitatively, we use the χ^2/d.o.f as a measure of the goodness of the fits. The χ^2/d.o.f for the rapidity and the p_T data are (.72, .72) for MC@NLO/HERWIRI1.031 and (.70,1.37) for MC@NLO/HERWIG6510 (PTRMS = 2.2 GeV) and (.70,2.23) for the MC@NLO/HERWIG6510 (PTRMS = 0 GeV) simulations.

It is expected that differences between the three calculations occur in the soft regime where $p_T \lesssim 7$ GeV, because the IR-improvement takes effect mainly in this regime. Therefore we see the main differences in the Fig. (6.2) between the three predictions is in the regime below 10 GeV. Taking a detailed snapshot of it in Fig. (6.3) with a finer binning of 0.5 GeV/c as compared to 3.0 GeV/c considered in the above figure, we see the differences in more detail. The Fig. (6.3) shows that the three theoretical predictions have significantly different shapes. These are testable with the precise data of the CMS and ATLAS experiments. Specifically with more than 10^7 events in each of ATLAS and CMS, the per mille level accuracy in the finer bins will give well more than 6σ significance for the differences in the three theories.

We note that above $p_T \cong 10$ GeV the three predictions in Fig. (6.2) approach one another. This is as it should be, as they all have the same exact NLO matrix element so that in the hard gluon regime they should approach the same result. This is an important cross check on the correctness of the NLO/ME matching calculus – it shows that the IR-improvement has not spoiled this calculus.

We also show in Fig. (6.4) the Z/γ^* mass spectrum for the MC@NLO/ HERWIRI1.031 (blue squares) and MC@NLO/HERWIG6510(PTRMS=2.2 GeV) (green squares) predictions when the lepton decay satisfies the LHC type requirement that their transverse momenta exceed 20 GeV. The peaks differ by 2.2%. With more than 10^7 events in each of ATLAS and CMS, even if the binning between $\pm\Gamma_Z$ of the resonance, where most of the events lie, is done at .25 GeV/bin, there will be per mille level accuracy on the bins near the peak. This means that 2.2% differences will be seen with well beyond 10σ significance. Here, $\Gamma_Z \cong 2.5$ GeV is the Z boson width. From this we see that the high precision data from LHC ATLAS and CMS experiments will allow one to distinguish between the two sets of theoretical predictions.

We may note that the differences seen in Figs. (6.3) and (6.4) are consistent with the results in Fig. (4.1) for the difference in the radiation probability between the IR-improved and the unimproved cases. The radiation probabilities differ mainly in the low virtuality regime, the soft regime. This led to the expectation that the main differences in Fig. (6.3) would be in the soft regime, as noted above. In Fig.(6.4), we see main differences in the regime near the Z peak, where, because of the small value of the Z width Γ_Z, only soft radiation is allowed so that again the soft regime is probed.

The results on the rapidity in Fig. (6.1) are also consistent with those in Fig. (4.1). This obtains because the rapidity distribution integrates over all values of p_T consistent with a given value of rapidity and the integrals of the curves in Fig. (4.1) are normalized to the same value when implemented on the MC.

Our results show that our new IR-improved MC realization opens the way to a rigorous path to the sub-1% precision regime for standard candle processes at the LHC, as required by the new LHC data. How does it compare with the existing paradigms in this connection? We turn to this question in the next section.

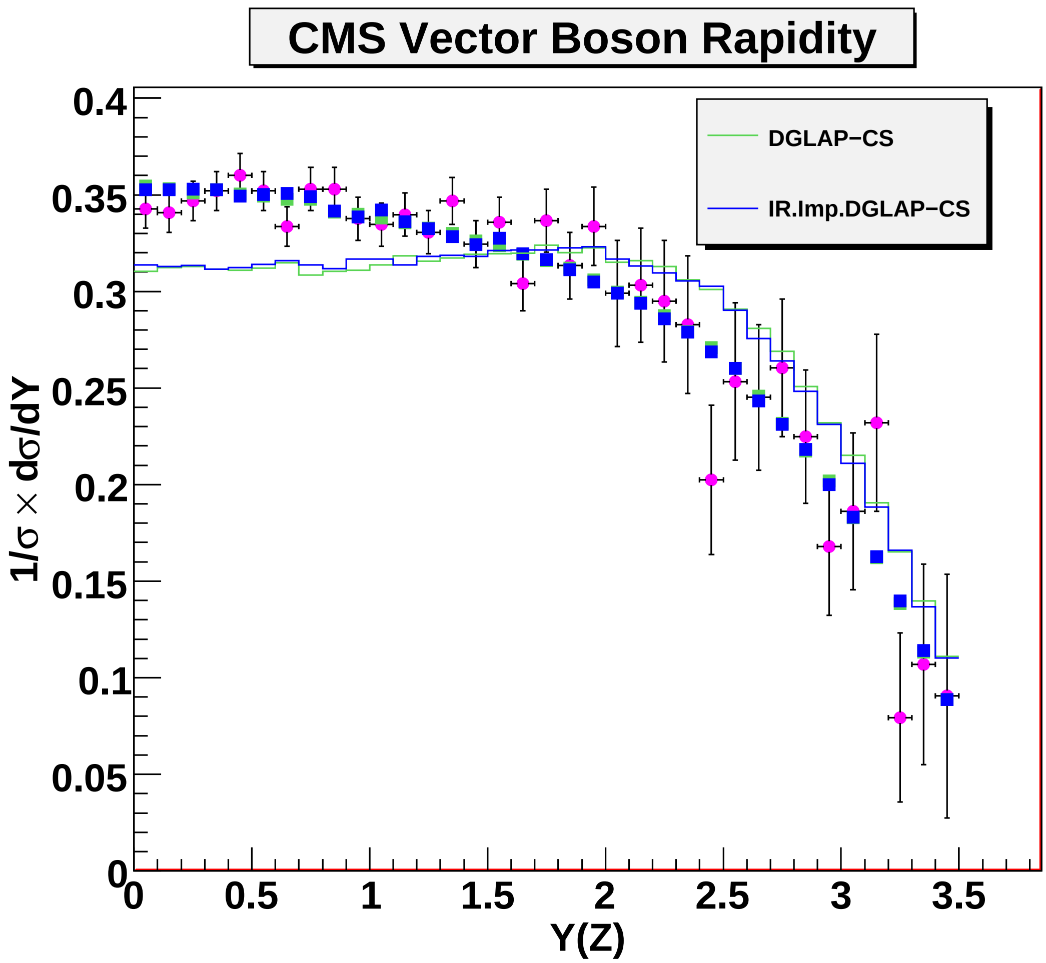

Figure 6.1: Comparison of the LHC data: CMS rapidity data on Z/γ^* production to e^+e^-, $\mu^+\mu^-$ pairs, the circular dots are the data, the green(blue) lines are HERWIG6.510(HERWIRI1.031), the blue(green) squares are MC@NLO/HERWIRI1.031(MC@NLO/HERWIG6.510(PTRMS=2.2 GeV)). [30, 33]

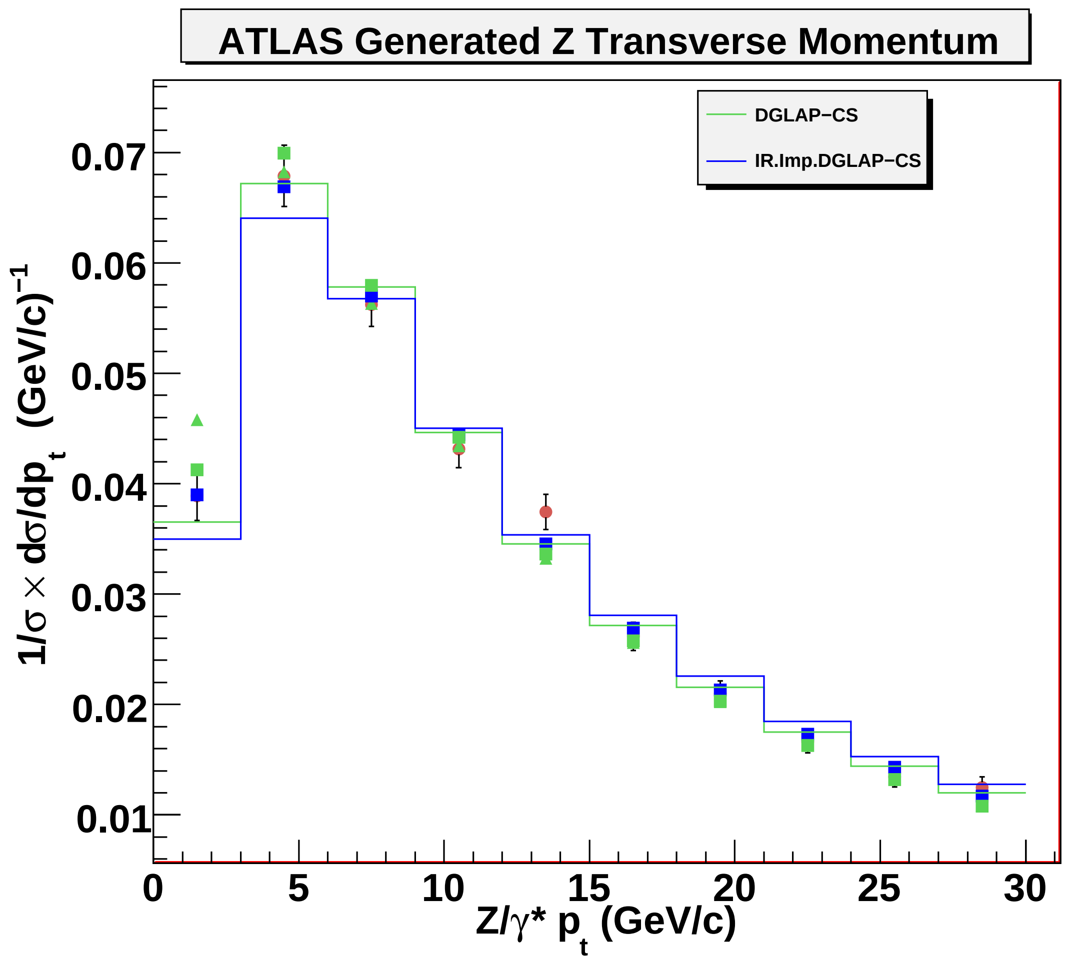

Figure 6.2: Comparison with LHC data: ATLAS p_T spectrum data on the Z/γ^* production to (bare) e^+e^- pairs, the circular dots are data, the blue(green)lines are HERWIRI1.031(HERWIG6.510), the blue(green) squares are MC@NLO/HERWIRI1.031(MC@NLO/HERWIG6.510(PTRMS=2.2 GeV)) and the green triangles are MC@NLO/HERWIG6.510(PTRMS=0). These are otherwise untuned theoretical results. [30, 34]

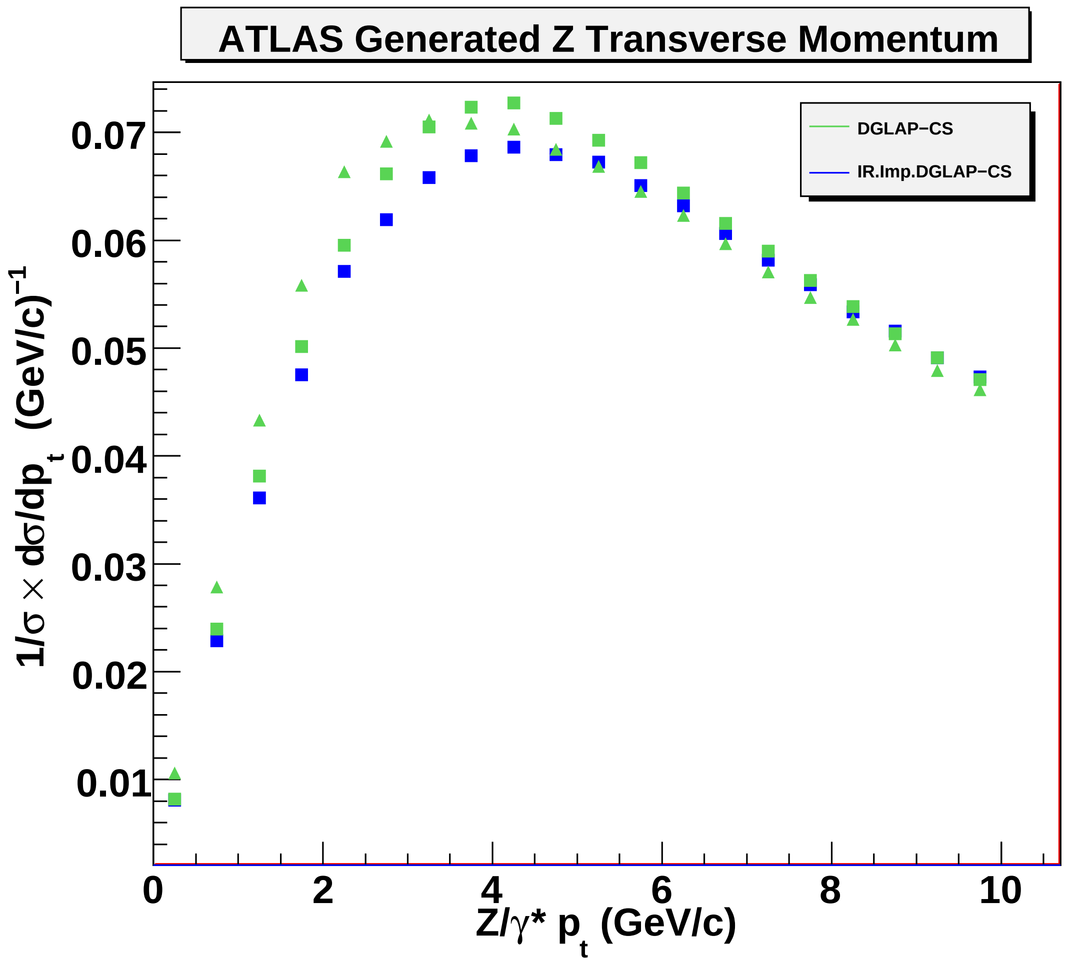

Figure 6.3: The normalized vector boson p_T spectrum at the LHC for the ATLAS cuts as exhibited in Fig. (6.2) for the same conventions on the notation for the theoretical results with vector boson $p_T < 10$ GeV to illustrate the differences between the three predictions. [30]

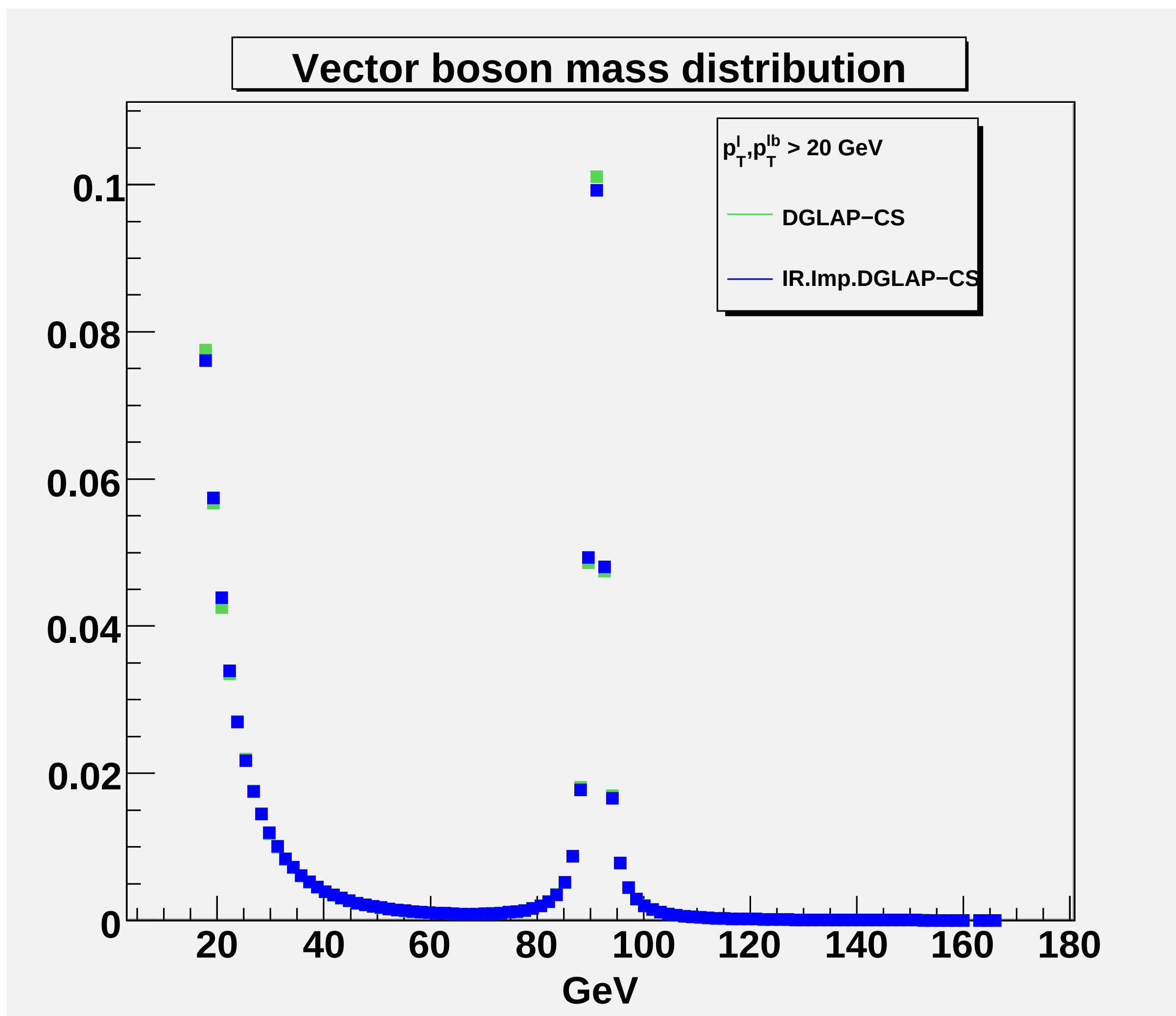

Figure 6.4: Normalized vector boson mass spectrum at the LHC for p_T(lepton) > 20 GeV. [30]

It is therefore seen that in order to reproduce the LHC data on the p_T distribution of the Z/γ^* in the pp collision the usual DGLAP-CS kernels require a hard intrinsic PTRMS. The hardness of the PTRMS required is completely ad-hoc, it is in disagreement with the already existing proton wave function models [35], where the scale of corresponding intrinsic PTRMS is found to $\lesssim 0.4$ GeV. Also it contradicts the the experimental observations of the precociousness of the Bjorken scaling [22]. (See Appendix E for the explanation of Bjorken scaling.)The SLAC-MIT experiment [36] on the deep inelastic electron-proton scattering process show that the Bjorken scaling occurs already at $Q^2 = 1_+$ GeV^2 for $Q^2 = -q^2$ where q is the 4-momentum transfer from the electron to proton. Since the corrections to Bjorken scaling from intrinsic p_T are $\mathcal{O}(p_T^2/Q^2)$, this precociousness is impossible for PTRMS $\cong 2$ GeV. What we therefore now advocate is that the ad hoc "hardness" of the PTRMS $\cong 2.2$ GeV value is just a phenomenological representation of the more fundamental dynamics described by the IR-improved DGLAP-CS theory because, if the proton constituents really had a Gaussian intrinsic p_T distribution with PTRMS $\cong 2$ GeV , the pioneering SLAC-MIT observations would not be possible.

In order to link the experimental results with the theoretical predictions we start with the fully differential representation of a hard LHC scattering process:

$$d\sigma = \sum_{i,j} \int dx_1 dx_2 F_i(x_1) F_j(x_2) d\hat{\sigma}_{res}(x_1 x_2 s), \tag{6.1}$$

where $\{F_j\}$ and $d\hat{\sigma}_{res}$ are the parton densities and the reduced hard differential cross section respectively. The subscript on $d\hat{\sigma}_{res}$ indicates that it has been resummed for all large EW and QCD higher order corrections in a manner consistent with achieving a total precision tag of 1% or better for the total theoretical precision of (6.1). The proof of the correctness of the value of the total theoretical precision $\Delta\sigma_{th}$ of (6.1) is the key theoretical issue for the realization of precision QCD for the LHC. The theoretical precision can therefore be written as [30]

$$\Delta\sigma_{th} = \Delta F \oplus \Delta\hat{\sigma}_{res}, \tag{6.2}$$

where ΔA is the contribution to the uncertainty on the quantity A to $\Delta\sigma_{th}$. Here we discuss the situation in which the two errors in (6.2) are independent. Therefore (6.2) has to be modified when the two errors are not independent. The proof of the correctness is indispensable to validate the application of a given theoretical prediction to precision experimental observations for the discussion of the background and the signals of both the SM and new physics (NP) studies, specifically the overall normalization in such studies. If a calculation is used with an unknown value of $\Delta\sigma_{th}$ the NP itself can very well be missed.

We note that $\Delta\sigma_{th}$ [37] is the total theoretical uncertainty that derives from the physical and technical precision contributions. The physical precision contribution, $\Delta\sigma_{th}^{phys}$, from sources such as missing graphs, approximations to graphs, truncations, etc. The technical precision contribution, $\Delta\sigma_{th}^{tech}$, from sources such as bugs in codes, numerical rounding errors, convergence issues, etc. When bugs in codes are referenced, we have in mind that all gross errors such as those that give obviously wrong results,as determined by cross checks, are eliminated and only programming errors are left such as those in the logic: suppose for programming error reasons a DO-loop ends at 999 steps instead of the intended 1000 steps, resulting in a per mille level error, that could alternate in sign from event to event. As per mille level accuracy is good enough in many applications, the program would remain reliable, but it would have what we call a technical precision error at the per mille level. With that understanding, we may write the total theoretical error as

$$\Delta\sigma_{th} = \Delta\sigma_{th}^{phys} \oplus \Delta\sigma_{th}^{tech}. \tag{6.3}$$

Even though the desired value for $\Delta\sigma_{th}$ depends on the specific requirements of the observations, as a general rule, it should fulfill $\Delta\sigma_{th} \leq f\Delta\sigma_{expt}$, where $\Delta\sigma_{expt}$ is the respective experimental error and $f \lesssim \frac{1}{2}$. This is so that the theoretical uncertainty does not adversely affect the physics analysis of the data.

In the interest of completeness we recapitulate the theory developed in Chapter 2 which is the QCD $\otimes$ QED resummation theory for the reduced cross section. The master formula, which applies to both to resummation of the reduced cross section and to the evolution of the parton densities, is identified as

$$\begin{aligned} d\bar{\sigma}_{res} = e^{SUM_{IR}(\text{QCED})} \sum_{n,m=0}^{\infty} \frac{1}{n!m!} \int \prod_{j_1=1}^{n} \frac{d^3 k_{j_1}}{k_{j_1}} \\ \prod_{j_2}^{m} \frac{d^3 k'_{j_2}}{k'_{j_2}} \int \frac{d^4 y}{(2\pi)^4} e^{iy\cdot(p_1+q_1-p_2-q_2-\sum_j k_j)+D_{\text{QCED}}} \\ * \tilde{\bar{\beta}}_{n,m}(k_1,\ldots,k_n;k'_1,\ldots,k'_m) \frac{d^3 p_2}{p_2^0} \frac{d^3 q_2}{q_2^0}, \end{aligned} \tag{6.4}$$

where $d\bar{\sigma}_{res}$ is either the reduced cross section $d\bar{\sigma}_{res}$ or the differential rate associated to the DGLAP-CS [3, 4] kernel involved in the evolution of the $\{F_j\}$ and where the new YFS residuals, $\tilde{\bar{\beta}}_{n,m}(k_1,\ldots,k_n;k'_1,\ldots,k'_m)$, with n hard gluons and m hard photons represent the successive application of the YFS expansion. In this case we again make the following replacements

$$\begin{aligned} B^{nls}_{\text{QCD}} &\rightarrow B^{nls}_{\text{QCD}} + B^{nls}_{\text{QED}} \equiv B^{nls}_{\text{QCED}} \\ \tilde{B}^{nls}_{\text{QCD}} &\rightarrow \tilde{B}^{nls}_{\text{QCD}} + \tilde{B}^{nls}_{\text{QED}} \equiv \tilde{B}^{nls}_{\text{QCED}} \\ \tilde{S}^{nls}_{\text{QCD}} &\rightarrow \tilde{S}^{nls}_{\text{QCD}} + \tilde{S}^{nls}_{\text{QED}} \equiv \tilde{S}^{nls}_{\text{QCED}} \end{aligned} \tag{6.5}$$

in the YFS [17] exponentiation algebra. Here the superscript *nls* denotes again the infrared functions are DGLAP-CS synthesized [3, 4]. Compared to chapter 2 we have interchanged the order of the gluons and photons without loss of physical content.

The infrared functions are now again given by

$$
\begin{aligned}
SUM_{IR}(\text{QCED}) &= 2\alpha_S \mathcal{R} B^{nls}_{\text{QCED}} + 2\alpha_S \tilde{B}^{nls}_{\text{QCED}} \\
D_{\text{QCED}} &= \int \frac{dk}{k^0}(e^{-iky} - \theta(K_{max} - k^0))\tilde{S}^{nls}_{\text{QCED}}
\end{aligned} \tag{6.6}
$$

which is independent of K_{max}. However again the dummies in QCD and QED were set to the same value for the purpose of the calculation. This is still denoted as Quantum ChromoElectroDynamics (QCED). In (6.6) $SUM_{IR}(\text{QCED})$ still sums up to the infinite order the maximal leading IR singular terms in the cross section for soft emission below a dummy parameter K_{max}, D_{QCED} [1] does the same for the regime above K_{max}, which therefore implies that (6.6) is independent of K_{max}, as interchanging the roles of gluons and photons does not affect the independence on K_{max}. Here the entire soft gluon phase space is included in the representation. In order to maintain exactness order by order in perturbation theory in both α and α_S in the presence of the resummed terms, we generate the residuals $\tilde{\bar{\beta}}_{n,m}$ by iterative computation to match the attendant exact results to all orders in α and α_S.Following Ref. [10], the new non-Abelian residuals $\tilde{\bar{\beta}}_{m,n}$ allow rigorous shower/ME matching via their shower subtracted analogs: in (6.4) we make the replacement

$$
\tilde{\bar{\beta}}_{n,m} \rightarrow \hat{\tilde{\bar{\beta}}}_{n,m} \tag{6.7}
$$

where the $\hat{\tilde{\bar{\beta}}}_{n,m}$ have had all effects in the shower associated to the $\{F_j\}$ removed from them.To see how contact is made with $\hat{\tilde{\bar{\beta}}}_{n,m}$ and the differential distributions in MC@NLO we see that the MC@NLO differential cross section is represented by

$$
\begin{aligned}
d\sigma_{MC@NLO} = {} & [B + V + \int (R_{MC} - C)d\Phi_R]d\Phi_B[\Delta_{MC}(0) + \int (R_{MC}/B)\Delta_{MC}(k_T d\Phi_R)] \\
& + (R - R_{MC})\Delta_C(k_T)d\Phi_B d\Phi_R
\end{aligned} \tag{6.8}
$$

[1] If we want to include more of the maximal exponentiating terms from the formalism of Ref. [21] in the two exponents $SUM_{IR}(\text{QCED})$, D_{QCED}, we may do so with a consequent change in the attendant residuals $\tilde{\bar{\beta}}_{n,m}$.

where B is the Born distribution, V is the regularized virtual contribution, C is the corresponding counter-term required at the exact NLO, R is the respective real emission distribution for exact NLO, $R_{MC} = R_{MC}(P_{AB})$ is the parton shower real emission distribution such that the Sudakov form factor is given by

$$\Delta_{MC}(p_T) = e^{\left[-\int d\Phi_R \frac{R_{MC}(\Phi_B,\Phi_R)}{B}\theta(k_T(\Phi_B,\Phi_R)-p_T)\right]} \tag{6.9}$$

where as usual it describes the respective no-emission probability. The respective Born and real emission differential phase spaces are denoted by $d\Phi_A$, A=B,R, respectively.

In Refs. [5, 6] it has been shown that our approach is consistent with the methods in Refs. [38, 39]. However the methods in [38, 39] gives approximations to the hard gluon residuals $\hat{\bar{\bar{\beta}}}_{n,0}$ as they are not exact results. In the threshold resummation methods in [38], the non-singular contributions to the cross sections at $z \to 1$ are dropped in resumming the logs in n-Mellin space using

$$\mid \int_0^1 dz z^{n-1} f(z) \mid \leq (\frac{1}{n}) \max_{z\in[0,1]} |f(z)|, \tag{6.10}$$

for any integrable function $f(z)$. In Ref. [39], the SCET theory, the terms of $\mathcal{O}(\lambda)$ are dropped at the amplitude level. There $\lambda = \sqrt{\frac{\Lambda}{Q}}$ with $\Lambda \sim .3$ GeV so that $\lambda \cong 5.5\%$ with $Q \sim 100$ GeV. As the two approaches are equivalent, the error in the threshold resummation is similar. Therefore these approaches can only be used as guide to the non-Abelian residuals $\hat{\bar{\bar{\beta}}}_{n,0}$ that are developed for the (sub-)1% precision regime.

We continue the consistency discussion with the Refs. [40, 41] which is again an approximate formalism. This theory is used widely at the LHC. The theory is also used in the data analysis for the Tevatron. See for example the recent analysis in Ref. [42] where this theory, as it is implemented in the MC integration program ResBos [43, 44, 45], is compared to recent LHC data and to recent analysis of Tevatron data. The question is whether the theory in Refs. [40, 41] can be used to reach $\leq 1\%$ physical precision for the QCD predictions. Let us note that the authors in Ref. [41] give us a hint to the answer to our question in their footnote on the journal page with number 215 for the paper, wherein they equate as 'negligible' 20% in discussing possible nonperturbative contributions in their formalism. Let us keep this footnote in mind in what follows.

The defining formula in the Refs. [40, 41] is that for the differential cross section for the p_T distribution for the production of heavy gauge bosons in the hadron-hadron collision. Here we specify the Drell-Yan γ^* production[2] , as

$$\frac{d\sigma}{dQ^2dydQ_T^2} \sim \frac{4\pi^2\alpha^2}{9Q^2s}\left\{\int \frac{d^2b}{(2\pi)^2}e^{i\vec{Q_T}.\vec{b}}\widetilde{W}(b;Q,x_A,x_B) + Y(Q_T;Q,x_A,x_B)\right\}, \quad (6.11)$$

where, $\vec{Q}_T = \vec{p}_T$ is the γ^* transverse momentum. A,B are the protons at LHC, s is the cms squared energy of the protons. Q^μ is the γ^* 4-momentum and Q^2 is the mass squared. $y = \frac{1}{2}\ln(\frac{Q^+}{Q^-})$ is the γ^* rapidity such that $x_A = e^y\frac{Q}{\sqrt{s}}$ and $x_B = e^{-y}\frac{Q}{\sqrt{s}}$. Also, Q is near M_Z here. The term involving $\widetilde{W}$ carries the effect from QCD resummation and the Y term includes those contributions which are regular at $Q_T = p_T \to 0$ as in Refs. [40, 41] that is, order by order in perturbation theory they are divided from parts of the hard scattering coefficients that are less singular than,$Q_T^2\times$(logs or 1) or $\delta(\vec{Q}_T)$ as $Q_T = p_T \to 0$. The Y term is perturbative and can be computed up to the required accuracy using the standard methods. Therefore, the question is regarding the precision of the $\widetilde{W}$.

Therefore, when $b << \frac{1}{\Lambda}$ where Λ is a hadronic mass scale like the inverse of the proton radius from Refs. [40, 41], we get

$$\widetilde{W}(b;Q,x_A,x_B) = \sum_{a,b}\int_{x_A}^1 d\xi_A\int_{x_B}^1 d\xi_B F_{\frac{a}{A}}(\xi_A;\mu)F_{\frac{b}{B}}(\xi_B;\mu)e^{-S_{SC}}$$
$$\times\sum_j e_j^2 C_{ja}(\frac{x_A}{\xi_A},b;\frac{C_1}{C_2};g(\mu),\mu)C_{jb}(\frac{x_B}{\xi_B},b;\frac{C_1}{C_2};g(\mu),\mu), \quad (6.12)$$

[2] The analogous results for the $W^\pm$ and Z/γ^* are obtained by straightforward substitutional manipulations of the EW aspects of the formula we record here as described in Ref. [41] so that we omit such manipulations here without loss of content of the QCD aspects of our discussion.

where [40, 41]

$$S_{SC} = \int_{\frac{C_1^2}{b^2}}^{C_2^2 Q^2} \frac{d\bar{\mu}^2}{\bar{\mu}^2} [\ln(\frac{C_2^2 Q^2}{\bar{\mu}^2}) A(g(\mu); C_1) + B(g(\bar{\mu}); C_1, C_2)]. \tag{6.13}$$

Here, we show the explicit dependences of the parton density functions $\{F_l\}$ and the dependences of the perturbatively calculable exponentiation and scattering coefficient functions A, B and C as given in the Refs. [40, 41]. The μ is usually set to $\frac{C_1}{b}$ and C_1 and C_2 are order 1 constant. The result for $\widetilde{W}$ is accurate up to terms $\mathcal{O}(\frac{m_q}{Q}, \frac{1}{(bQ)})$ when $\frac{1}{Q} << b << \frac{1}{\Lambda}$ where m_q represents the quark masses. Also, according to Refs. [40, 41] the terms of $\mathcal{O}(\frac{m_q}{Q}, \frac{Q_T}{Q})$ are dropped in the regime $0 \leq Q_T << Q$ in (6.11).

Now considering the regime $b \gtrsim \frac{1}{\Lambda}$, according to Refs. [40, 41] the functions A,B and C have to be replaced according to

$$\begin{aligned}
&A(g(\bar{\mu}); C_1) \to A(g(\bar{\mu}), m_q/\bar{\mu}; C_1) \\
&B(g(\bar{\mu}); C_1, C_2) \to B(g(\bar{\mu}), m_q/\bar{\mu}; C_1, C_2) \\
&\sum_{a,b} \int_{x_A}^1 d\xi_A \int_{x_B}^1 d\xi_B F_{a/A}(\xi_A; \mu) F_{b/B}(\xi_B; \mu) \sum_j e_j^2 C_{ja}(x_A/\xi_A, b; C_1/C_2; g(\mu), \mu) \\
&\times C_{jb}(x_B/\xi_B, b; C_1/C_2; g(\mu), \mu) \to \sum_j e_j^2 \bar{\mathcal{P}}_{j/A}(x_A, b; C_1/C_2) \bar{\mathcal{P}}_{j/B}(x_B, b; C_1/C_2).
\end{aligned} \tag{6.14}$$

It can be seen then the quark masses cannot be neglected anymore and the convolutions $C * F$ are no longer appropriate.

From Refs. [40, 41], the two results for the regimes $b << \frac{1}{\Lambda}$ and $b \gtrsim \frac{1}{\Lambda}$ are joined as follows. Define

$$\widetilde{W}(b; Q, x_A, x_B) \equiv \sum_j e_j^2 \widetilde{W}_j(b; Q, x_A, x_B), \tag{6.15}$$

which is well defined in both the regimes. Considering b_{max} to be a parameter in the perturbative regime we can write

$$\widetilde{W}_j(b; Q, x_A, x_B) = \widetilde{W}_j(b^*; Q, x_A, x_B) e^{\{-\ln(Q^2/Q_0^2) g_1(b) - g_{j/A}(x_A, b) - g_{j/B}(x_B, b)\}}, \tag{6.16}$$

where g_1,$g_{j/A}$,$g_{j/B}$ have non-perturbative content and

$$b^* = b/\sqrt{1+b^2/b^2_{\rm max}}. \tag{6.17}$$

With the definition above, Refs. [40, 41] arrive at the following conclusion

$$\frac{d\sigma}{dQ^2dydQ_T^2} \sim \frac{4\pi^2\alpha^2}{9Q^2s}\left\{\int\frac{d^2b}{(2\pi)^2}e^{i\vec{Q}_T\cdot\vec{b}}\sum_j e_j^2\widetilde{W}_j(b^*;Q,x_A,x_B)\right.$$
$$\left.\times\, e^{\{-\ln(Q^2/Q_0^2)g_1(b)-g_{j/A}(x_A,b)-g_{j/B}(x_B,b)\}} \;+\; Y(Q_T;Q,x_A,x_B)\right\}. \tag{6.18}$$

Now in ResBos in Refs. [43, 44] the following three realizations of the non-perturbative functions are used:

$$\ln(Q^2/Q_0^2)g_1(b) + g_{j/A}(x_A,b) + g_{j/B}(x_B,b)$$
$$= \begin{cases} [g_1+g_2\ln(Q/(2Q_0))]b^2, \text{ DWS [46]} \\ [g_1+g_2\ln(Q/(2Q_0))]b^2 + g_1g_3\ln(100x_Ax_B)b, \text{ LY [43]} \\ [g_1+g_2\ln(Q/(2Q_0)) + g_1g_3\ln(100x_Ax_B)]b^2, \text{ BLNY [44].} \end{cases} \tag{6.19}$$

The g_i are the parameters on the RHS of (6.19). The best fit to the data considered in Ref. [44] was obtained from the BLNY parametrization with the values

$$g_1 = 0.21^{+0.01}_{-0.01}\ \text{GeV}^2,\ g_2 = 0.68^{+0.01}_{-0.02}\ \text{GeV}^2,\ g_3 = -0.6^{+0.05}_{-0.04} \tag{6.20}$$

when $b_{max} = 0.5\ \text{GeV}^{-1}$ and $Q_0 = 1.6$ GeV.

On the question of the physical precision of (6.18) it is observed that, with the errors shown on the constants g_i for the best BLNY parametrization, the -0.02 error on g_2 represents already a 1.5% uncertainty at the saddle point position for the integration over b in the respective Z analogue of (6.11). This exceeds the theory error budget in precision QCD that we advocate here. On the LHS of (6.18) the g_l which do not (do) multiply $\ln(\frac{Q}{Q_0})$ are unspecified *functions* of $x_j, b(b)$ that are required to vanish at $b=0$ while on the RHS these dependencies are simplified to second order polynomials in b and either no or linear $\ln(x_A x_B)$ dependence on x_j. These simplifications are generically ad hoc and cannot be considered as a rigorous platform for testing the fundamental QCD theory.[3]

Now, on the question of the physical precision of (6.18), we note that in the regime $0 \leq Q_T \leq Q$ it has an error of $\mathcal{O}(Q_T/Q)$ as such terms have been dropped, order by order in perturbation theory in the construction of $\widetilde{W}_j$. For $Q = M_Z$ and $Q_T = 5$ GeV, there is an error of $\cong 5.5\%$ and it is twice this size at $Q_T = 10$ GeV. This shows that the formalism in [40, 41] cannot be used for (sub-)1% theory predictions for the heavy gauge boson p_T spectrum at the LHC.[4] At $Q_T = 0$ following Parisi and Petronzio in Refs. [47], the integral over $\vec{b}$ in (6.11)is dominated by a saddle point at

$$b_{SP} = \frac{1}{\Lambda}(\frac{Q}{\Lambda})^{-A^{(1)}/(A^{(1)}+\beta_1)} \tag{6.21}$$

where we have $A = \sum_N A^{(N)}(\alpha_S/\pi)^N$ and $\beta_1 = \frac{1}{12}(33 - 2N_F)$ where N_F is the number of effective quark flavors which we take as 5 here. Then we have $A^{(1)} = 4/3$ so that

$$b_{SP} = \frac{1}{\Lambda}(\frac{Q}{\Lambda})^{-0.41}. \tag{6.22}$$

---

[3] Note that, with the IR-improvement of the parton shower in HERWIRI1.031, there is no longer any need even for an IR cut-off parameter, as all formerly IR-divergent integrals now converge; there is no issue of the validity of perturbation theory in the shower because the shower resums the large logs in it to all orders in α_S; the shower runs down to the hadronization scale ~ 1 GeV and the transition to hadrons is a smooth one due to local parton hadron duality [46]and the precociousness of Bjorken scaling [22, 36] which occurs already at 1_+ GeV^2 – the properties of the shower such as its p_T and its energy are independent of the transition to hadrons to very high accuracy. No arbitrary ad hoc parameters that affect resummed results from the shower such as the parameters in (6.19) appear – even the un-IR-improved parton shower in HERWIG6.5 is well-behaved at small p_T and no part of the result of $\mathcal{O}(Q_T/Q)$ in (6.4) is just dropped as it is in (6.18).

[4] We stress that in any given realization of (6.18) such as that in Ref. [45] the quantity Y is known only to a finite order in α_S, in the latter reference this is to first order in α_S. This means that the physical precision error $\mathcal{O}(Q_T/Q)$ on the part of the resummed singular part of (6.18) from $\mathcal{O}(\alpha_S^n)$, $n \geq 2$, cannot be compensated by Y in Ref. [45], for example. If Y is known to $\mathcal{O}(\alpha_S^n)$, physical precision error $\mathcal{O}(Q_T/Q)$ from the $\widetilde{W}_j$ part of (6.18) from $\mathcal{O}(\alpha_S^m)$, $m \geq n+1$, cannot be compensated by Y even in principle.

For $Q = M_Z$ we get, $b_{SP} \cong .48\ \mathrm{GeV}^{-1}$ and we take $\Lambda = 0.15$ GeV [41]. This result for b_{SP} is in the perturbative regime. Also, from [40, 41] we know that the error on the Z production analogue of $\widetilde{W}_j$ at this point is $\mathcal{O}(1/(b_{SP}M_Z)) \cong 2.3\%$.Thus, even when (6.12) is reliable in the perturbative regime, the error is too large. From comparison of ATLAS and Tevatron data related to the p_T spectrum in single Z/γ^* in Ref. [42] it can be seen that ResBos misses the data by 2% for the p_T near 0 and it misses the data by $\gtrsim 5\%$ for the regime of $p_T \gtrsim 10$ GeV, and is consistent with our estimate of the physical precision. The non-perturbative factor in (6.18) compromises the predictive power of the formalism in Refs. [40, 41]. In the Ref. [46] it is argued that for W, Z production considered here the prediction in (6.18) is insensitive to the non-perturbative parametrization in (6.19) in the regime 6 GeV $< Q_T <$ 16 GeV. This indicates that the effects discussed above are the main obstacles to using Refs. [40, 41] for the precision QCD physics predictions at the LHC in the latter regime for the precision at or below 1%. Ref. [48] presents another version of (6.11) with the same physical precision as realized in ResBos with different treatment of the non-perturbative regime. So comparison to the data in Ref. [42] in the perturbative regime, our physical precision estimate for this regime also applies to the realization of (6.11) in Ref. [48]. It cannot be therefore used for the study of 1% precision LHC physics.

Ref. [48] discusses the uncertainty in their results as a function of the variation of the values associated with their renormalization, factorization and resummation scales. They estimate, for example, that this is at the level of 10% near the peak of the Q_T spectrum in the single Z/γ^* production at the LHC. These uncertainties can in principle be reduced by computing the perturbative terms in their results to higher and higher orders. Also an additional PDF error is estimated at this region at the level of 2%. This in principle can be reduced by improving the determination of the respective PDF's. The error in the defining result (6.18) derived in Refs. [40, 41]

on which their results are based is an error of $\mathcal{O}(Q_T/Q)$ that applies order by order in the perturbation theory - it is separate from the scale and PDF errors discussed in Ref. [48].

The SCET theory approach used in Ref. [49] is used to recover (6.18) and it is explicitly shown that the improvement of the perturbative scale errors indeed occurs when higher order corrections are included in the calculation of the perturbative terms in the respective SCET realization of (6.18). The error that we discuss here of $\mathcal{O}(Q_T/Q)$ due to the approximations in the defining derivations of (6.18)in Refs. [40, 41] also applies to the order-by-order results in Ref. [49]. As noted above, SCET involves for single Z production at the LHC the defining error $\sqrt{\Lambda/M_Z} \equiv 5.7\%$ for the typical hadronic transverse size $\Lambda \cong 0.3$ GeV and this is consistent with the approximations made in Refs. [40, 41]. Such approximations cannot be used for the 1% precision QCD theory.

In summary we see that even though a new variable Q_T-related variable [50] is used in some of the comparisons, $\phi^*_\eta = \tan\left(\frac{1}{2}(\pi - \Delta\phi)\right)\sin\theta^* \cong |\sum \frac{p_{iT}\sin\phi_i}{Q}| + \mathcal{O}(\frac{p_{iT}^2}{Q^2})$, where $\Delta\phi = \phi_1 - \phi_2$ is the azimuthal angle between the two leptons which have transverse momenta p_{iT}, $i = 1, 2$ and θ^* is the scattering angle of the dilepton system relative to the beam direction when one boosts to the frame along the beam direction such that the leptons are back to back, it is seen that $\phi^*_\eta-$comparisons also show the underlying physical precision error associated with defining (6.11); as expected the comparisons are somewhat better than the Q_T spectra comparisons because this ϕ^*_η is more inclusive - two different values of Q_T with corresponding compensating differences in the attendant ϕ_i can have the same value of ϕ^*_η. From the discussions just completed, we see that, in order to have a strict control on the theoretical precision in (6.1), we need both the resummation of the reduced cross section and that of the attendant evolution of $\{F_j\}$.

To demonstrate the above from Ref. [34] in Fig. (6.5) we compare the measurement to the predictions of pQCD calculations as well as of different generators. The $\mathcal{O}(\alpha_S)$ and $\mathcal{O}(\alpha_S^2)$ pQCD predictions of the p_T dependent cross section are obtained using FEWZ and MSTW PDF sets. Around the scale $\mu_R = \mu_F = M_Z$ with the constraint $0.5 \leq \mu_R/\mu_F \leq 2$, the uncertainties on the normalized predictions are evaluated by variation of the normalization and factorization scales by factors of 2, with a range corresponding to 90% confidence-level limits, by variation of α_S and by using the PDF error eigenvector sets. With a dominant contribution of 9% and 6.5% from the scale variations, the above amount to $\sim$ 10% and $\sim$ 8% for $\mathcal{O}(\alpha_S)$ and $\mathcal{O}(\alpha_S^2)$ prediction respectively. The p_T distribution suffers from scale uncertainty. This indicates non-negligible missing higher order corrections. The above measurements are also compared to the predictions of RESBOS and various other event generators. The RESBOS prediction is based on CTEQ6.6. The general consistency with data is verified using a χ^2 test. The data deviates from RESBOS by 2.5% for low p_T and by 5% for larger value of p_T. Continuing to further demonstrate, following Ref. [42] we show in Fig. (6.6) the ratio of combined normalized differential cross section to RESBOS [43, 44, 45], a QCD calculation by A. Banfi [48] and that obtained from FEWZ. The CTEQ6M PDF set is used in [48]. For FEWZ the PDF set CT10 is used. The uncertainties are evaluated as explained above. The difference between RESBOS prediction and data is $\sim$ 2% for $\phi^*_\eta < 0.1$, increasing to 5% for higher ϕ^*_η values. The description provided by A. Banfi [48] is not better than RESBOS. The prediction of FEWZ undershoots the data by $\sim$ 10%. The predictions of FEWZ is only given for $\phi^*_\eta > 0.1$, as it diverges away from the data for lower values - it needs IR-improvement.

These results corroborate the physical precision error estimates made above for attendant approaches. What this means is that we have opened the way to something fundamentally new: a practical way to achieve sub 1% precision results via

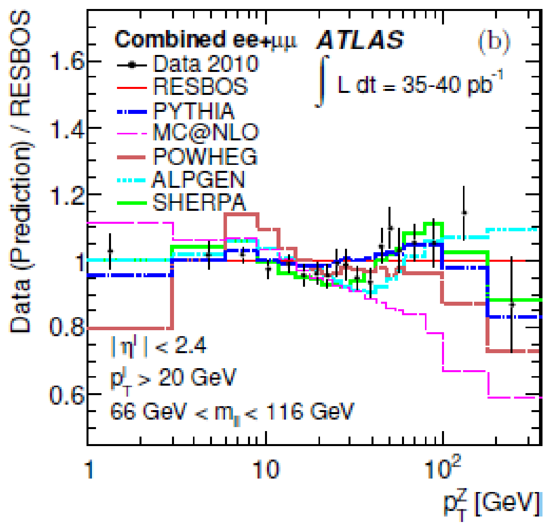

Figure 6.5: Ratios of the combined data and various predictions over the RESBOS predictions for the normalized differential cross section as a function of p_T: predictions from PYTHIA [51], MC@NLO [25], POWHEG [26],ALPGEN and SHERPA [52]. The data points are shown with combined statistical and systematic uncertainties [34].

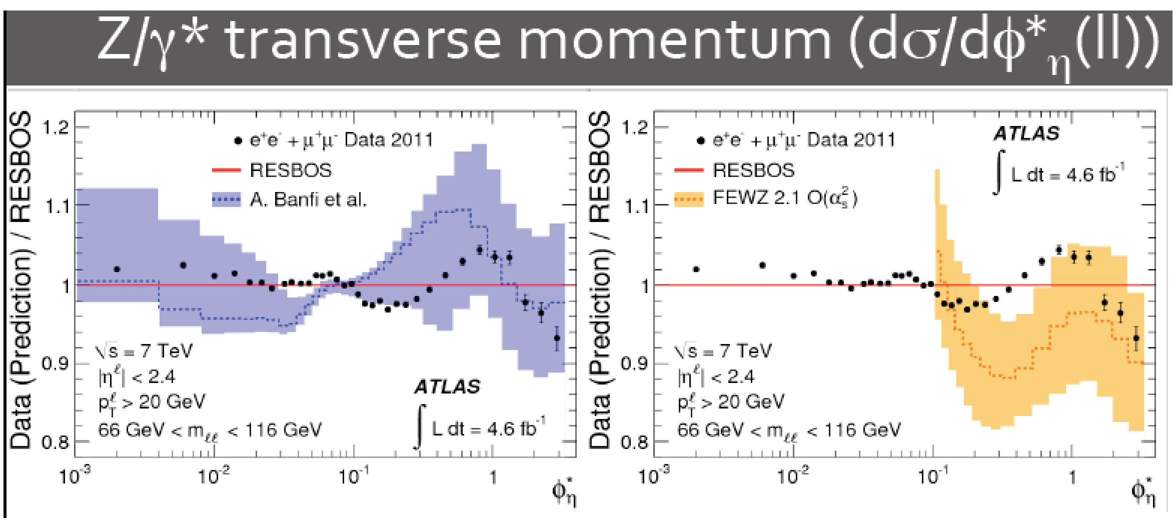

Figure 6.6: The ratio of the combined differential cross section $1/\sigma \cdot d\sigma/d\phi^*_\eta$ to RESBOS predictions as a function of ϕ^*_η. The inner and outer error bars on the data points represent the statistical and total uncertainties, respectively. The uncertainty due to QED FSR is included in the total uncertainties. The measurements are also compared to predictions, which are represented by a dashed line from Ref. [48] and FEWZ. Uncertainties associated with these two calculations are represented by shaded bands. The prediction for FEWZ is only presented for $\phi^*_\eta > 0.1$.

MC methods. This allows arbitrary detector cuts so that contact with experimental data is manifest. We used single Z/γ^* production as our prototypical process. But HERWIRI1.031 runs the same set of processes as does HERWIG6.510. Thus the entire set of standard candle processes and the BSM processes at the LHC is within our approach.

CHAPTER SEVEN

Conclusion

In this thesis we have shown that the realization of IR-improved DGLAP-CS theory in HERWIRI1.031, when used in the MC@NLO/HERWIRI1.031 exact $\mathcal{O}(\alpha_S)$ ME matched parton shower framework, affords one the opportunity to explain, on an event-to-event basis, both the rapidity and the p_T spectra of the Z/γ^* in pp collisions in the recent LHC data from CMS and ATLAS, respectively, without the need of an unexpectedly hard intrinsic Gaussian p_T distribution with rms value of PTRMS$\cong$ 2 GeV in the proton's wave function. Therefore it can be interpreted as providing a rigorous basis for the phenomenological correctness of such unexpectedly hard distributions insofar as describing these data using the usual DGLAP-CS showers is concerned. It is further emphasized that the precociousness of Bjorken scaling argues against the fundamental correctness of the *hard* scale intrinsic p_T ansatz with the unexpectedly hard value of PTRMS$\cong$ 2 GeV, as do the successful models of the proton's wave function, which would predict this value to be $\lesssim$ 0.4 GeV. We also point-out that the fundamental description in MC@NLO/HERWIRI1.031 can be systematically improved to the NNLO parton shower/ME matched level - a level which we anticipate is a key ingredient in achieving the (sub-)1% precision tag for such processes as single heavy gauge boson production at the LHC. We conclude that the physical precision of the other more approximate approaches are the above 1% precision tag that is now aspired. However, it is to be noted that there is no contradiction between the other more approximate approaches and the exact IR-improved DGLAP-CS theory.

APPENDICES

APPENDIX A

Herwiri1.031

HERWIRI1.031 is a Monte Carlo package for simulating high energy radiation with IR improvement. The functions modified in HERWIG are

HWBRAN

HWBSUD

HWBSU1

HWBSU2

HWBSUG

HWIGIN

HWSGQQ (modified in version 1.02)

HWSFBR (modified in version 1.031)

The new functions in HERWIRI1.031 are

IRNF Computes the number of active flavours based on Q.

IREI Computes the exponential integral Ei(x) for x ¿ 0.

IRQQBAR Newton-Raphsons method to solve an algebraic equation of the form F(x)=0.

A.1 hwmain.f

```
PROGRAM HWIGPR
C—COMMON BLOCKS ARE INCLUDED AS FILE HERWIG65.INC
INCLUDE 'HERWIG65.INC'
INTEGER N
EXTERNAL HWUDAT
```

C—MAX NUMBER OF EVENTS THIS RUN

MAXEV= 1000

C—BEAM PARTICLES

PART1='P'

PART2='P'

open (unit = 1, file = "output.dat")

C—BEAM MOMENTA

PBEAM1=7000.

PBEAM2=7000.

C—PROCESS

IPROC=1353

C—INITIALISE OTHER COMMON BLOCKS

CALL HWIGIN

C—USER CAN RESET PARAMETERS AT THIS POINT, OTHERWISE DEFAULT

C VALUES IN HWIGIN WILL BE USED.

NOWGT = .TRUE.

PRVTX = .FALSE.

MAXPR = 5

C PTMIN=100.

PTMIN = 5 C—COMPUTE PARAMETER-DEPENDENT CONSTANTS

CALL HWUINC

C—CALL HWUSTA TO MAKE ANY PARTICLE STABLE

CALL HWUSTA('PI0 ')

C—USER'S INITIAL CALCULATIONS

CALL HWABEG

C—INITIALISE ELEMENTARY PROCESS

```
CALL HWEINI
C—LOOP OVER EVENTS
DO 100 N=1,MAXEV
C—INITIALISE EVENT
CALL HWUINE
C—GENERATE HARD SUBPROCESS
CALL HWEPRO
C—GENERATE PARTON CASCADES
CALL HWBGEN
C—FINISH EVENT
CALL HWUFNE
C—USER'S EVENT ANALYSIS
CALL HWRAP
100 CONTINUE
C—TERMINATE ELEMENTARY PROCESS
CALL HWEFIN
C—USER'S TERMINAL CALCULATIONS
CALL HWAEND
close(1)
STOP
END
SUBROUTINE HWABEG
C USER'S ROUTINE FOR INITIALIZATION
C————————————————————————————-
END
C————————————————————————————-
SUBROUTINE HWAEND
```

```
C USER'S ROUTINE FOR TERMINAL CALCULATIONS, HISTOGRAM OUT-
PUT, ETC
C——————————————————————————————-
END
C——————————————————————————————-
SUBROUTINE HWRAP
C USER'S ROUTINE TO CALCULATE THE RAPIDITY DISTRIBUTION OF
THE Z
C ZLOW : MINIMUM VALUE OF Z FOR CUT
C PTLCUT : CUT ON LEPTON MOMENTUM
C ETACUT : CUT ON LEPTON RAPIDITY
C——————————————————————————————-
INCLUDE 'HERWIG65.INC'
INTEGER IST, I
LOGICAL ZCUT, PTTEST, PLUS, MINUS
DOUBLE PRECISION ZLOW, PX, PY, PT, PTLP,PTLM, ETAL,
& PTLCUT, MUPLUS, MUMINUS, E, PZ, ETA,
& ETAFNL, ETACUT
ETACUT = 50
ZLOW = 40
PTLCUT = 5
IF (IERROR.NE.0) RETURN
ZCUT = .FALSE.
PLUS = .FALSE.
MINUS =.FALSE.
DO 30 I=1, NHEP
IST = ISTHEP(I)
```

```
C MAKE CUT ON Z
IF((IST .EQ. 120) .AND. (IDHEP(I) .EQ. 23)) THEN
IF(PHEP(5,I) .GT. ZLOW) THEN
E = PHEP(4,I)
PZ= PHEP(3,I)
ETAFNL = 0.5*LOG((E+PZ)/(E-PZ))
ZCUT = .TRUE.
ENDIF
ENDIF C MAKES CUT ON PT and Y FOR MU-MINUS
IF ((IST .EQ. 190) .AND.(IDHEP(I) .EQ. 13) ) THEN
PX = PHEP(1,I)
PY = PHEP(2,I)
E = PHEP(4,I)
PZ = PHEP(3,I)
ETA = 0.5*LOG((E+PZ)/(E-PZ))
PTLM = SQRT(PX*PX + PY*PY)
IF((PTLM .GT. PTLCUT) .AND. (ABS(ETA) .LT.ETACUT )) THEN
PLUS = .TRUE.
ENDIF
ENDIF
C MAKES CUT ON PT and Y FOR MU-PLUS
IF ((IST .EQ. 190) .AND.(IDHEP(I) .EQ. -13) ) THEN
PX = PHEP(1,I)
PY = PHEP(2,I)
E = PHEP(4,I)
PZ = PHEP(3,I)
ETA = 0.5*LOG((E+PZ)/(E-PZ))
```

```
PTLP = SQRT(PX*PX + PY*PY)
IF((PTLP .GT. PTLCUT) .AND. (ABS(ETA) .LT.ETACUT)) THEN
MINUS = .TRUE.
ENDIF
ENDIF
30 CONTINUE
IF(ZCUT) THEN
C ONYLY WRITE EVENTS THAT PASS LEPTON TEST
IF(PLUS .AND. MINUS) THEN
WRITE(1,*), ETAFNL
ENDIF
ENDIF
END
C————————————————————————————
```

APPENDIX B

Sample Run Data

INPUT CONDITIONS FOR THIS RUN

BEAM 1 (P) MOM. = 7000.00

BEAM 2 (P) MOM. = 7000.00

PROCESS CODE (IPROC) = 1353

NUMBER OF FLAVOURS = 6

STRUCTURE FUNCTION SET = 8

AZIM SPIN CORRELATIONS = T

AZIM SOFT CORRELATIONS = T

QCD LAMBDA (GEV) = 0.1800

DOWN QUARK MASS = 0.3200

UP QUARK MASS = 0.3200

STRANGE QUARK MASS = 0.5000

CHARMED QUARK MASS = 1.5500

BOTTOM QUARK MASS = 4.9500

TOP QUARK MASS = 174.3000

GLUON EFFECTIVE MASS = 0.7500

EXTRA SHOWER CUTOFF (Q)= 0.4800

EXTRA SHOWER CUTOFF (G)= 0.1000

PHOTON SHOWER CUTOFF = 0.4000

CLUSTER MASS PARAMETER = 3.3500

SPACELIKE EVOLN CUTOFF = 2.5000

INTRINSIC P-TRAN (RMS) = 0.0000

DECAY SPIN CORRELATIONS= T

SUSY THREE BODY ME = T

SUSY FOUR BODY ME = F

MIN MASS FOR DRELL-YAN = 10.0000

MAX MASS FOR DRELL-YAN =14000.0001

NO EVENTS WILL BE WRITTEN TO DISK

B_d: Delt-M/Gam =0.7000 Delt-Gam/2*Gam =0.0000

B_s: Delt-M/Gam = 10.00 Delt-Gam/2*Gam =0.2000

PDFLIB NOT USED FOR BEAM 1

PDFLIB NOT USED FOR BEAM 2

Checking consistency of particle properties

WRITING SUDAKOV TABLE ON UNIT 77

WRITING MATRIX ELEMENT TABLE ON UNIT 88

CHECKING SUSY DECAY MATRIX ELEMENTS

PARTICLE TYPE 21=PI0 SET STABLE

INITIAL SEARCH FOR MAX WEIGHT

PROCESS CODE IPROC = 1353

RANDOM NO. SEED 1 = 1246579

SEED 2 = 8447766

NUMBER OF SHOTS = 10000

NEW MAXIMUM WEIGHT = 9.666181036104836

NEW MAXIMUM WEIGHT = 19.14190263622064

HWWARN CALLED FROM SUBPROGRAM HWSMRS: CODE = 4

EVENT 0: SEEDS = 17673 & 63565 WEIGHT = 0.0000E+00

EVENT SURVIVES. EXECUTION CONTINUES

WARNING: MRST98 CALLED WITH X OUTSIDE ALLOWED RANGE!

X VALUE=1.261E-06, MINIMUM=1.000E-05, MAXIMUM=1.000E+00

NO FURTHER WARNINGS WILL BE ISSUED

NEW MAXIMUM WEIGHT = 21.25145338674105

INITIAL SEARCH FINISHED

OUTPUT ON ELEMENTARY PROCESS

N.B. NEGATIVE WEIGHTS NOT ALLOWED

NUMBER OF EVENTS = 0

NUMBER OF WEIGHTS = 10000

MEAN VALUE OF WGT = 6.0962E+00

RMS SPREAD IN WGT = 4.4149E+00

ACTUAL MAX WEIGHT = 2.0496E+01

ASSUMED MAX WEIGHT = 2.1251E+01

PROCESS CODE IPROC = 1353

CROSS SECTION (PB) = 6096.

ERROR IN C-S (PB) = 44.15

EFFICIENCY PERCENT = 28.69

SUBROUTINE TIMEL CALLED BUT NOT LINKED.

DUMMY TIMEL WILL BE USED. DELETE DUMMY

AND LINK CERNLIB FOR CPU TIME REMAINING.

HWWARN CALLED FROM SUBPROGRAM HWSMRS: CODE = 5

EVENT 1: SEEDS = 17673 & 63565 WEIGHT = 0.6096E+01

EVENT SURVIVES. EXECUTION CONTINUES

WARNING: MRST98 CALLED WITH Q OUTSIDE ALLOWED RANGE!

Q VALUE=1.540E+04, MINIMUM=1.118E+00, MAXIMUM=3.162E+03

NO FURTHER WARNINGS WILL BE ISSUED

EVENT 1: 7000.00 GEV/C P ON 7000.00 GEV/C

P PROCESS: 1353

SEEDS: 17673 & 63565 STATUS: 40 ERROR: 0

WEIGHT: 6.0962E+00

Table B.1. INITIAL STATE

IHEP	ID	IDPDG	IST	M01	M02	DA1	DA2	P-X	P-Y	P-Z	ENERGY	MASS
1	P	2212	101	0	0	0	0	0.00	0.00	7000.0	7000.0	0.94
2	P	2212	102	0	0	0	0	0.00	0.00	-7000.0	7000	0.94
3	CMF	0	103	1	2	0	0	0.00	0.00	0.01400	0.01400	0.00

EVENT 2: 7000.00 GEV/C P ON 7000.00 GEV/C P PROCESS: 1353

SEEDS: 1794949213 & 1372457633 STATUS: 40 ERROR: 0 WEIGHT: 6.0962E+00

EVENT 3: 7000.00 GEV/C P ON 7000.00 GEV/C P PROCESS: 1353

SEEDS: 655683739 & 1202914484 STATUS: 40 ERROR: 0 WEIGHT: 6.0962E+00

Table B.2. HARD SUBPROCESS

IHEP	ID	IDPDG	IST	M01	M02	DA1	DA2	P-X	P-Y	P-Z	ENERGY	MASS
4	UQRK	2	121	6	5	9	5	0.00	0.00	-0.4	0.5	0.32
5	UQRK	-2	122	6	4	16	4	0.00	0.00	-635.0	635.0	0.32
6	Z0/GAMA*	23	120	4	5	7	8	-6.43	-0.77	-635.4	635.6	11.76

Table B.3. H/W/Z BOSON DECAYS

IHEP	ID	IDPDG	IST	M01	M02	DA1	DA2	P-X	P-Y	P-Z	ENERGY	MASS
7	MU-	13	123	6	7	21	7	5.46	1.88	-377.1	377.2	0.11
8	MU+	-13	124	6	8	22	8	-5.46	-1.88	-258.3	258.4	0.11

Table B.4. PARTON SHOWERS

IHEP	ID	IDPDG	IST	M01	M02	DA1	DA2	P-X	P-Y	P-Z	ENERGY	MASS
9	UQRK	94	141	4	6	11	15	-6.81	-1.97	80.4	-80.3	-8.56
10	CONE	0	149	9	12	0	0	1.00	0.08	-62.6	62.6	0.00
11	GLUON	21	149	9	12	0	20	1.64	-0.38	-15.8	15.9	0.75
12	GLUON	21	149	9	13	0	11	2.16	0.04	-28.9	29.0	0.75
13	GLOUN	21	149	9	14	0	12	3.04	1.16	-29.7	29.9	0.75
14	GLUON	21	149	9	15	0	13	-0.03	1.14	-5.7	5.9	0.75
15	UD	2101	147	9	18	0	14	0.00	0.00	6999.7	6999.7	-2.30
16	UBAR	94	142	5	6	18	20	0.38	1.20	-715.9	715.9	-1.76
17	CONE	0	100	5	4	0	0	-0.96	0.26	-42.8	42.8	0.00
18	UQRK	2	149	16	19	0	15	-1.09	-0.31	-877.9	877.9	0.32
19	UU	2203	148	16	20	0	18	0.00	0.00	-3223.7	3223.7	0.35
20	DQRK	1	149	16	11	0	19	0.71	-0.89	-2182.4	2182.5	0.32
21	MU-	13	190	7	6	0	0	3.11	1.60	-201.9	201.9	0.11
22	MU+	-13	190	8	6	0	0	-9.54	-2.37	-433.5	433.7	0.11

Table B.5. INITIAL STATE

IHEP	ID	IDPDG	IST	M01	M02	DA1	DA2	P-X	P-Y	P-Z	ENERGY	MASS
1	P	2212	101	0	0	0	0	0.00	0.00	7000.0	7000.0	0.94
2	P	2212	102	0	0	0	0	0.00	0.00	-7000.0	7000.0	0.94
3	CMF	0	103	1	2	0	0	0.00	0.00	0.01400	0.01400	0.00

Table B.6. HARD SUBPROCESS

IHEP	ID	IDPDG	IST	M01	M02	DA1	DA2	P-X	P-Y	P-Z	ENERGY	MASS
4	DQRK	1	121	6	5	9	5	0.00	0.00	957.9	957.9	0.32
5	DBAR	-1	122	6	4	11	4	0.00	0.00	0.6	0.7	0.32
6	Z0/GAMA*	23	120	4	5	7	8	1.40	-2.41	958.5	958.6	12.30

Table B.7. H/W/Z BOSON DECAYS

IHEP	ID	IDPDG	IST	M01	M02	DA1	DA2	P-X	P-Y	P-Z	ENERGY	MASS
7	MU-	13	123	6	7	20	7	4.10	3.69	-690.7	690.7	0.11
8	MU+	-13	124	6	8	21	8	-4.10	-3.69	267.9	267.9	0.11

Table B.8. PARTON SHOWERS

IHEP	ID	IDPDG	IST	M01	M02	DA1	DA2	P-X	P-Y	P-Z	ENERGY	MASS
9	DQRK	94	141	4	6	10	10	0.00	0.00	1194.5	1194.5	0.32
10	UU	2203	147	9	13	0	19	0.00	0.00	5805.5	5805.5	0.47
11	DBAR	94	142	5	6	13	19	1.40	-2.41	-235.9	-235.8	-6.85
12	CONE	0	100	5	4	0	0	0.98	-0.17	116.9	116.9	0.00
13	DQRK	1	149	11	14	0	10	0.30	1.27	0.5	1.4	0.32
14	UU	2203	148	11	15	0	13	0.00	0.00	-6988.2	6988.2	-3.67
15	DQRK	1	149	11	16	0	14	0.78	0.80	-11.2	11.3	0.32
16	GLUON	21	149	11	17	0	15	-1.33	-0.56	22.3	22.4	0.75
17	GLUON	21	149	11	18	0	16	-0.28	0.67	35.2	35.2	0.75
18	GLUON	21	149	11	19	0	17	-0.96	1.21	87.8	87.8	0.75
19	GLUON	21	149	11	10	0	18	0.08	-0.97	89.6	89.6	0.75
20	MU-	13	190	7	6	0	0	4.78	2.52	665.2	665.2	0.11
21	MU+	-13	190	8	6	0	0	-3.38	-4.93	293.4	293.4	0.11

Table B.9. INITIAL STATE

IHEP	ID	IDPDG	IST	M01	M02	DA1	DA2	P-X	P-Y	P-Z	ENERGY	MASS
1	P	2212	101	0	0	0	0	0.00	0.00	7000.0	7000.0	0.94
2	P	2212	102	0	0	0	0	0.00	0.00	-7000.0	7000.0	0.94
3	CMF	0	103	1	2	0	0	0.00	0.00	0.01400	0.01400	0.00

EVENT 5: 7000.00 GEV/C P ON 7000.00 GEV/C P PROCESS: 1353

SEEDS: 1264112893 & 538273190 STATUS: 40 ERROR: 0 WEIGHT: 6.0962E+00

Table B.10. HARD SUBPROCESS

IHEP	ID	IDPDG	IST	M01	M02	DA1	DA2	P-X	P-Y	P-Z	ENERGY	MASS
4	UBAR	-2	121	6	5	9	5	0.00	0.00	73.6	73.6	0.32
5	UQRK	2	122	6	4	15	4	0.00	0.00	-0.4	0.5	0.32
6	Z0/GAMA*	23	120	4	5	7	8	-4.22	-0.94	73.2	74.2	11.24

Table B.11. H/W/Z BOSON DECAYS

IHEP	ID	IDPDG	IST	M01	M02	DA1	DA2	P-X	P-Y	P-Z	ENERGY	MASS
7	MU-	13	123	6	7	17	7	-1.71	-2.01	3.9	4.7	0.11
8	MU+	-13	124	6	8	18	8	1.71	-2.01	69.3	69.4	0.11

Table B.12. PARTON SHOWERS

IHEP	ID	IDPDG	IST	M01	M02	DA1	DA2	P-X	P-Y	P-Z	ENERGY	MASS
9	UBAR	94	141	4	6	11	14	-4.22	-0.94	73.8	73.7	-4.99
10	CONE	0	100	4	5	0	0	-0.73	0.68	4.5	4.6	0.00
11	UQRK	2	149	9	12	0	16	2.30	0.35	1042.5	1042.5	0.32
12	UD	2101	147	9	13	0	11	0.00	0.00	4099.1	4099.1	0.31
13	UQRK	2	149	9	14	0	12	0.89	-0.71	1742.1	1742.1	0.31
14	GLUON	21	149	9	16	0	13	1.04	1.30	42.5	42.5	0.75
15	UQRK	94	142	5	6	16	16	0.00	0.00	-0.5	0.5	0.01
16	UD	2101	148	15	11	0	14	0.00	0.00	-6999.5	6999.5	0.37
17	MU-	13	190	7	6	0	0	-4.03	1.49	9.4	10.3	0.11
18	MU+	-13	190	8	6	0	0	-0.19	-2.43	63.9	63.9	0.11

Table B.13. INITIAL STATE

IHEP	ID	IDPDG	IST	M01	M02	DA1	DA2	P-X	P-Y	P-Z	ENERGY	MASS
1	P	2212	101	0	0	0	0	0.00	0.00	7000.0	7000.0	0.94
2	P	2212	102	0	0	0	0	0.00	0.00	-7000.0	7000.0	0.94
3	CMF	0	103	1	2	0	0	0.00	0.00	0.01400	0.01400	0.00

OUTPUT ON ELEMENTARY PROCESS

N.B. NEGATIVE WEIGHTS NOT ALLOWED

NUMBER OF EVENTS = 1000

NUMBER OF WEIGHTS = 3473

Table B.14. HARD SUBPROCESS

IHEP	ID	IDPDG	IST	M01	M02	DA1	DA2	P-X	P-Y	P-Z	ENERGY	MASS
4	UQRK	2	121	6	5	9	5	0.00	0.00	458.9	458.9	0.32
5	UBAR	-2	122	6	4	15	4	0.00	0.00	-0.4	0.5	0.32
6	Z0/GAMA*	23	120	4	5	7	8	-3.28	-0.67	458.5	459.5	30.29

Table B.15. H/W/Z BOSON DECAYS

IHEP	ID	IDPDG	IST	M01	M02	DA1	DA2	P-X	P-Y	P-Z	ENERGY	MASS
7	MU-	13	123	6	7	24	7	2.92	-2.82	450.6	450.6	0.11
8	MU+	-13	124	6	8	25	8	-2.92	2.82	7.9	8.9	0.11

Table B.16. PARTON SHOWERS

IHEP	ID	IDPDG	IST	M01	M02	DA1	DA2	P-X	P-Y	P-Z	ENERGY	MASS
9	UQRK	94	141	4	6	11	14	-1.92	3.85	503.6	503.5	-10.81
10	CONE	0	100	4	5	0	0	-0.01	1.00	11.2	11.2	0.00
11	GLUON	21	149	9	12	0	23	0.99	-0.45	15.9	16.0	0.75
12	GLUON	21	149	9	13	0	11	0.81	-1.33	37.8	37.9	0.75
13	GLUON	21	149	9	14	0	12	0.12	-2.06	713.2	713.2	0.75
14	UD	2101	147	9	17	0	13	0.00	0.00	5729.5	5729.5	0.36
15	UBAR	94	142	5	6	17	23	-1.36	-4.51	-45.1	-44.0	-11.00
16	CONE	0	100	5	4	0	0	0.93	0.38	20.3	20.3	0.00
17	UQRK	2	149	15	18	0	14	-0.61	0.93	-5.2	5.3	0.32
18	UU	2203	148	15	19	0	17	0.00	0.00	-6932.3	6932.3	0.25
19	DQRK	1	149	15	20	0	18	-0.46	1.10	-61.4	61.4	0.32
20	GLUON	21	149	15	21	0	19	1.01	-0.65	0.9	1.7	0.75
21	GLUON	21	149	15	22	0	20	0.94	0.58	14.2	14.2	0.75
22	GLUON	21	149	15	22	0	21	0.35	0.87	8.3	8.4	0.75
23	GLUON	21	149	15	11	0	22	0.14	1.69	20.6	20.7	0.75
24	MU-	13	190	7	6	0	0	1.30	-3.15	445.4	445.4	0.11
25	MU+	-13	190	8	6	0	0	-4.58	2.49	13.1	14.1	.11

MEAN VALUE OF WGT = 6.0018E+00

RMS SPREAD IN WGT = 4.4205E+00

ACTUAL MAX WEIGHT = 2.0460E+01

ASSUMED MAX WEIGHT = 2.1251E+01

PROCESS CODE IPROC = 1353

CROSS SECTION (PB) = 6002.

ERROR IN C-S (PB) = 75.01

EFFICIENCY PERCENT = 28.24

APPENDIX C

CMS Data Used

Table C.1: Measurement of the normalized differential cross section ($\sigma \frac{d\sigma}{d|y|}$) for the Drell-Yan lepton pairs in the Z-boson mass region ($60 < M_{ll} < 120$ GeV) as a function of the absolute value of rapidity, separately for the muon and electron channels and combined. Detector geometry and trigger uniformity requirements limit the muon channel measurement to $|y| < 2.0$. The uncertainties shown are the combined statistical and systematic uncertainties. [33]

	Normalized Differential Cross section		
$\lvert y\rvert$ Range	Muon	Electron	Combined
[0.0,0.1]	0.324±0.012	0.359±0.015	0.337±0.010
[0.1, 0.2]	0.338±0.013	0.326±0.016	0.335±0.010
[0.2, 0.3]	0.338±0.013	0.344±0.017	0.341±0.010
[0.3, 0.4]	0.341±0.013	0.355±0.017	0.346±0.010
[0.4, 0.5]	0.363±0.013	0.339±0.017	0.354±0.011
[0.5, 0.6]	0.342±0.013	0.351±0.018	0.346±0.010
[0.6, 0.7]	0.312±0.013	0.360±0.018	0.328±0.010
[0.7, 0.8]	0.354±0.013	0.331±0.018	0.347±0.011
[0.8, 0.9]	0.343±0.014	0.355±0.018	0.347±0.011
[0.9, 1.0]	0.332±0.014	0.332±0.018	0.332±0.011
[1.0, 1.1]	0.336±0.014	0.316±0.018	0.329±0.011
[1.1, 1.2]	0.324±0.014	0.352±0.019	0.334±0.011
[1.2, 1.3]	0.321±0.014	0.332±0.019	0.325±0.011
[1.3, 1.4]	0.355±0.016	0.321±0.019	0.341±0.012
[1.4, 1.5]	0.326±0.016	0.313±0.019	0.319±0.012
[1.5, 1.6]	0.331±0.018	0.330±0.020	0.330±0.013
[1.6, 1.7]	0.294±0.018	0.306±0.022	0.299±0.014
[1.7, 1.8]	0.331±0.021	0.332±0.024	0.331±0.016
[1.8, 1.9]	0.324±0.025	0.294±0.024	0.308±0.017
[1.9, 2.0]	0.328±0.032	0.328±0.026	0.038±0.020
[2.0, 2.1]		0.294±0.027	0.294±0.027
[2.1, 2.2]		0.298±0.029	0.298±0.029
[2.2, 2.3]		2.290±0.031	2.290±0.031
[2.3, 2.4]		0.278±0.035	0.278±0.035
[2.4, 2.5]		0.199±0.038	0.199±0.038
[2.5, 2.6]		0.249±0.040	0.249±0.040
[2.6, 2.7]		0.241±0.037	0.241±0.037
[2.7, 2.8]		0.256±0.035	0.256±0.035
[2.8, 2.9]		0.221±0.034	0.221±0.034
[2.9, 3.0]		0.165±0.035	0.165±0.035
[3.0, 3.1]		0.183±0.040	0.183±0.040
[3.1, 3.2]		0.228±0.045	0.228±0.045
[3.2, 3.3]		0.078±0.043	0.078±0.043
[3.3, 3.4]		0.105±0.051	0.105±0.051
[3.4, 3.5]		0.089±0.062	0.089±0.062

Table C.2: Measurement of the normalized differential cross section for the Drell-Yan lepton pairs in the Z-boson mass region ($60 < M_{ll} < 120$ GeV) as a function of p_T, separately for muon and electron channels and for the combination of the two channels. The distribution is normalized by the cross section for the Z-bosons with both leptons having $|\eta| < 2.1$ and $p_T > 20$ GeV. The uncertainties listed in the table are the combined statistical and systematic uncertainties. [33]

p_T Range (GeV)	Muon Channel	Electron Channel	Combination
[0.0,2.5]	$(3.21 \pm 0.14) \times 10^{-2}$	$(3.24 \pm 0.25) \times 10^{-2}$	$(3.22 \pm 0.13) \times 10^{-2}$
[2.5, 5.0]	$(5.89 \pm 0.21) \times 10^{-2}$	$(6.03 \pm 0.32) \times 10^{-2}$	$(5.92 \pm 0.17) \times 10^{-2}$
[5.0, 7.5]	$(5.51 \pm 0.21) \times 10^{-2}$	$(5.32 \pm 0.32) \times 10^{-2}$	$(5.50 \pm 0.16) \times 10^{-2}$
[7.5, 10.0]	$(3.90 \pm 0.18) \times 10^{-2}$	$(4.20 \pm 0.30) \times 10^{-2}$	$(3.96 \pm 0.14) \times 10^{-2}$
[10.0, 12.5]	$(3.49 \pm 0.16) \times 10^{-2}$	$(3.60 \pm 0.28) \times 10^{-2}$	$(3.53 \pm 0.12) \times 10^{-2}$
[12.5, 15.0]	$(2.74 \pm 0.15) \times 10^{-2}$	$(2.70 \pm 0.25) \times 10^{-2}$	$(2.72 \pm 0.12) \times 10^{-2}$
[15.0, 17.5]	$(2.23 \pm 0.14) \times 10^{-2}$	$(2.00 \pm 0.22) \times 10^{-2}$	$(2.16 \pm 0.10) \times 10^{-2}$
[17.5, 20.0]	$(1.68 \pm 0.12) \times 10^{-2}$	$(1.59 \pm 0.20) \times 10^{-2}$	$(1.65 \pm 0.09) \times 10^{-2}$
[20.0, 30.0]	$(1.14 \pm 0.04) \times 10^{-2}$	$(1.20 \pm 0.05) \times 10^{-2}$	$(1.16 \pm 0.04) \times 10^{-2}$
[30.0, 40.0]	$(6.32 \pm 0.28) \times 10^{-3}$	$(5.62 \pm 0.31) \times 10^{-3}$	$(5.98 \pm 0.27) \times 10^{-3}$
[40.0, 50.0]	$(3.53 \pm 0.21) \times 10^{-3}$	$(3.18 \pm 0.24) \times 10^{-3}$	$(3.38 \pm 0.18) \times 10^{-3}$
[50.0, 70.0]	$(1.74 \pm 0.10) \times 10^{-3}$	$(1.90 \pm 0.12) \times 10^{-3}$	$(1.81 \pm 0.09) \times 10^{-3}$
[70.0, 90.0]	$(7.76 \pm 0.71) \times 10^{-4}$	$(7.86 \pm 0.77) \times 10^{-4}$	$(7.79 \pm 0.54) \times 10^{-4}$
[90.0, 110.0]	$(4.87 \pm 0.55) \times 10^{-14}$	$(4.57 \pm 0.59) \times 10^{-4}$	$(4.75 \pm 0.42) \times 10^{-4}$
[110.0, 150.0]	$(1.79 \pm 0.22) \times 10^{-4}$	$(2.18 \pm 0.26) \times 10^{-4}$	$(1.93 \pm 0.17) \times 10^{-4}$
[150.0, 190.0]	$(7.10 \pm 1.40) \times 10^{-5}$	$(4.82 \pm 1.31) \times 10^{-5}$	$(6.00 \pm 0.99) \times 10^{-5}$
[190.0, 250.0]	$(1.17 \pm 0.51) \times 10^{-5}$	$(2.05 \pm 0.64) \times 10^{-5}$	$(1.51 \pm 0.43) \times 10^{-5}$
[250.0, 600.0]	$(2.24 \pm 0.78) \times 10^{-6}$	$(0.81 \pm 0.52) \times 10^{-6}$	$(1.29 \pm 0.44) \times 10^{-6}$

APPENDIX D

ATLAS Data Used

Table D.1: The measured normalized differential cross section $\frac{1}{\sigma}\frac{d\sigma}{dp_T}$ in bins of p_T for $Z/\gamma^* \rightarrow e^+e^-$. The cross sections are to be multiplied by the factor k corresponding to bare electrons. The relative statistical (stat.) and total systematic (syst.) uncertainties are given. [34]

p_T bin (GeV)	$\frac{1}{\sigma}\frac{d\sigma}{dp_T}$ GeV^{-1} $Z/\gamma^* \rightarrow e^+e^-$		uncert. (%)	
	bare electron	k	stat.	syst.
0 - 3	3.21	$.10^{-2}$	3.3	4.7
3 - 6	5.60	$.10^{-2}$	2.4	3.3
6 - 9	4.64	$.10^{-2}$	2.7	2.3
9 - 12	3.56	$.10^{-2}$	3.1	2.4
12 - 15	3.09	$.10^{-2}$	3.3	2.7
15 - 18	2.16	$.10^{-2}$	3.9	3.0
18 - 21	1.73	$.10^{-2}$	4.4	3.3
21 - 24	1.37	$.10^{-2}$	4.8	3.6
24 - 27	1.11	$.10^{-2}$	5.5	3.8
27 - 30	1.03	$.10^{-2}$	6.5	4.0
30 - 36	7.26	$.10^{-3}$	4.8	4.2
36 - 42	4.85	$.10^{-3}$	5.8	4.5
42 - 48	3.59	$.10^{-3}$	7.0	4.8
48 - 54	3.20	$.10^{-3}$	7.8	5.0
54 - 60	2.08	$.10^{-3}$	9.2	5.4
60 - 80	1.17	$.10^{-3}$	6.5	5.7
80 - 100	5.44	$.10^{-4}$	9.8	5.9
100 - 180	1.67	$.10^{-4}$	9.6	6.1
180 - 350	0.73	$.10^{-5}$	27.0	7.8

APPENDIX E

Parton Model of Hadron Structure – Bjorken Scaling

The following chapter follows the explanation of the parton model and Bjorken scaling in Quantum Field Theory by Peskin and Schroeder [16].

The cross section for e^+e^- annihilation to hadrons can be computed using a model in which quarks are treated as non-interacting fermions which gives an accurate formula for the cross section. Now we consider the case of proton-proton collision. At high energy, collisions of protons in the center of mass produce a large number of pions. These pions are produced mostly with momenta collinear with the collision axis. This limited transverse momentum led to the modelling of hadron as a loosely bound assembly of many components. So when a proton is struck with another proton, it shatters into a cloud of pieces. In a high energy collision, the two initial hadrons have almost lightlike momenta. The pieces of the hadron forming the cloud possess lightlike momenta parallel to the original momentum vectors as well. So by exchanging momenta q among the pieces in a way such that even if the components of q are large, q^2 is always small, the final state can be produced. As ejection of a hadron at large transverse momenta requiring large q^2 is rare, it can be stated that hadrons are loose clouds of constituents which cannot absorb large q^2.

The SLAC-MIT [36] deep inelastic scattering experiments put the above model to test. The experiments saw hard scattering of electrons from the protons. Only in rare cases a single proton emerged from the scattering processes. The deep inelastic region of the phase space contributed the largest part of the rate. Therefore, Bjorken and Feynman gave a simple model called the parton model to explain the above. In this theory it was assumed that the proton was made of a small number of components called partons. These includes quarks and antiquarks and neutral species that are responsible for their binding. Now in a scattering, the hadrons produced are collinear with the direction of the original struck proton.

We now consider the electron-proton inelastic scattering in Fig. (E.1).

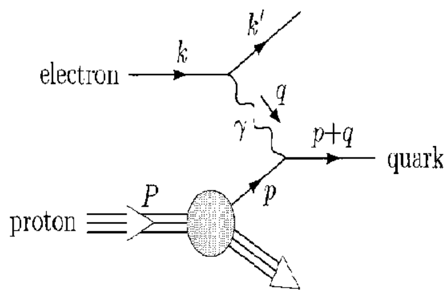

Figure E.1. Kinematics of deep inelastic electron scattering in the parton [16].

As q^μ is a spacelike vector, we can express its invariant square in terms of

$$Q^2 = -q^2, \tag{E.1}$$

where Q is a positive quantity. The Mandelstam variable $\hat{t}$ is given by $-Q^2$. A given parton can be characterized by the fraction of the proton's momentum that it carries(ξ). Here it is assumed $0 < \xi < 1$. So the total momentum of the parton is given by $p = \xi P$, where P is the momentum of the proton. So if k be the initial momentum of the electron, the Mandelstam variable $\hat{s}$ is given by

$$\hat{s} = (p + k)^2 = 2p.k = 2\xi P.k = \xi s. \tag{E.2}$$

Here s is the center of mass energy squared. The mass of scattered parton is small compared to s and Q^2, so we get

$$\begin{aligned} 0 &\approx (p + q)^2 \\ &= 2p.q + q^2 \\ &= 2\xi P.q - Q^2. \end{aligned} \tag{E.3}$$

This leads to

$$\xi = x \text{ where } x \equiv \frac{Q^2}{2P.q}. \tag{E.4}$$

It is possible to determine Q^2 and x for the scattering process from each electron. The cross section at $\xi = x$ is

$$\frac{d^2\sigma}{dxdQ^2} = \sum_i f_i(x)Q_i^2 \cdot \frac{2\pi\alpha^2}{Q^4}\left[1 + \left(1 - \frac{Q^2}{xs}\right)^2\right], \tag{E.5}$$

where $f_i(x)$ is the parton distribution function at $\xi = x$. When the cross section is divided by $\frac{1+(1-Q^2/xs)^2}{Q^4}$, we get a quantity that depends only on x. This is known as the *Bjorken Scaling* [22, 36]. According to Bjorken scaling the proton structure appears to be the same irrespective of how hard the proton is struck.

APPENDIX F

χ^2 Test

The formula for χ^2 is given by

$$\chi^2 = \sum \frac{(\text{experimental value} - \text{theoretical prediction})^2}{\text{theoretical prediction}}. \tag{F.1}$$

Degrees of freedom is defined as

$$df = n - 1, \tag{F.2}$$

where n is the number of classes.

BIBLIOGRAPHY

[1] F. Gianotti, in *Proc. ICHEP2012*, in press; J. Incandela, *ibid.*, 2012, in press; G. Aad *et al.*[ATLAS Collaboration], Phys. Lett. B**716** (2012) 1, arXiv:1207.7214; D. Abbaneo *et al.*, S. Chatrchyan *et al.*[CMS COllaboration] Phys. Lett. B**716** (2012) 30, arXiv:1207.7235;

[2] F. Englert and R. Brout, Phys. Rev. Lett. **13** (1964) 312; P.W. Higgs, Phys. Lett. **12** (1964) 132; Phys. Rev. Lett. **13** (1964) 508; G.S. Guralnik, C.R. Hagen and T.W.B. Kibble, *ibid.* **13** (1964) 585.

[3] G. Altarelli and G. Parisi, *Nucl. Phys.* **B126** (1977) 298; Yu. L. Dokshitzer, *Sov. Phys. JETP* **46** (1977) 641; L. N. Lipatov, *Yad. Fiz.* **20** (1974) 181; V. Gribov and L. Lipatov, *Sov. J. Nucl. Phys.* **15** (1972) 675, 938; see also J.C. Collins and J. Qiu, *Phys. Rev. D***39** (1989) 1398.

[4] C.G. Callan, Jr., *Phys. Rev. D***2** (1970) 1541; K. Symanzik, *Commun. Math. Phys.* **18** (1970) 227, and in *Springer Tracts in Modern Physics*, **57**, ed. G. Hoehler (Springer, Berlin, 1971) p. 222; see also S. Weinberg, *Phys. Rev. D***8** (1973) 3497.

[5] B.F.L. Ward, *Adv. High Energy Phys.* **2008** (2008) 682312.

[6] B.F.L. Ward, Ann. Phys. **323** (2008) 2147.

[7] S. Joseph *et al.*, Phys. Lett. B**685** (2010) 283; Phys. Rev. D**81** (2010) 076008.

[8] G. Corcella *et al.*, hep-ph/0210213; J. High Energy Phys. **0101** (2001) 010; G. Marchesini *et al.*, Comput. Phys. Commun.**67** (1992) 465.

[9] B.F.L. Ward, S.K. Majhi and S.A. Yost, in PoS(**RADCOR2011**) (2012) 022.

[10] C. Glosser, S. Jadach, B.F.L. Ward and S.A. Yost, Mod. Phys. Lett. A **19**(2004) 2113; B.F.L. Ward, C. Glosser, S. Jadach and S.A. Yost, in *Proc. DPF 2004*, Int. J. Mod. Phys. A **20** (2005) 3735; in *Proc. ICHEP04, vol. 1*, eds. H. Chen *et al.*,(World. Sci. Publ. Co., Singapore, 2005) p. 588; B.F.L. Ward and S. Yost, preprint BU-HEPP-05-05, in *Proc. HERA-LHC Workshop*, CERN-2005-014; in *Moscow 2006, ICHEP, vol. 1*, p. 505; Acta Phys. Polon. B **38** (2007) 2395; arXiv:0802.0724, PoS**(RADCOR2007)**(2007) 038; B.F.L. Ward *et al.*, arXiv:0810.0723, in *Proc. ICHEP08*; arXiv:0808.3133, in *Proc. 2008 HERA-LHC Workshop*,DESY-PROC-2009-02, eds. H. Jung and A. De Roeck, (DESY, Hamburg, 2009)pp. 180-186, and references therein.

[11] Z. Xu, D.-H. Zhang, and L. Chang, Nucl. Phys. B**291** (1987) 392; Tsingua University preprint TUTP-84/3, 1984.

[12] CALKUL Collaboration, F.A. Berends *et al.*, Phys. Lett. B**103** (1981) 124; B**105** (1981) 215; B**114** (1982) 203; Nucl. Phys. B**206** (1982) 53; B**206** (1982) 61; B**239** (1984) 382.

[13] R. Kleiss and W.J. Stirling, Nucl. Phys. B**262**, 235 1985; Phys. Lett. B **179**, 159 1986.

[14] B.F.L. Ward Phys. Rev. D 83(2011) 113014.

[15] Quarks and Leptons, Halzen and Martin.

[16] An Introduction to Quantum Field Theory, Peskin and Schroeder.

[17] D. R. Yennie, S. C. Frautschi, and H. Suura, Ann. Phys. **13** (1961) 379; see also K. T. Mahanthappa, Phys. Rev. **126** (1962) 329, for a related analysis.

[18] See also S. Jadach and B.F.L. Ward, *Comput. Phys. Commun.* **56**(1990) 351; *Phys.Lett. B* **274** (1992) 470; S. Jadach *et al.*, *Comput. Phys. Commun.* **102** (1997) 229; S. Jadach, W. Placzek and B.F.L Ward, *Phys. Lett. B* **390** (1997) 298; S. Jadach, M. Skrzypek and B.F.L. Ward,*Phys. Rev. D* **55** (1997) 1206; S. Jadach, W. Placzek and B.F.L. Ward, *Phys. Rev. D* **56** (1997) 6939; S. Jadach, B.F.L. Ward and Z. Was,*Phys. Rev. D* **63** (2001) 113009; *Comp. Phys. Commun.* **130** (2000) 260; *ibid.***124** (2000) 233; *ibid.***79** (1994) 503; *ibid.***66** (1991) 276; S. Jadach *et al.*, *ibid.***140** (2001) 432, 475; S. Jadach, B.F.L. Ward and Z. Was, Phys. Rev. D**88**(2013) 114022.

[19] B.F.L. Ward and S. Jadach, Mod. Phys. Lett. A**14** (1999) 491.

[20] S. Jadach, B.F.L. Ward and Z. Was, *Eur. Phys. J.* C22(2001) 423.

[21] J.G.M. Gatheral, Phys. Lett. B **133** (1983) 90.

[22] J. Bjorken, in *Proc. 3rd International Symposium on the History of Particle Physics: The Rise of the Standard Model, Stanford, CA, 1992*, eds. L. Hoddeson *et al.* (Cambridge Univ. Press, Cambridge, 1997) p. 589, and references therein.

[23] B.I. Ermolaev, M. Greco and S.I. Troyan, *PoS DIFF2006* (2006) 036, and references therein.

[24] G. Altarelli, R.D. Ball and S. Forte, *PoS RADCOR2007* (2007) 028.

[25] S. Frixione and B.Webber, J. High Energy Phys. **0206** (2002) 029; S. Frixione *et al.*, arXiv:1010.0568; B. Webber, talk at CERN, 03/30/2011; S. Frixione, talk at CERN, 05/04/2011.

[26] P. Nason, J. High Energy Phys. **0411** (2004) 040.

[27] B.R. Webber, *Ann.Rev. Nucl. Part. Sci.* **B**(1986) 253-286.

[28] C. Galea, in *Proc. DIS 2008*, London, 2008, `http://dx.doi.org/10.3360/dis.2008.55`.

[29] V.M. Abasov *et al.*, Phys. Rev. Lett. **100**, 102002 (2008).

[30] S. K Majhi , A. Mukhopadhyay, B.F.L. Ward, S.A. Yost Phys. Lett. B **719** (2013) 367; S. K Majhi , A. Mukhopadhyay, B.F.L. Ward, S.A. Yost, arXiv: 1305.0023; B.F.L. Ward, S. K Majhi , A. Mukhopadhyay, S.A. Yost, arXiv:1302.0758; B.F.L. Ward, S. K Majhi , A. Mukhopadhyay, S.A. Yost, RADCOR 2013, arXiv:1312.0874.

[31] M. Seymour, "Event Generator Physics for the LHC", CERN Seminar, 2011.

[32] P. Skands, private communication, 2011, finds a similar behavior in PYTHIA8 simulations.

[33] S. Chatrchyan *et al.*, arXiv:1110.4973; Phys. Rev. D**85** (2012) 032002.

[34] G. Aad *et al.*, arXiv:1107.2381; Phys. Lett. B**705** (2011) 415.

[35] R.P. Feynman, M. Kislinger and F. Ravndal, Phys. Rev. D**3** (1971) 2706; R. Lipes, *ibid.***5** (1972) 2849; F.K. Diakonas, N.K. Kaplis and X.N. Mawita, *ibid.* **78** (2008) 054023; K. Johnson, *Proc. Scottish Summer School Phys. 17* (1976) p. 245; A. Chodos et al., Phys. Rev. D**9** (1974) 3471; *ibid.* **10** (1974) 2599; T. DeGrand *et al.*, *ibid.* **12** (1975) 2060.

[36] See for example R.E. Taylor, Phil. Trans. Roc. Soc. Lond. **A359** (2001) 225, and references therein.

[37] See for example S. Jadach *et al.*, in *Physics at LEP2, vol. 2*, (CERN, Geneva, 1995) pp. 229-298.

[38] G. Sterman, Nucl. Phys. B **281**, 310 (1987); S. Catani and L. Trentadue, Nucl. Phys. B **327**, 323 (1989); *ibid.* **353**, 183 (1991).

[39] See for example C. W. Bauer, A.V. Manohar and M.B. Wise, Phys. Rev. Lett. **91** (2003) 122001; Phys. Rev. D **70** (2004) 034014; C. Lee and G. Sterman, Phys. Rev. D **75** (2007) 014022.

[40] J.C. Collins and D.E. Soper, Nucl. Phys. B**193** (1981) 381; *ibid.***213**(1983) 545; *ibid.* **197**(1982) 446.

[41] J.C. Collins, D.E. Soper and G. Sterman, Nucl. Phys. B**250**(1985) 199; in *Les Arcs 1985, Proceedings, QCD and Beyond*, pp. 133-136.

[42] S. Hassani, in Proc. Recntres de Moriond EW, 2013, in press; H. Yin, *ibid.*, 2013, in press; G. Aad *et al.*, arXiv:1211.6899, and references therein.

[43] G. Ladinsky and C. Yuan, Phys. Rev. D**50** (1994) 4239.

[44] F. Landry *et al.*, Phys. Rev. D**63** (2003) 073016.

[45] C. Balazs and C. Yuan, Phys. Rev. D**56** (1997) 5558.

[46] C. Davies, B. Webber and W. Stirling, Nucl. Phys. B**256** (1985) 413.

[47] Yu.L. Dokshitser, D.I. D'yakonov and S.I. Troyan, Phys. Lett. B**78** (1978) 290; Proc. 13th Winter School of the LPNI, Leneingrad(1978); Phys. Rept. **58** (1980) 271; G. Parisi and R. Petronzio, Nucl. Phys. B **154** (1979) 427; G. Curci, M. Greco and R. Srivastava, Phys. Rev. Lett. **43** (1979) 834; Nucl. Phys. B **159** (1979) 451; P. Chiappetta and M. Greco, Nucl.Phys. B**199** (1982) 77; *ibid.* 221 (1983) 268; Phys. Lett. B**135** (1984) 187; F. Halzen, A.D. Martin and D.M. Scott, Phys. Rev. D**25** (1982) 754; P. Aurenche and R. Kinnunen, Phys. Lett. B **135** (1984) 493; A. Nakamura, G. Pancheri and Y. Srivastava, Z. Phys. **21** (1984) 243; G. Altarelli, R.K. Ellis, M. Greco and G. Martinelli, Nucl. Phys. B **246** (1984) 12.

[48] A. Banfi *et al.*, Phys. Lett. B**715**(2012) 152 and references therein.

[49] T. Becher, M. Neubert and D. Wilhelm, arXiv:1109.6027; T. Becher, M. Neubert, Eur. Phys. J. C**71** (2011) 1665, and references therein.

[50] A. Banfi *et al.*, Eur. Phys. J. C**71** (2011) 1600.

[51] T. Sjostrand, S. Mrenna and P. Z. Skands, Comput. Phys. Commun. **178** (2008) 852-867.

[52] T. Gleisberg *et al.*, J.High Energy Phys. **0902** (2009) 007.